Design and Control of a 10 DOF Biped Robot

By: Weigang Gu
Supervised by: Dr. Xiaoping Liu

A thesis submitted to the faculty of graduate studies
Lakehead University
in partial fulfillment of the requirements for the degree of
Master of Science in Control Engineering

Faculty of Engineering
Thunder Bay, Ontario
P7B 5E1

April, 2009

Abstract

Compared to wheeled robots, biped robots have their advantages. Biped robots have better mobility. Biped robots can walk in human environments, such as rough terrain and the place that contains obstacles, and can also climb stairs or ladders. A biped robot has "discrete" footholds; therefore, it does not require a continuous path of support as wheeled robots. Moreover, biped robots can turn around in a small area. However, it is more difficult to balance and control the biped robot, especially on the rough or slope surface, compared to wheeled robots.

In this thesis, a 10 degree-of-freedom (DOF) biped robot is built. There are 2 DOFs for each ankle joint, 1 DOF for each knee joint and 2 DOFs for each hip-leg joint. The prototype of the biped robot is designed by using AutoCAD. The biped robot is made with aluminum. All the joints are actuated by gear-head DC motors. Limit switches are installed on the joints to prevent links from overturning, which may damage the gears or other mechanical parts. Potentiometers are used for the position feedback. Two eZdspF2812 development boards based on the Texas Instruments TMS320F2812 Digital Signal Processor (DSP) are used to control the biped robot. The electrical circuit boards are designed, fabricated and assembled for the biped robot. Proportional-Derivative (PD) controllers with gravity compensation are used for joint trajectory tracking control. The controllers are applied to each joint individually.

For walking pattern planning, a whole walking cycle starting from the home position is divided into the following phases: shift weight toward the left leg, swing the right leg forward, shift weight back, keep the current position, shift weight toward the right leg, swing the left leg forward, shift weight back, keep the current position. For the swing phases, three points are selected for both ankle and hip joint trajectories, which are used to generate smooth trajectories for the ankle joints and hip joint by the third-order spline interpolation method. Based on the smooth trajectories for the ankle joints and hip joint, the desired trajectories for joint angles are calculated by using inverse kinematics. The zero moment point (ZMP) for the biped robot is also calculated. The ZMP must always be inside the contact area between the feet and the ground to make sure that the robot will not fall down during the walking.

Simulation results show that the desired trajectories guarantee that the ZMP of the biped robot is always within the contact area between the feet and the ground, which means that the biped robot is able to walk stably if the desired trajectories are followed. The experiment results show that the robot is able to walk on the flat surface by following the planned trajectories with the approximate speed of 8cm/min.

Acknowledgements

I am glad to express my gratitude to the following people for their contributions to help me complete this thesis.

I am deeply indebted to my supervisor, Dr. Xiaoping Liu, for his supervision. He has offered me valuable ideas, suggestions and criticisms. I thank him for generously sharing his knowledge and time. His patience and kindness are greatly appreciated.

I would like to thank Dr. Abdelhamid Tayebi for his guidance in robotics and his great lectures in my academic study.

I would also like to thank Mr. Manfred Klein, Mr. Bruce Misner, Mr. Warren Paju and Mr. Kailash Bhatia, who gave me a lot of helps to build the robot prototype.

I want to thank my former colleague, Mr. Wenguang Li, for his help, support, interesting and valuable hints for my research.

Finally, I would like to give the special thanks to my parents for their love, support and understanding throughout my graduate study.

Contents

List of Figures

List of Tables

List of Acronym

ADC	analog-to-digital converter
CoG	center of gravity
CoP	center of pressure
DS	double-support
DSP	digital signal processor
D-H	Denavit-Hartenberg
DOF	degree-of-freedom
FS	force sensor
GPIO	General Purpose I/O
IC	integrated circuit
PCB	printed circuit board
PWM	pulse-width modulation
PD	proportional -derivative
SCI	serial communications interface
SPI	serial peripheral interface
SS	single-support
ZMP	zero moment point

Chapter 1

Introduction

1.1 Literature Review

A robot is a machine that performs certain tasks automatically. Robots can be classified into stationary robots, such as manipulators used in industries, and mobile robots, such as autonomous underwater vehicles, unmanned aerial vehicles, wheeled robots, legged robots, etc. Stationary robots are fixed in one place and tethered to a computer, so they cannot move from place to place while mobile robots are not fixed to one physical location and have the capability to move around in their environment. Legged robots are one kind of mobile robots. Biped robots, also called humanoid robots, are legged robots with human-like appearance. In general, biped robots have a torso with a head, two arms, and two legs. Some biped robots may also have a face with eyes and mouth. Biped robots are designed to function like human, allowing interaction with made-for-human tools or environments. Biped robots are able to perform many tasks that most wheeled robots cannot, such as climbing stairs or moving over rough terrain. However, compared wheeled robots, biped robots are more complex in structure and more difficult to control. Building a biped robot is not as simple as building a wheeled robot. Many issues, such as balance, proper gait and complexity, to name a few, need to be dealt with when designing a biped robot.

Much of the current interest in legged robots comes from the appeal of machines that can operate in rough terrain, or environments with discontinuous supports, such as

the rungs of ladder. In particular, the study of biped robots has been motivated by diverse sociological and commercial interests, ranging from the restoration of motion in the disabled, such as leg prosthesis, to the desire to replace humans in hazardous environments, such as nuclear power plants. Biped robots could also find their possible applications in industries, hospitals, households, space explorations, to name a few. Therefore, biped robots have attracted a lot of attention from doctors, engineers, etc. The intensive study of biped robots first began in Japan at the end of the '60s [1]. WAP-1 is known as the first biped robot, which was designed and developed at Waseda University, Tokyo, Japan, in 1969. WAP-1 was actuated with the artificial muscles made of rubber. Planar biped locomotion was realized by teaching-playback control of its artificial muscles. In 1971, WAP-3 was constructed with DC motors as actuators, which was able to move its center of gravity on the frontal plane. WAP-3, considered as the first biped robot to be able to perform three-dimensional automatic walking, can walk on a flat surface, climb a slope or a staircase and make a turn. In 1984, WL-10R, the first robot with dynamic walking, was developed at Waseda University. The torque sensors are attached to the ankle and hip joints to allow flexible control of a change-over phase (transition-phase from standing on one leg to standing on the other leg) using torque feedback. In 1986, the Honda Motor Company, Japan, began their research on biped robots [2]. Eleven biped prototypes have been developed by Honda from 1989 to present. The latest prototype of Honda biped robot, named as ASIMO, has 34 degree-of-freedom (DOF), which is 1.3m high and 54kg in weight. ASIMO is conceived to function in an actual human living environment. It is able to move freely within the human living environment, all with a people-friendly design. Some humanoid robot prototypes are

developed in other countries. In 2005, the Beijing University of Science and Engineering, China, revealed the robot BHR-1 to the world [3]. The BHR-1 is 1.58m tall, weighs 76kg and has 32 DOF. This robot is capable of talking to people and performing the ancient arts of swordplay and shadow boxing (Tai Chi). The Korea Advanced Institute of Science and Technology (KAIST) developed the humanoid robot KHR-3 in 2005 [4]. The KAIST's research on biped robots began in 2000 and the fist prototype, KHR-1, was developed without a head or arms in 2003, followed by KHR-2 in 2004. The KHR-3, 1.2m tall and 55kg in weight, has voice recognition and synthesis facilities as well as a sophisticated vision system. The 41-DOF biped robot, KHR-3, is equipped with force-torque sensors, inertia sensors, servo drivers and has the real-time distributed control architecture.

Similar to industrial manipulators, biped robots are composed of sensors, actuators, and controllers, which are connected to each other with mechanical parts, such as links, shafts, bearings, etc., and electric devices, such as amplifiers, signal conditioning circuits, computers, and so on. Sensors commonly used on biped robots include position sensors, torque and force sensors, speed sensors, tilt sensors, etc. Actuators could be either electric, pneumatic, or hydraulic. Most of biped robots are driven by electric actuators, such as DC motors.

Unlike stationary robots and wheeled robots, it is important to maintain dynamic balance during the walk. The solution to this problem relies on a major concept, the Zero Moment Point (ZMP), which was first introduced by Vukobratovic [5] in 1973. ZMP is defined as the point on the ground about which the sum of all the moments of the active forces equals zero. ZMP is defined mathematically in [6], which can be determined

experimentally by measuring the ground/feet contact forces, see, for example, [7]. It is known from the viewpoint of mechanics that if the ZMP is within the contact area between the feet and the ground, the biped robot is able to keep dynamic balance during the walk. ZMP is a very important concept in the motion planning for biped robots. Since biped robots behave like an inverted pendulum during the walk, the dynamic balance of their whole body has to be maintained by properly planning the motion. In 1984, the first practical demonstration of ZMP took place on the first dynamically balanced robot WL-10R of the robotic family WABOT in laboratory of Ichiro Kato at Waseda University in Japan [8]. Since then, ZMP has been extensively used for walking pattern planning of biped robots.

Walking pattern planning is very important in biped robot research. There are two main methods for walking pattern planning. One of them is to design a desired ZMP trajectory first and then generate joint trajectories to achieve the desired ZMP trajectory. The other method is to design the desired joint trajectories first and then to check if ZMP maintains within the contact area between the feet and the ground. Both methods have been used in walking pattern planning, see, for example, [9] and [10] for the application of the first method and [11] and [12] for the second method. In [9], the dynamics of a biped robot is modeled as a running cart on a table, which gives a convenient representation to treat ZMP. After reviewing conventional methods of ZMP-based pattern generation, a ZMP tracking servo controller is designed by adopting the preview control that uses the future ZMP reference. The preview controller can be used to compensate the ZMP error caused by the difference between the simple cart-table model and the precise multi-body model. The drawback of the design in [9] is that the walking lacks naturalness

because the ZMP is kept fixed in the middle of the sole of the support foot during the stepping motion. [10] points out that the ZMP in human walking does not stay fixed, but moves forward under the support foot. To achieve naturalness in the walk, the human-like ZMP reference trajectories are designed by using Fourier series approximation techniques. In [11], both ankle movement and hip movement are first modeled by some parameters, which can be adjusted to adapt to different ground conditions. After that, the third-order spline interpolation method is used to determine the ankle and hip trajectories. Then joint trajectories are calculated by inverse kinematics. Finally, ZMP is computed to check the dynamic balance of the biped robot. [12] presents a trajectory planning method based on the third-order spline interpolation, which aims to achieve a smooth motion by reducing the instant velocity change, which occurs at the time of collision between the swing leg with the ground. The ZMP is calculated based on the pre-determined trajectories in both [11] and [12] to ensure that the biped robot is able to walk. By following the desired trajectories, the biped robot is able to perform static walking. In static walking, the projection of Center of Gravity (CoG) on the horizontal plane must be within the support polygon [13]. The support polygon is the polygon that minimally encloses the soles on the horizontal plate. On the other hand, in dynamic walking, the projection of CoG on the horizontal plane can be outside of the support polygon.

In order to make a biped robot walk stably subject to external disturbances or in various environments, such as rough terrain, up and down slopes, up and down stairs, the biped robot has to be able to perform dynamic walking. Research on dynamic balance control concentrates on ZMP compensation. In [13] [14], force sensors are installed at the four corners of each foot. The real-time ZMP is calculated based on the measurements

from force sensors. Then the compensating torque is computed and injected into the ankle-joint of the foot of the robot to improve the dynamic stability. The effectiveness of ZMP compensation was verified on the humanoid robots, Kondo KHR-1 [13] and MANUS-I [14]. With the compensation technique, KHR-1 is able to stand firmly on the ground even when a big disturbance force, a 700 g pendulum, is applied. MANUS-I can carry an additional weight of 390 g (17% of the body weight) while walking. In addition, it can walk up a 10 degree slope and down a 3 degree slope. In order to control the balance of the biped robot in unknown environments, [15] proposes a control method to maintain the biped balance by adjusting the ankle joint against an unknown periodic external force with a known period. The period of the external force is assumed to be known, because the external force can be expanded to a Fourier series. The balance control in unknown environments is achieved by using feedback of ground reaction forces and a learning rule of the torque profile by estimating the exerted external forces.

Biped robot walking contains two phases, double-support phase and single-support phase. During the double-support phase, both feet are in contact with the ground. During the single-support phase, while one foot is stationary on the ground, the other foot swings from the rear to the front [11]. A biped robot in single-support phase can be represented by a simple inverted pendulum model with a compliant joint. With this model, [16] introduces the balance control for single-support phase. The damping controller that increases system damping and reduces oscillation is proposed as a balance controller. A landing orientation controller at the ankle joints is used to achieve fast and stable landing. A landing position controller is implemented in order to modify the prescribed trajectory of the swing foot and to reduce the landing impact during unexpected landing. For the

double-support phase, [17] developed an advanced control system for a 12-DOF biped robot in the double-support phase. A constrained dynamic model for the robot is formulated and a reduced order model is derived for the double-support phase. Control strategies based on feed forward compensation and linear state feedback are designed for tracking specified joint trajectories.

In summary, intensive research has been done related to biped robots and many biped prototypes have been built for the experimental study on walking robots. For details, see [18] and [19] for recent reviews on biped robots.

The objective of this robot research is to design, build and control a 10 DOF biped robot. The strategies to achieve this objective includes building a reliable robot structure, performing walking pattern planning so that the ZMP is within the contact area between the feet and ground, and designing PD controllers.

1.2 Thesis Outline

The outline and brief description of this thesis is as follows:

Chapter 2 gives the forward kinematics and inverse kinematics analysis for the 10 DOF biped robot built for this thesis. The Denavit-Hartenberg (D-H) model of single support phase with right leg support is described. The link parameters for D-H representation are provided. With D-H model and link parameters, both forward kinematics problem and inverse kinematics problem are solved.

A procedure to generate a smooth walking pattern for the 10 DOF biped robot is given in Chapter 3. Third-order spline interpolation method is used for ankles and hip trajectories planning. The joint variables are calculated by inverse kinematics and third-order spline interpolation method. The ZMP for the biped robot is analyzed for dynamic balance.

The mechanical structure design, electrical circuit design and printed circuit board (PCB) design are discussed in Chapter 4. This Chapter also explains the method that converts the desired trajectories in degree to voltage.

Chapter 5 introduces control program for the biped robot system. The controller with PD control plus gravity compensation is also described. All controller parameters that are determined by trial- and-error method are listed in this Chapter.

The experiment results are provided in Chapter 6. The home position adjustment for the 10 DOF biped robot is also introduced in this Chapter.

Chapter 7 summarizes this thesis and discusses future work.

Chapter 2

Forward Kinematics and Inverse Kinematics

Robot kinematics is the study of the motion of robots, which includes both forward kinematics and inverse kinematics. The objective of forward kinematics is to calculate the position of any point on the robot given the link parameters, such as link length and joint angles. However, in inverse kinematics, joint angles are calculated by given the position of the point on the robot. This Chapter is devoted to solving both forward kinematics and inverse kinematics problems.

2.1 Forward Kinematics

To solve the forward kinematics problem or inverse kinematics problem, appropriate reference frames have to be established first. A commonly used convention for selecting reference frames in robotic applications is the Denavit-Hartenberg (D-H) convention. Fig. 2-1 shows the scenario that the right foot is on the floor while the left foot is in the air. It is single-support phase with right leg support. In this case, the left foot is considered as the end-effector.

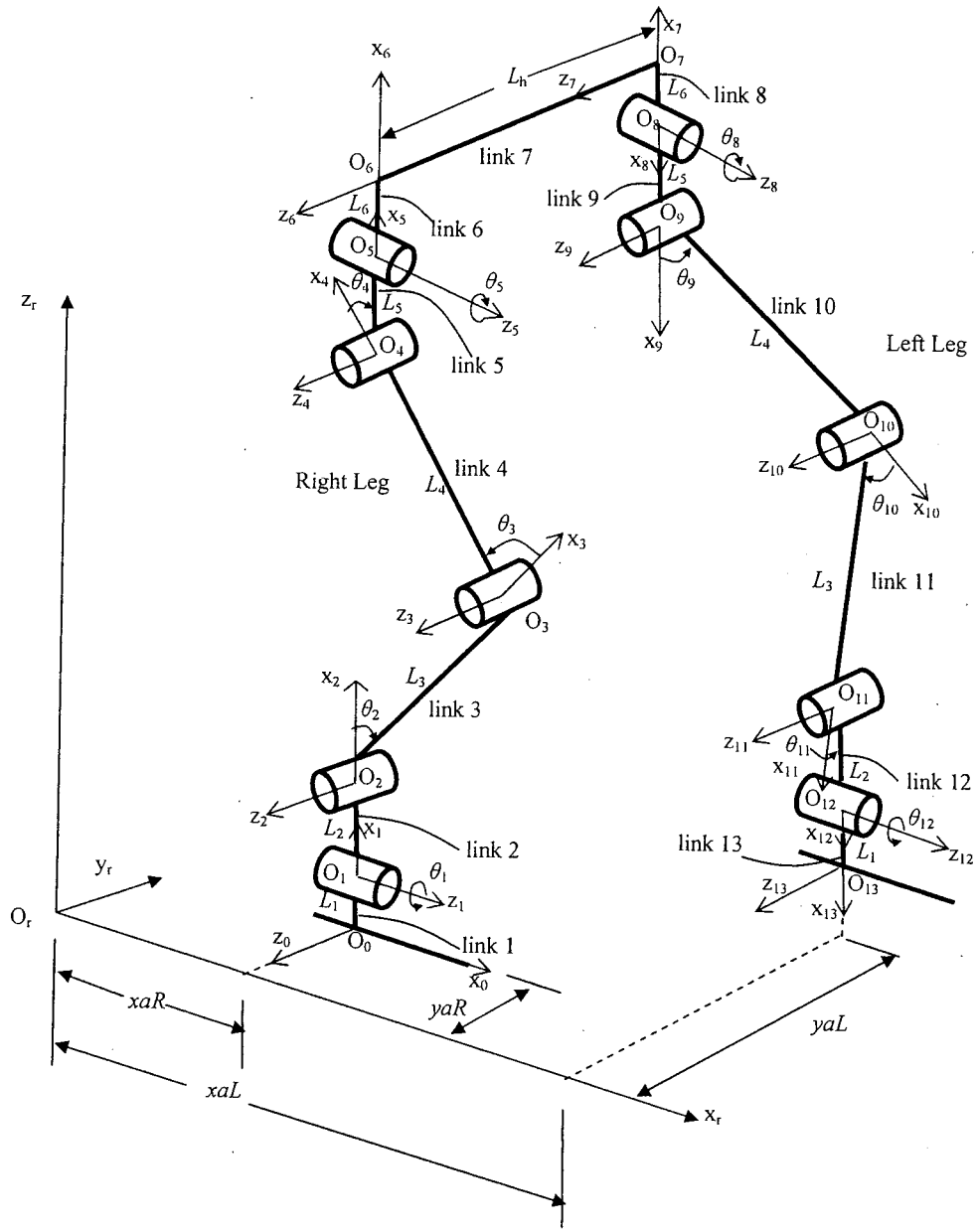

Fig.2-1 D-H representation for single-support phase with right leg support

For the purpose of solving the kinematics problems, the scenarios shown as Fig. 2-1 can be modeled by a system with 13 links to indicate the location of the biped robot with respect to frame 0. There are 14 frames for the robot model, which is marked as 0 to 13. The 13 links are numbered from 1 to 13. The joint O_i is the point in space where links i and i+1 are connected. The i-th joint variable is the rotating angle denoted by θ_i. From Fig. 2-1, the joint variables in this 10 DOF biped robot are θ_1, θ_2, θ_3, θ_4, θ_5, θ_8, θ_9, θ_{10}, θ_{11} and θ_{12}, which are the rotating angle for joint O_1, O_2, O_3, O_4, O_5, O_8, O_9, O_{10}, O_{11} and O_{12}. There are no joint variables for the rest of the joints. The joint variables are indicated in Table 2-1.

Table 2-1 List of Joint Variables

			Joint	Joint Variable
Hip	Left	Pitch	O_9	θ_9
		Roll	O_8	θ_8
	Right	Pitch	O_4	θ_4
		Roll	O_5	θ_5
Knee	Left	Pitch	O_{10}	θ_{10}
	Right	Pitch	O_3	θ_3
Ankle	Left	Pitch	O_{11}	θ_{11}
		Roll	O_{12}	θ_{12}
	Right	Pitch	O_2	θ_2
		Roll	O_1	θ_1

From the D-H model of the 10 DOF biped robot, frame i is rigidly attached to link i, which means that, whatever motion the biped robot executes, the coordinates of each point on link i are constant when expressed in frame i. Table 2-2 list the D-H parameters for the models in Fig. 2-1.

Table 2-2: D-H Parameters for Single-Support Phase with Right Leg Support

Link	a_i	d_i	α_i	θ_i	A_i
1	L_1	0	90°	90°	A_1
2	L_2	0	-90°	θ_1	A_2
3	L_3	0	0°	θ_2	A_3
4	L_4	0	0°	θ_3	A_4
5	L_5	0	90°	θ_4	A_5
6	L_6	0	-90°	θ_5	A_6
7	0	$-L_h$	0°	0°	A_7
8	L_6	0	-90°	180°	A_8
9	L_5	0	90°	θ_8	A_9
10	L_4	0	0°	θ_9	A_{10}
11	L_3	0	0°	θ_{10}	A_{11}
12	L_2	0	-90°	θ_{11}	A_{12}
13	L_1	0	90°	θ_{12}	A_{13}

The homogeneous matrix that transforms the coordinates of a point from frame i to frame i-1 is denoted as A_i. Each homogeneous transformation A_i can be represented as a product of four "basic" transformations, that is,

$$
\begin{aligned}
A_i &= Rot_{z,\theta_i} Trans_{z,d_i} Trans_{x,a_i} Rot_{x,\alpha_i} \\
&= \begin{bmatrix} \cos\theta_i & -\sin\theta_i & 0 & 0 \\ \sin\theta_i & \cos\theta_i & 0 & 0 \\ 0 & 0 & 1 & 0 \\ 0 & 0 & 0 & 1 \end{bmatrix} \begin{bmatrix} 1 & 0 & 0 & 0 \\ 0 & 1 & 0 & 0 \\ 0 & 0 & 1 & d_i \\ 0 & 0 & 0 & 1 \end{bmatrix} \begin{bmatrix} 1 & 0 & 0 & a_i \\ 0 & 1 & 0 & 0 \\ 0 & 0 & 1 & 0 \\ 0 & 0 & 0 & 1 \end{bmatrix} \begin{bmatrix} 1 & 0 & 0 & 0 \\ 0 & \cos\alpha_i & -\sin\alpha_i & 0 \\ 0 & \sin\alpha_i & \cos\alpha_i & 0 \\ 0 & 0 & 0 & 1 \end{bmatrix} \\
&= \begin{bmatrix} \cos\theta_i & -\sin\theta_i\cos\alpha_i & \sin\theta_i\sin\alpha_i & a_i\cos\theta_i \\ \sin\theta_i & \cos\theta_i\cos\alpha_i & -\cos\theta_i\sin\alpha_i & a_i\sin\theta_i \\ 0 & \sin\alpha_i & \cos\alpha_i & d_i \\ 0 & 0 & 0 & 1 \end{bmatrix}
\end{aligned}
\qquad (2\text{-}1)
$$

where the four quantities a_i, d_i, α_i and θ_i are parameters of link i and joint i. a_i is called the length, which is the distance along x_i from O_i to the intersection of x_i and z_{i-1} axes. d_i is called the offset, which is the distance along z_{i-1} from O_{i-1} to the intersection of x_i and z_{i-1} axes. α_i is called the twist, which is the angle between z_{i-1} and z_i measured about x_i. θ_i is called the angle, which is the angle between x_{i-1} and x_i measured about z_{i-1}.

The homogeneous transformation matrix that transforms the coordinates of a point from frame j to frame i, named as the transformation matrix ${}_i^jT$, is calculated by:

$${}_i^jT = A_{i+1}A_{i+2}...A_{j-1}A_j, \quad if \quad i < j \tag{2-2}$$

Note that ${}_i^jT$ is a four by four matrix and the x, y and z coordinates of the origin of frame j, referred to the frame i, can be read from the first three elements in the fourth column of transformation matrix ${}_i^jT$.

For this 10 DOF biped robot, the transformation matrix that transforms the coordinates of a point from frame 0 to the reference frame (frame r with the origin O_r) need to be obtained first. The transformation matrix from frame 0 to frame r is determined as

$${}_r^0T = Rot_{x,\frac{\pi}{2}}Trans_{x,x_{aR}}Trans_{z,y_{aR}}$$

$$= \begin{bmatrix} 1 & 0 & 0 & 0 \\ 0 & 0 & -1 & 0 \\ 0 & 1 & 0 & 0 \\ 0 & 0 & 0 & 1 \end{bmatrix} \begin{bmatrix} 1 & 0 & 0 & x_{aR} \\ 0 & 1 & 0 & 0 \\ 0 & 0 & 1 & 0 \\ 0 & 0 & 0 & 1 \end{bmatrix} \begin{bmatrix} 1 & 0 & 0 & 0 \\ 0 & 1 & 0 & 0 \\ 0 & 0 & 1 & -y_{aR} \\ 0 & 0 & 0 & 1 \end{bmatrix} = \begin{bmatrix} 1 & 0 & 0 & x_{aR} \\ 0 & 0 & -1 & y_{aR} \\ 0 & 1 & 0 & 0 \\ 0 & 0 & 0 & 1 \end{bmatrix} \tag{2-3}$$

Then the forward kinematics for the single-support phase with right leg support can be performed as

$$\begin{cases} {}_r^1T = {}_r^0TA_1 \\ {}_r^2T = {}_r^1TA_2 \\ {}_r^3T = {}_r^2TA_3 \\ {}_r^4T = {}_r^3TA_4 \\ {}_r^5T = {}_r^4TA_5 \\ {}_r^6T = {}_r^5TA_6 \\ {}_r^7T = {}_r^6TA_7 \\ {}_r^8T = {}_r^7TA_8 \\ {}_r^9T = {}_r^8TA_9 \\ {}_r^{10}T = {}_r^9TA_{10} \\ {}_r^{11}T = {}_r^{10}TA_{11} \\ {}_r^{12}T = {}_r^{11}TA_{12} \\ {}_r^{13}T = {}_r^{12}TA_{13} \end{cases} \tag{2-4}$$

For the forward kinematics for the single-support phase with left leg support, the transformation matrices can be calculated as

$$\begin{cases} {}^{12}_{r}T = {}^{13}_{r}T\left(A_{13}\right)^{-1} \\ {}^{11}_{r}T = {}^{12}_{r}T\left(A_{12}\right)^{-1} \\ {}^{10}_{r}T = {}^{11}_{r}T\left(A_{11}\right)^{-1} \\ {}^{9}_{r}T = {}^{10}_{r}T\left(A_{10}\right)^{-1} \\ {}^{8}_{r}T = {}^{9}_{r}T\left(A_{9}\right)^{-1} \\ {}^{7}_{r}T = {}^{8}_{r}T\left(A_{8}\right)^{-1} \\ {}^{6}_{r}T = {}^{7}_{r}T\left(A_{7}\right)^{-1} \\ {}^{5}_{r}T = {}^{6}_{r}T\left(A_{6}\right)^{-1} \\ {}^{4}_{r}T = {}^{5}_{r}T\left(A_{5}\right)^{-1} \\ {}^{3}_{r}T = {}^{4}_{r}T\left(A_{4}\right)^{-1} \\ {}^{2}_{r}T = {}^{3}_{r}T\left(A_{3}\right)^{-1} \\ {}^{1}_{r}T = {}^{2}_{r}T\left(A_{2}\right)^{-1} \\ {}^{0}_{r}T = {}^{1}_{r}T\left(A_{1}\right)^{-1} \end{cases} \tag{2-5}$$

where $(A_i)^{-1}$ is the inverse matrix of A_i defined in Equation (2-1), and ${}^{13}_{r}T$ can be determined as

$$\begin{aligned} {}^{13}_{r}T &= Rot_{x,\frac{\pi}{2}} Rot_{z,-\frac{\pi}{2}} Trans_{y,x_{aL}} Trans_{z,-y_{aL}} \\ &= \begin{bmatrix} 1 & 0 & 0 & 0 \\ 0 & 0 & -1 & 0 \\ 0 & 1 & 0 & 0 \\ 0 & 0 & 0 & 1 \end{bmatrix} \begin{bmatrix} 0 & 1 & 0 & 0 \\ -1 & 0 & 0 & 0 \\ 0 & 0 & 1 & 0 \\ 0 & 0 & 0 & 1 \end{bmatrix} \begin{bmatrix} 1 & 0 & 0 & 0 \\ 0 & 1 & 0 & x_{aL} \\ 0 & 0 & 1 & 0 \\ 0 & 0 & 0 & 1 \end{bmatrix} \begin{bmatrix} 1 & 0 & 0 & 0 \\ 0 & 1 & 0 & 0 \\ 0 & 0 & 1 & -y_{aL} \\ 0 & 0 & 0 & 1 \end{bmatrix} = \begin{bmatrix} 0 & 1 & 0 & x_{aL} \\ 0 & 0 & -1 & y_{aL} \\ -1 & 0 & 0 & 0 \\ 0 & 0 & 0 & 1 \end{bmatrix} \end{aligned} \tag{2-6}$$

For the case of the single-support phase with right leg support, the matrices A_i and ${}^{j}_{i}T$ are calculated in Appendix A, with the assumption that θ_1, θ_5, θ_8 and θ_{12} are zero. Furthermore, the coordinates of the hips and ankles are also derived in Appendix A, which will be used for solving the inverse kinematics problem.

2.2 Inverse Kinematics

Given a desired position and orientation for the end-effector of the robot, a set of joint variables that achieve the desired position and orientation can be determined by inverse kinematics.

The inverse kinematics for the 10 DOF biped robot is very complicated. To simplify the calculation, the inverse kinematics is performed with the following assumptions:

A2.2.1 The joint variables θ_1, θ_5, θ_8 and θ_{12} are all set to zero.

A2.2.2 The position and orientation of the ankle joints and hip joints are given.

With these assumptions, the inverse kinematics problem is simplified to calculate the joint variables θ_2, θ_3, θ_4, θ_9, θ_{10} and θ_{11}. In what follows, these angles will be determined.

2.2.1 Calculate θ_2, θ_3 and θ_4

The x, y and z coordinates for the right ankle joint O_2 and right hip joint O_4 with respect to the reference frame r are determined, see Appendix A, as follows:

$$\text{Right Ankle: } \begin{cases} x_{O_2} = x_{aR} \\ y_{O_2} = y_{aR} \\ z_{O_2} = l_{an} \end{cases} \tag{2-7}$$

$$\text{Right Hip: } \begin{cases} x_{O_4} = x_{aR} - L_3 \sin\theta_2 - L_4 \sin(\theta_2 + \theta_3) \\ y_{O_4} = y_{aR} \\ z_{O_4} = l_{an} + L_3 \cos\theta_2 + L_4 \cos(\theta_2 + \theta_3) \end{cases} \tag{2-8}$$

where $l_{an} = L_1 + L_2$.

It follows from Equations (2-7) and (2-8) that:

$$\begin{cases} x_{O_4} - x_{O_2} = -(L_3 + L_4 \cos\theta_3)\sin\theta_2 - L_4 \sin\theta_3 \cos\theta_2 \\ z_{O_4} - z_{O_2} = (L_3 + L_4 \cos\theta_3)\cos\theta_2 - L_4 \sin\theta_3 \sin\theta_2 \end{cases} \tag{2-9}$$

By calculating $\left(x_{O_4}-x_{O_2}\right)^2+\left(z_{O_4}-z_{O_2}\right)^2$, $\cos\theta_3$ can be determined as

$$\cos\theta_3=\frac{\left(x_{O_4}-x_{O_2}\right)^2+\left(z_{O_4}-z_{O_2}\right)^2-L_3^2-L_4^2}{2L_3L_4} \tag{2-10}$$

From Fig. 2-1 and Table 2-2, the range for θ_3 is $0\le\theta_3<\pi$, so

$$\sin\theta_3=\sqrt{1-\cos^2\theta_3} \tag{2-11}$$

Finally, θ_3 can be calculated as:

$$\theta_3=\tan^{-1}\left(\frac{\sin\theta_3}{\cos\theta_3}\right) \tag{2-12}$$

$\cos\theta_2$ and $\sin\theta_2$ can be solved from (2-9) as

$$\begin{cases}\sin\theta_2=-\dfrac{\left(x_{O_4}-x_{O_2}\right)(L_3+L_4\cos\theta_3)+\left(z_{O_4}-z_{O_2}\right)L_4\sin\theta_3}{L_3^2+L_4^2+2L_3L_4\cos\theta_3}\\ \cos\theta_2=\dfrac{\left(z_{O_4}-z_{O_2}\right)(L_3+L_4\cos\theta_3)-\left(x_{O_4}-x_{O_2}\right)L_4\sin\theta_3}{L_3^2+L_4^2+2L_3L_4\cos\theta_3}\end{cases} \tag{2-13}$$

Then, θ_2 can be determined by

$$\theta_2=\tan^{-1}\left(\frac{\sin\theta_2}{\cos\theta_2}\right) \tag{2-14}$$

Fig. 2-2 shows the geometric relation among joint variables θ_2, θ_3 and θ_4. According to Fig. 2-1 and Table 2-2, θ_2 and θ_4 are negative angle and θ_3 is positive. Therefore, θ_4 can be determined by

$$\theta_4=-\theta_2-\theta_3 \tag{2-15}$$

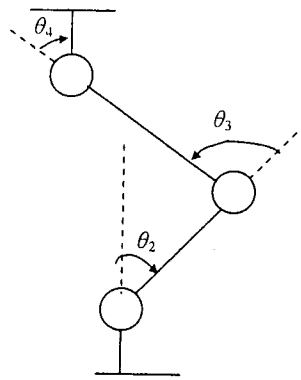

Fig. 2-2 The geometric relation among θ_2, θ_3 and θ_4

2.2.2 Calculate θ_9, θ_{10} and θ_{11}

The x, y and z coordinates for the right ankle joint O_{11} and right hip joint O_9 with respect to the reference frame r are determined as follows, see Appendix A:

Left Ankle:

$$\begin{cases} x_{O_{11}} = x_{aR} - L_3\sin\theta_2 - L_4\sin(\theta_2+\theta_3) + L_4\sin(\theta_2+\theta_3+\theta_4+\theta_9) \\ \qquad +L_3\sin(\theta_2+\theta_3+\theta_4+\theta_9+\theta_{10}) \\ y_{O_{11}} = y_{aR} + L_h \\ z_{O_{11}} = L_1 + L_2 + L_3\cos\theta_2 + L_4\cos(\theta_2+\theta_3) - L_4\cos(\theta_2+\theta_3+\theta_4+\theta_9) \\ \qquad -L_3\cos(\theta_2+\theta_3+\theta_4+\theta_9+\theta_{10}) \end{cases} \quad (2\text{-}16)$$

Left Hip:

$$\begin{cases} x_{O_9} = x_{aR} - L_3\sin\theta_2 - L_4\sin(\theta_2+\theta_3) \\ y_{O_9} = y_{aR} + L_h \\ z_{O_9} = L_1 + L_2 + L_3\cos\theta_2 + L_4\cos(\theta_2+\theta_3) \end{cases} \quad (2\text{-}17)$$

It is easily seen that:

$$\begin{cases} x_{O_9} - x_{O_{11}} = -(L_4 + L_3\cos\theta_{10})\sin(\theta_2+\theta_3+\theta_4+\theta_9) - L_3\sin\theta_{10}\cos(\theta_2+\theta_3+\theta_4+\theta_9) \\ z_{O_9} - z_{O_{11}} = (L_4 + L_3\cos\theta_{10})\cos(\theta_2+\theta_3+\theta_4+\theta_9) - L_3\sin\theta_{10}\sin(\theta_2+\theta_3+\theta_4+\theta_9) \end{cases} \quad (2\text{-}18)$$

As a result,

$$\left(x_{O_9} - x_{O_{11}}\right)^2 + \left(z_{O_9} - z_{O_{11}}\right)^2 = L_3^2 + L_4^2 + 2L_3L_4\cos\theta_{10} \tag{2-19}$$

$$\text{Therefore, } \theta_{10} = \tan^{-1}\left(\frac{\sin\theta_{10}}{\cos\theta_{10}}\right), \qquad (-\pi < \theta_{10} \le 0) \tag{2-20}$$

$$\text{where, } \begin{cases} \cos\theta_{10} = \dfrac{\left(x_{O_9} - x_{O_{11}}\right)^2 + \left(z_{O_9} - z_{O_{11}}\right)^2 - L_3^2 - L_4^2}{2L_3L_4} \\ \sin\theta_{10} = -\sqrt{1-\cos^2\theta_{10}} \end{cases}$$

From Equation (2-18), $\theta_2 + \theta_3 + \theta_4 + \theta_9$ can be solved as

$$\begin{cases} \sin(\theta_2 + \theta_3 + \theta_4 + \theta_9) = -\dfrac{\left(x_{O_9} - x_{O_{11}}\right)\left(L_4 + L_3\cos\theta_{10}\right) + \left(z_{O_9} - z_{O_{11}}\right)L_3\sin\theta_{10}}{L_3^2 + L_4^2 + 2L_3L_4\cos\theta_{10}} \\ \cos(\theta_2 + \theta_3 + \theta_4 + \theta_9) = \dfrac{\left(z_{O_9} - z_{O_{11}}\right)\left(L_4 + L_3\cos\theta_{10}\right) - \left(x_{O_9} - x_{O_{11}}\right)L_3\sin\theta_{10}}{L_3^2 + L_4^2 + 2L_3L_4\cos\theta_{10}} \end{cases} \tag{2-21}$$

which means that

$$\theta_9 = -\theta_2 - \theta_3 - \theta_4 + \tan^{-1}\left(\frac{\sin(\theta_2 + \theta_3 + \theta_4 + \theta_9)}{\cos(\theta_2 + \theta_3 + \theta_4 + \theta_9)}\right) \tag{2-22}$$

Fig. 2-3 displays the geometric relation among joint variables θ_9, θ_{10} and θ_{11}. According to Fig. 2-1 and Table 2-2, θ_9 and θ_{11} are positive angle and θ_{10} is negative. Therefore, θ_{11} can be solved by

$$\theta_{11} = -\theta_9 - \theta_{10} \tag{2-23}$$

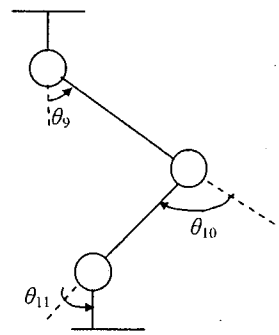

Fig. 2-3 The geometric relation among θ_9, θ_{10} and θ_{11}

Chapter 3

Walking Trajectory Planning

For a biped robot to be able to walk stably, the desired trajectory for each joint has to be properly designed, otherwise the biped robot would either tip over, or fall back, or turn over. The existing research results show that the biped robot can walk stably if the ZMP is maintained within the contact area between the feet and the ground. Therefore, the objective of walking trajectory planning is to design trajectories for all the robot joints so that the ZMP is always within the contact area between the feet and the ground.

In the literature, there are two main methods for walking pattern planning. One of them is to design a desired ZMP trajectory first and then generate joint trajectories to achieve the desired ZMP trajectory. The other method is to design the desired joint trajectories first and then test if the desired joint trajectories result in a stable walking pattern by calculating the ZMP. In this thesis, the second method is used.

Similar to human walking, biped robot walking is periodic motion. A complete walking cycle is composed of two phases: a double-support phase and a single-support phase. The double-support phase is defined as the period during which both feet are in contact with the ground, while the single-support phase is referred to as the period during which one foot is stationary on the ground and the other foot swings from the rear to the front. In order to avoid the biped robot from falling over to one side during the single-support phase; the double-support phase is designed so that the weight is shifted to the support leg before lifting the swing leg and back to home position after landing the swing

leg. On the other hand, in order to prevent the biped robot from tipping over or falling back, the single-support phase is designed so that the weight is transferred forward.

To simplify analysis, it is assumed that the feet are always level with the ground, that is, the foot soles are always parallel with the ground; the upper body is always maintained at the upright position, that is, the upper body is always vertical; and the walking cycle starts from the home position. For further understanding the walking pattern, Fig. 3-1 is provided to show the process of one walking cycle.

To facilitate the design of walking trajectories, the walking cycle is further divided into the following movements:

1. Shift the weight towards the left leg and stay there for a short period of time.
2. Lift the right leg, swing it forward and land it on the ground and stay there for a short period of time.
3. Shift the weight back and stay there for a short period of time.
4. Shift the weight towards the right leg and stay there for a short period of time.
5. Lift the left leg, swing it forward and land it on the ground and stay there for a short period of time.
6. Shift the weight back and stay there for a short period of time.

To achieve the walking cycle designed above, the desired trajectories for the joint angles θ_1, θ_2, θ_3, θ_4, θ_5, θ_8, θ_9, θ_{10}, θ_{11} and θ_{12} have to be properly designed. It is difficult to design the trajectories directly for the joint angles θ_2, θ_3, θ_4, θ_9, θ_{10} and θ_{11}. Therefore, for simplification, the ankle and hip trajectories are designed first and then the trajectories for the joint angles θ_2, θ_3, θ_4, θ_9, θ_{10} and θ_{11} are calculated by inverse kinematics. The details for designing the trajectories for the joint angles θ_2, θ_3, θ_4, θ_9, θ_{10} and θ_{11} will be

given in §3.2, §3.3 and §3.4. However, the trajectories for the joint angles θ_1, θ_5, θ_8 and θ_{12} can be easily determined directly, which will be discussed in §3.5. The details on checking the ZMP will be provided in §3.7.

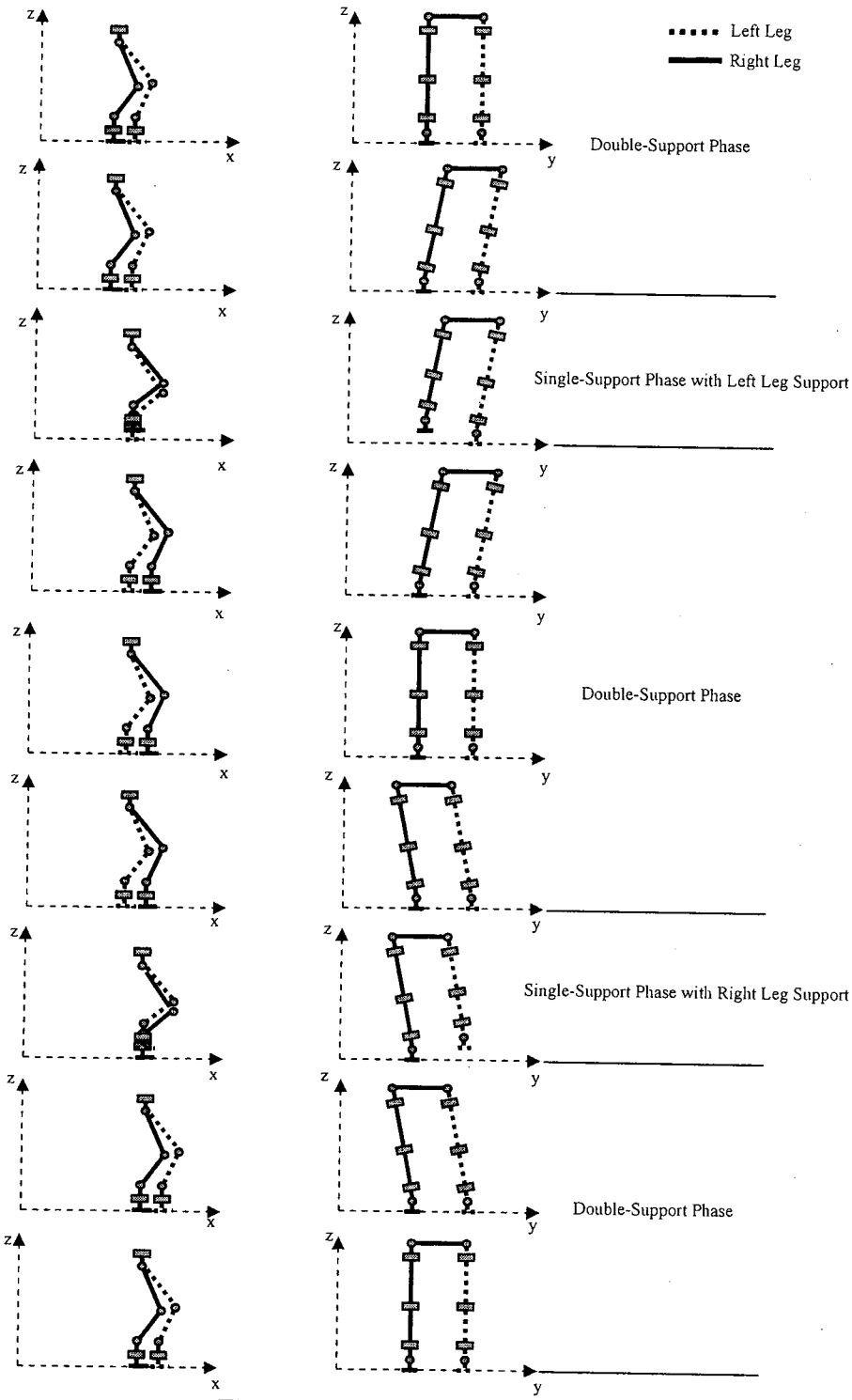

Fig. 3-1 Robot walking cycle

3.1 Third-Order Spline Interpolation

Spline interpolation method can be used to find a polynomial, which goes exactly through the given points. The main advantage of spline interpolation is its stability and calculation simplicity. A set of linear equations, which should be solved to construct splines, are well-conditioned, therefore, the polynomial coefficients are calculated precisely.

The linear spline and second-order spline are the splines, which consist of first-degree polynomials and second-degree polynomials. These two spline interpolation methods provide low precision and the smoothness of the resulting curve are not guaranteed. In this thesis, the third-order spline interpolation method is used. The third-order spline is able to generate the smooth curve for given points, possessing the following properties: the first and second derivatives are continuous and the first derivatives are zero at the start and end points.

For given three points, point 1, point 2 and point 3 with coordinates (t_1, v_{11}), (t_2, v_{12}) and (t_3, v_{13}), a smooth curve $p(t)$ that goes through these points, that is,

$$p(t)=\begin{cases} v_{11} & t=t_1 \\ v_{12} & t=t_2 \\ v_{13} & t=t_3 \end{cases} \tag{3-1}$$

can be determined by the third-order spline interpolation method. This smooth curve is composed of two parts, p_1 and p_2. p_1 is the curve from point 1 to point 2 and p_2 is the curve from point 2 to point 3. p_1 and p_2 are third-order polynomials, which can be expressed as

$$\begin{cases} p_1(t)=c_1+c_2(t-t_1)+c_3(t-t_1)^2+c_4(t-t_1)^3, & t_1 \le t \le t_2 \\ p_2(t)=c_5+c_6(t-t_2)+c_7(t-t_2)^2+c_8(t-t_2)^3, & t_2 \le t \le t_3 \end{cases} \tag{3-2}$$

It is easily seen that

$$\begin{cases} c_1 = p_1(t_1) = v_{11} \\ c_5 = p_2(t_2) = v_{12} \end{cases} \tag{3-3}$$

The following conditions can be used to determine the rest of coefficients.

1. Polynomial p_1 passes through (t_2, v_{12}) and polynomial p_2 passes through (t_3, v_{13}) :

$$\begin{cases} f_1 = c_2 h_1 + c_3 h_1^2 + c_4 h_1^3 \\ f_2 = c_6 h_2 + c_7 h_2^2 + c_8 h_2^3 \end{cases} \tag{3-4}$$

where $h_1 = t_2 - t_1$, $h_2 = t_3 - t_2$, $f_1 = p_1(t_2) - p_1(t_1)$, $f_2 = p_2(t_3) - p_2(t_2)$.

2. First derivatives match at the middle points: $\left.\frac{dp_1(t)}{dt}\right|_{t=t_2} = \left.\frac{dp_2(t)}{dt}\right|_{t=t_2}$, that is,

$$c_2 + 2c_3 h_1 + 3c_4 h_1^2 - c_6 = 0 \tag{3-5}$$

3. Second derivatives match at the middle points: $\left.\frac{dp_1^2(t)}{dt^2}\right|_{t=t_2} = \left.\frac{dp_2^2(t)}{dt^2}\right|_{t=t_2}$, that is,

$$2c_3 + 6c_4 h_1 - 2c_7 = 0 \tag{3-6}$$

4. First derivatives vanish at the end points: $\left.\frac{dp_1(t)}{dt}\right|_{t=t_1} = 0$, $\left.\frac{dp_2(t)}{dt}\right|_{t=t_3} = 0$

$$\begin{cases} c_2 = 0 \\ c_6 + 2c_7 h_2 + 3c_8 h_2^2 = 0 \end{cases} \tag{3-7}$$

The coefficients c_i can be calculated from Equation (3-3) to Equation (3-7) as follows:

$$A\begin{bmatrix} c_1 \\ c_2 \\ c_3 \\ c_4 \\ c_5 \\ c_6 \\ c_7 \\ c_8 \end{bmatrix} = \begin{bmatrix} 0 \\ 0 \\ 0 \\ f_1 \\ 0 \\ f_2 \\ v_{11} \\ v_{12} \end{bmatrix} \tag{3-8}$$

where

$$A = \begin{bmatrix} 0 & 1 & 0 & 0 & 0 & 0 & 0 & 0 \\ 0 & 1 & 2h_1 & 3h_1^2 & 0 & -1 & 0 & 0 \\ 0 & 0 & 2 & 6h_1 & 0 & 0 & -2 & 0 \\ 0 & h_1 & h_1^2 & h_1^3 & 0 & 0 & 0 & 0 \\ 0 & 0 & 0 & 0 & 0 & 1 & 2h_2 & 3h_2^2 \\ 0 & 0 & 0 & 0 & 0 & h_2 & h_2^2 & h_2^3 \\ 1 & 0 & 0 & 0 & 0 & 0 & 0 & 0 \\ 0 & 0 & 0 & 0 & 1 & 0 & 0 & 0 \end{bmatrix}$$

With some simple mathematical operations, the coefficient c_i can be determined as

$$\begin{bmatrix} c_1 \\ c_2 \\ c_3 \\ c_4 \\ c_5 \\ c_6 \\ c_7 \\ c_8 \end{bmatrix} = A^{-1}\begin{bmatrix} 0 \\ 0 \\ 0 \\ f_1 \\ 0 \\ f_2 \\ v_{11} \\ v_{12} \end{bmatrix} = \begin{bmatrix} v_{11} \\ 0 \\ \frac{1.5}{h_1(h_1+h_2)}\left(2f_1 + \frac{f_1h_2}{h_1} - \frac{f_2h_1}{h_2}\right) \\ -\frac{0.5}{h_1^2(h_1+h_2)}\left(4f_1 + \frac{f_1h_2}{h_1} - 3\frac{f_2h_1}{h_2}\right) \\ v_{12} \\ \frac{1.5}{h_1+h_2}\left(\frac{f_1h_2}{h_1} + \frac{f_2h_1}{h_2}\right) \\ -\frac{3}{h_1+h_2}\left(\frac{f_1}{h_1} - \frac{f_2}{h_2}\right) \\ -\frac{0.5}{h_2^2(h_1+h_2)}\left(\frac{f_2h_1}{h_2} - 3\frac{f_1h_2}{h_1} + 4f_2\right) \end{bmatrix} = \begin{bmatrix} v_{11} \\ 0 \\ 1.5c_a\left(2a_{11} + a_{12} - a_{21}\right) \\ -0.5c_a\left(4a_{11} + a_{12} - 3a_{21}\right)/h_1 \\ v_{12} \\ 1.5c\left(a_{12} + a_{21}\right) \\ -3c\left(M_1 - M_2\right) \\ -0.5c_b\left(a_{21} - 3a_{12} + 4a_{22}\right)/h_2 \end{bmatrix} \tag{3-9}$$

$$\text{where} \begin{cases} a_{11} = f_1, & a_{22} = f_2 \\ M_1 = \dfrac{f_1}{h_1}, & M_2 = \dfrac{f_2}{h_2} \\ a_{12} = M_1 h_2, & a_{21} = M_2 h_1 \\ c = \dfrac{1}{h_1 + h_2}, & c_a = \dfrac{c}{h_1}, \quad c_b = \dfrac{c}{h_2} \end{cases}$$

The coefficients (c_1 c_2 .... c_8) determined above will be used in Equation (3-2) to calculate the smooth curve passing through point 1, point 2 and point 3.

3.2 Ankle Trajectories

It can be observed from Fig. 3-1 that the position of the ankle on the leg, which swings forward, is changing with time. For simplicity, it is assumed that the y coordinate of the ankle joint is constant. Then the movement of the ankle can be illustrated as Fig. 3-2. In Fig. 3-2, three positions are specified, which are positions 1, 2 and 3. Positions 1 and 3 represent the beginning and end of the single-support phase, respectively. On the other hand, the ankle reaches its highest point at position 2. *Hao* denotes the z coordinate of the highest point and *lao* is the distance between the position 1 and position 2 along the x-axis. It is assumed that position 2 is located halfway in between position 1 and position 3 and it is reached at the middle of the single-support phase. l_{an} denotes the ankle length along z-axis.

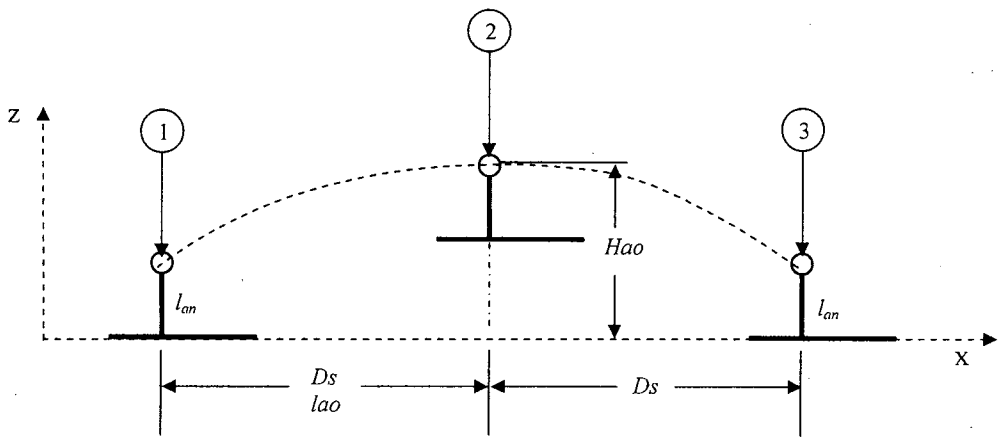

Fig. 3-2 Walking parameters for ankle

The period for one walking step is T_c. The K^{th} step is the step from KT_c to $(K+1)T_c$, where K is the number of the steps. The swing distance is $2D_s$, where D_s is the distance between two ankles at the beginning of single-support phase. The time from position 1 to position 2 is $0.5T_c$ second. In the trajectory design, the right foot trajectory is considered only

because the left foot trajectory is the same as the right foot trajectory but with a delay of T_c.

Mathematically, the x and z coordinates of the ankle in Fig.3-2 can be written as

$$x_R = \begin{cases} v_{11} = kD_s, & t = t_1 = kT_c \\ v_{12} = kD_s + lao, & t = t_2 = kT_c + 0.5T_c \\ v_{13} = (k+2)D_s, & t = t_3 = (k+1)T_c \end{cases} \tag{3-10}$$

$$z_R = \begin{cases} v_{11} = l_{an}, & t = t_1 = kT_c \\ v_{12} = Hao, & t = t_2 = kT_c + 0.5T_c \\ v_{13} = l_{an}, & t = t_3 = (k+1)T_c \end{cases} \tag{3-11}$$

With Equation (3-10) or (3-11), the coefficients c_i used in the third-order interpolation can be determined by using Equation (3-9), and the trajectories for the x and z coordinates of the ankle can be calculated by Equation (3-2).

3.3 Hip Trajectories

For simplicity, only the x and z coordinates of the hip are considered for the hip trajectory design with the y coordinate being assumed to be constant.

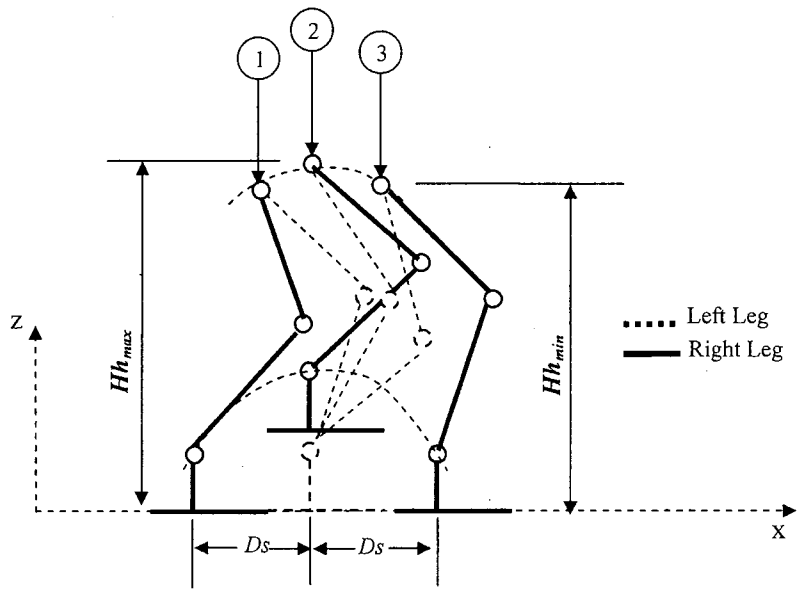

Fig. 3-3 Walking parameters for hip

Fig. 3-3 shows the walking parameters for the hip trajectory. The hip reaches its highest position (position 2) at the middle of the single-support phase and the height at this point is marked as Hh_{max}. At this point, the ankle and hip joints are assumed to be on the same vertical line. The hip gets its lowest position at the beginning (position 1) and end (position 3) of the single-support phase and the height is marked as Hh_{min}. At position 1 or position 3, the hip is located halfway in between two ankle joints on the x-axis.

Based on Fig. 3-3, the following constraints should be satisfied during the single-support phase

$$z_h = \begin{cases} v_{11} = Hh_{\min}, & t = t_1 = kT_c \\ v_{12} = Hh_{\max}, & t = t_2 = kT_c + 0.5T_c \\ v_{13} = Hh_{\min}, & t = t_3 = (k+1)T_c \end{cases} \tag{3-12}$$

$$x_h = \begin{cases} v_{11} = kD_s + lao - 0.5lao, & t = t_1 = kT_c \\ v_{12} = kD_s + lao, & t = t_2 = kT_c + 0.5T_c \\ v_{13} = kD_s + lao + 0.5lao, & t = t_3 = (k+1)T_c \end{cases} \tag{3-13}$$

With Equation (3-12) or (3-13), the coefficients c_i used in the third-order interpolation can be determined by using Equation (3-9), and the trajectories for the x and z coordinates of the hip can be calculated by Equation (3-2).

3.4 Trajectories for Joint Variables θ_2, θ_3, θ_4, θ_9, θ_{10} and θ_{11}

For the case of the left leg support, with the ankle and hip trajectories determined in §3.2 and §3.3, the trajectories for joint variables θ_2, θ_3, θ_4, θ_9, θ_{10} and θ_{11} can be calculated by using the related inverse kinematics equations discussed in §2.2.

Similarly, for the case of the right leg support, the same method can be used to determine the trajectories for joint variables θ_2, θ_3, θ_4, θ_9, θ_{10} and θ_{11}. However, the design procedure can be simplified by directly referring the results for the case of the left leg support to the case of the right leg support because of the symmetry of the walking pattern. The walking trajectories for right leg support can be determined as

$$\begin{cases} \theta_2 = -\theta_{11L} \\ \theta_3 = -\theta_{10L} \\ \theta_4 = -\theta_{9L} \\ \theta_9 = -\theta_{4L} \\ \theta_{10} = -\theta_{3L} \\ \theta_{11} = -\theta_{2L} \end{cases} \tag{3-14}$$

where the subscript "L" indicates the trajectory with left leg support.

3.5 Trajectories for Joint Variables θ_1, θ_5, θ_8 and θ_{12}

This subsection is devoted to designing the joint angles θ_1, θ_5, θ_8 and θ_{12} to shift the weight from side to side for dynamic balance sideway. It is assumed that there is no forward motion when the biped robot shifts weight from side to side, that is, the joint angles θ_2, θ_3, θ_4, θ_9, θ_{10} and θ_{11} are kept constant. Therefore, only the trajectories for θ_1, θ_5, θ_8 and θ_{12} are required for weight shifting.

3.5.1 Trajectories for Joint Variables θ_1 and θ_{12}

For simplicity, the following three values are specified first.

$$\theta_k = \begin{cases} v_{11} = 0, & t = t_1 = 0 \\ v_{12} = \theta\_SW\_A, & t = t_2 = T_c\_SW \\ v_{13} = 0, & t = t_3 = 2T_c\_SW \end{cases} \text{, where } k\text{=1, 12} \qquad (3\text{-}15)$$

where θ_SW_A is the angle by which the joint O_1 or O_{12} turns at the end of weight shifting and T_c_SW is the time it takes for the joint to turn from zero to θ_SW_A.

By following the same procedure indicated in §3.1, the coefficient c_i can be determined by Equation (3-9), which can be used to determine the trajectories for θ_1 and θ_{12}.

In the actual walking cycle, θ_k will change from v_{11} to v_{12} in T_c_SW seconds before the single support phase begins. Then θ_k will remain at v_{12} for the entire single support phase. After the single support phase ends, θ_k will change back from v_{12} to v_{13} in another T_c_SW seconds.

It is easily seen from Fig. 3-1 that the trajectories for θ_1 and θ_{12} with the weight shifting to the left and to the right are the same in magnitude but in the opposite direction.

3.5.2 Trajectories for Joint Variables θ_5 and θ_8

For the weight shifting phase, the trajectories for θ_5 and θ_8 are determined by specifying the following three points

$$\theta_k = \begin{cases} v_{11} = 0, & t = t_1 = 0 \\ v_{12} = \theta\_SW\_H, & t = t_2 = T_c\_SW \\ v_{13} = 0, & t = t_3 = 2T_c\_SW \end{cases}, \text{ where } k=5, 8 \tag{3-16}$$

where θ_SW_H is the angle by which the joint O_5 or O_8 turns at the end of weight shifting and T_c_SW is the time it takes for the joint to turn from zero to θ_SW_H.

By using the third order spline interpolation method discussed in §3.1, the coefficient c_i can be determined by Equation (3-9), which can be used to calculate the trajectories for θ_5 and θ_8 in the weight shifting phase.

For the single support phase, the trajectory for θ_5 or θ_8 is determined by specifying the following three points

$$\theta_k = \begin{cases} v_{11} = \theta\_SW\_H, & t = t_1 = 0 \\ v_{12} = \theta\_HSS, & t = t_2 = 0.5T_c \\ v_{13} = \theta\_SW\_H, & t = t_3 = T_c \end{cases}, \text{ where } k=5 \text{ or } 8 \tag{3-17}$$

where θ_HSS is the angle by which the joint O_5 or O_8 turns at the middle of the single-support phase. T_c is the period for single-support phase.

Equation (3-17) can be used to determine the trajectory for θ_5 or θ_8 in the single support phase by first calculating the coefficients c_i using Equation (3-9) and then computing the trajectory using Equation (3-2).

In the actual walking cycle, for the single-support phase with left leg support, θ_k will turn from v_{11} to v_{12} in T_c_SW seconds by following the trajectories determined by Equation (3-16) before the single support phase begins; θ_5 will remain at v_{12} in Equation

(3-16) and θ_8 will turn from v_{11} to v_{13} determined by Equation (3-17) for the single support phase; and θ_k will turn back to the home position from v_{12} to v_{13} in another T_c_SW seconds by following the trajectories determined by Equation (3-16) after the single support phase ends. On the other hand, for the single-support phase with right leg support, θ_k will turn from v_{11} to v_{12} in T_c_SW seconds by following the trajectories determined by Equation (3-16) before the single support phase begins; θ_8 will remain at v_{12} in Equation (3-16) and θ_5 will turn from v_{11} to v_{13} determined by Equation (3-17) for the single support phase; and θ_k will turn back to the home position from v_{12} to v_{13} in another T_c_SW seconds by following the trajectories determined by Equation (3-16) after the single support phase ends.

3.6 Simulation Results on Trajectory Planning

For completeness, the robot parameters and walking parameters are listed in Table 3-1.

Table 3-1: Parameters for the Biped Robot

Symbol	Description	Value	Unit
L_1	distance between O_0 and O_1 along the link	0.028	m
L_2	distance between O_1 and O_2 along the link	0.04	m
l_{an}	ankle length	L_1+L_2	m
l_{af}	foot front part length	0.14	m
l_{ab}	foot back part length	0.1	m
L_3	shin length (between O_2 and O_3)	0.19	m
L_4	thigh length (between O_3 and O_4)	0.27	m
L_5	distance between O_4 and O_5 along the link	0.04	m
L_6	distance between O_5 and O_6 along the link	0.028	m
L_h	hip width	0.145	m
D_s	step length	0.04	m
lao	distance on x-axis of reference frame from start point to the highest point for O_2	D_s	m
Hao	height of highest ankle position	l_{an}+0.03	m
$Hh_{\min}$	height of lowest hip position	L_3+L_4+l_{an}-0.03	m
$Hh_{\max}$	height of highest hip position	Hh_{min}+0.005	m
T_c	period for one walking step	6	s
T_c_SW	time that shifts the weight to the support leg and shift back	6	s
θ_SW_A	θ_1 or θ_{12} for weight shifting	15	deg
θ_SW_H	θ_5 or θ_8 for weight shifting	15 (for swing leg) 13 (for support leg)	deg
θ_HSS	θ_5 or θ_8 at the middle of single-support phase for the support leg	10.5	deg
T_s	Sampling time	0.001	s

Some MATLAB programs were written to generate the desired trajectories for the biped robot.

3.6.1 Ankle and Hip Trajectories

For the single support phase with left leg support, the trajectories for both ankle and hip joints are calculated by using the third order spline interpolation method. The simulation results are shown in Fig. 3-4 to Fig. 3-7.

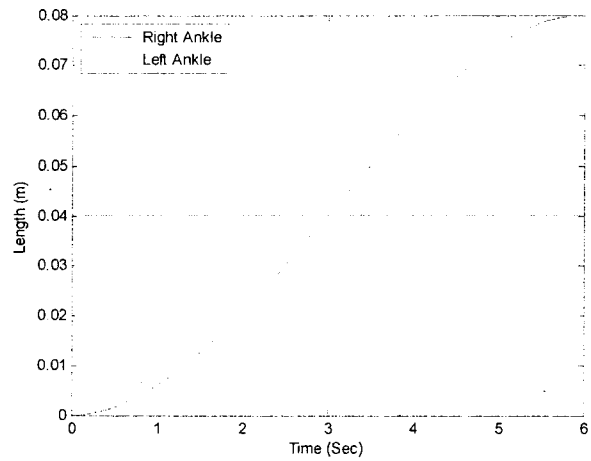

Fig. 3-4 Plot for x_R and x_L

Fig. 3-4 shows that the right ankle starts from zero and moves forward along the x-axis by 0.08 m, at the same time the left ankle stays at 0.04 m.

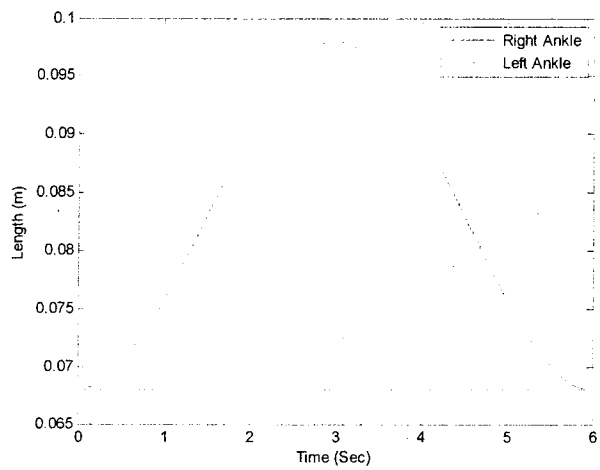

Fig. 3-5 Plot for z_R and z_L

Fig. 3-5 shows that alone the z-axis, the right ankle starts from 0.068 m, lifts to the highest point of 0.098 m at 3 second, and then comes back to 0.068 m at 6 second, while the left ankle stays at 0.068 m.

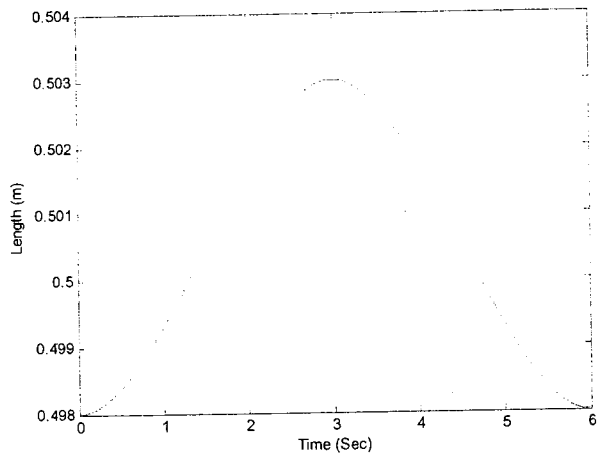

Fig. 3-6 Plot for z_h

Fig. 3-6 shows that the hip moves up from 0.498 m, reaches the highest point of 0.503 m at 3 second, and then comes back to 0.498 m at 6 second.

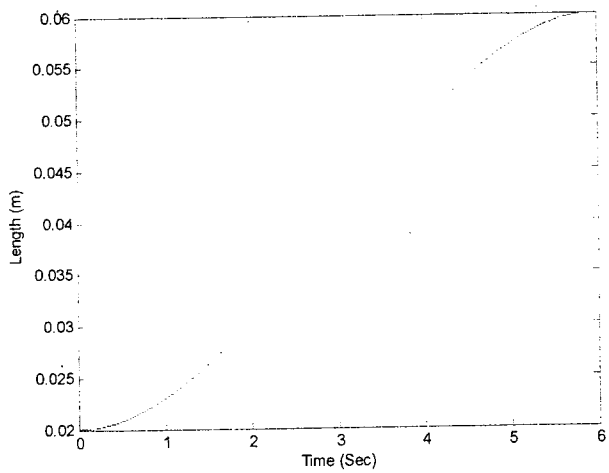

Fig. 3-7 Plot for x_h

Fig. 3-7 shows that the hip moves forward from 0.02 m to 0.06 m in 6 seconds.

3.6.2 Simulation Results for Joint Trajectories

The complete walking cycle contains the following steps:

1. Initialization

   The first 15 seconds are used for the initialization. The biped robot is powered at 3 second, controlled to the home position in 6 seconds, and then held at the home position for 6 seconds.

2. Shift weight to the left

   The walking cycle starts at this step. From 15 second to 23 second, the robot shifts weight to the left leg in 6 seconds and then holds that position for 2 seconds. The period from the step 1 to step 2 is the double-support phase.

3. Swing the right leg

   From 23 second to 29 second, the robot lifts the right leg, swings it from the rear to the front and lands it on the ground. This is the single-support phase with left leg support.

4. Shift weight back

   After the right foot lands on the ground, from 29 second to 31 second, the robot holds that position for 2 seconds, and then from 31 second to 37 second, the robot shifts weight back.

5. Hold the current position

   The robot holds the current position from 37 second to 43 second. Up to now, the robot completes the first half of the complete walking cycle.

6. Shift weight to right

The second half of the complete walking cycle begins with the robot shifting weight to the right leg from 43 second to 49 second and holding for 2 seconds. The period from step 4 to step 6 is the double-support phase.

7. Swing the left leg

   The period from 51 second to 57 second is the second single-support phase. The robot lifts the left leg, swings it from the rear to the front, lands it on the ground.

8. Shift weight back

   The robot holds the position from 57 second to 59 second after lands the left foot. Then from 59 second to 65 second, the robot shifts the weight back.

9. Hold the current position

   The robot holds the current position from 65 second to 69 second.

The next walking cycle starts from step 2 and repeats steps from 2 to 9.

3.6.2.1 The Desired Trajectories in Degrees

The complete walking trajectories in degrees are shown in Fig. 3-8 to Fig. 3-17

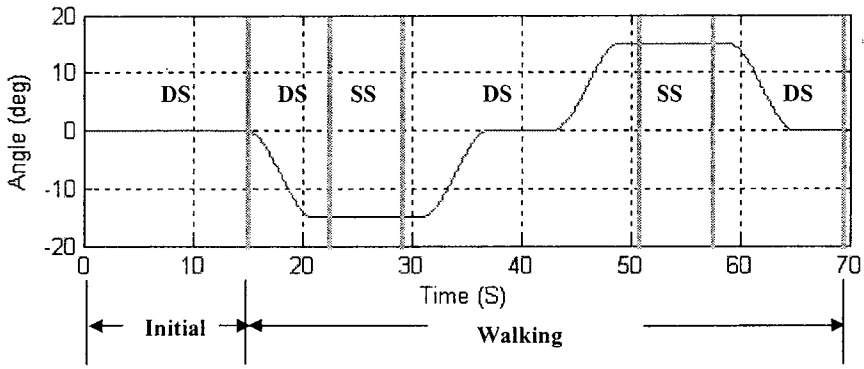

Fig. 3-8 Desired trajectory for joint variable θ_1

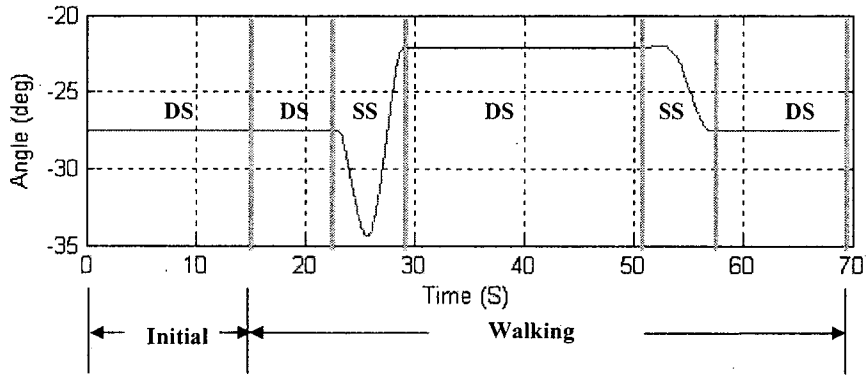

Fig. 3-9 Desired trajectory for joint variable θ_2

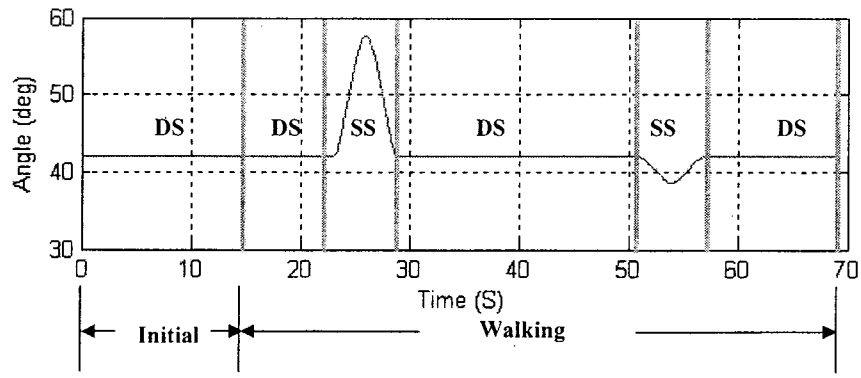

Fig. 3-10 Desired trajectory for joint variable θ_3

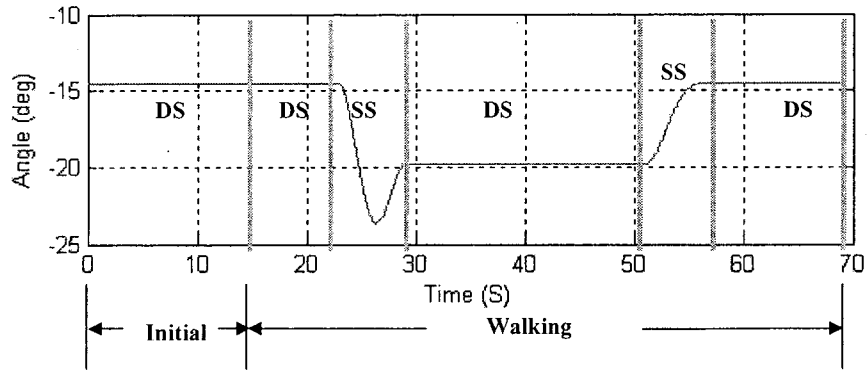

Fig. 3-11 Desired trajectory for joint variable θ_4

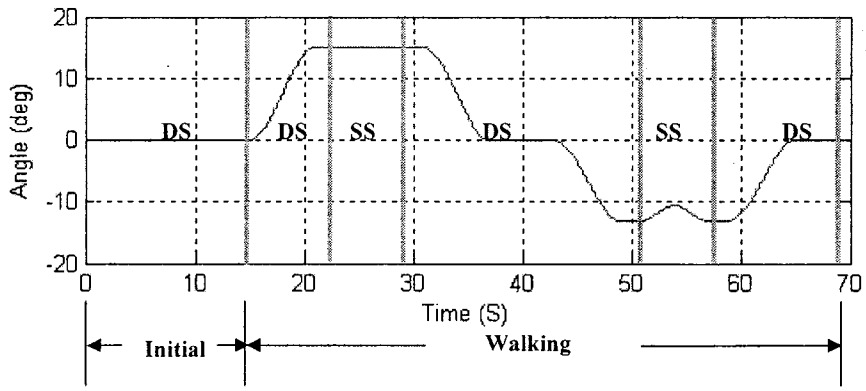

Fig. 3-12 Desired trajectory for joint variable θ_5

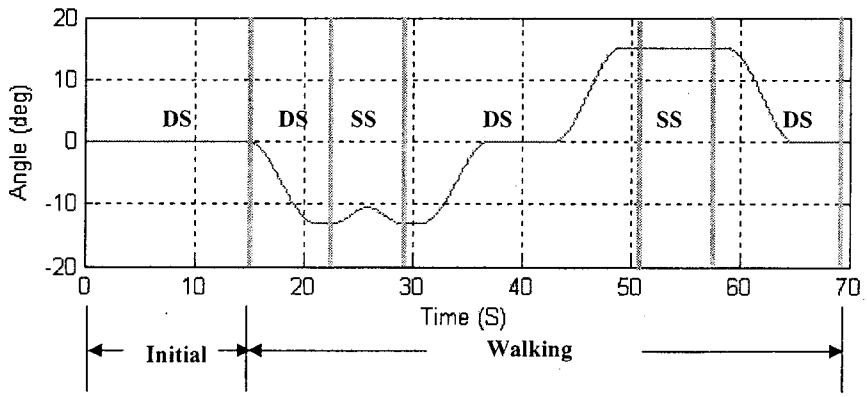

Fig. 3-13 Desired trajectory for joint variable θ_8

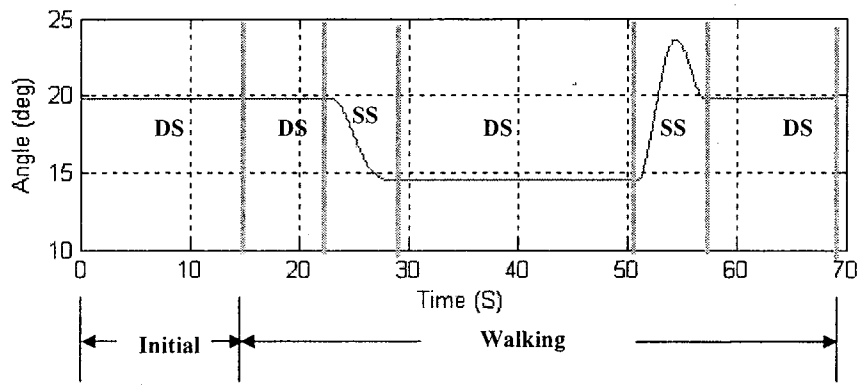

Fig. 3-14 Desired trajectory for joint variable θ_9

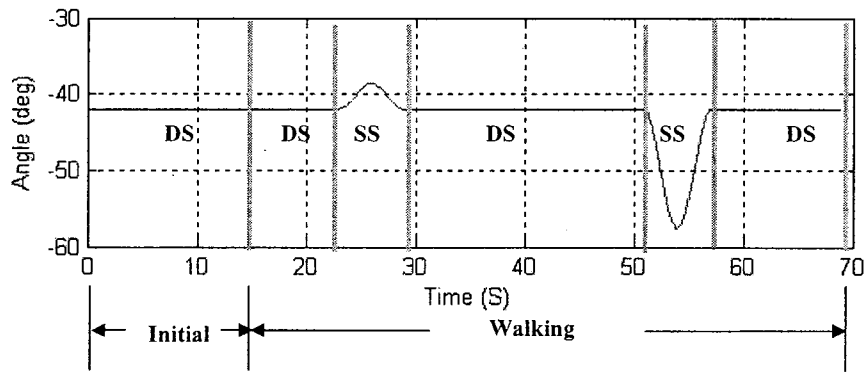

Fig. 3-15 Desired trajectory for joint variable θ_{10}

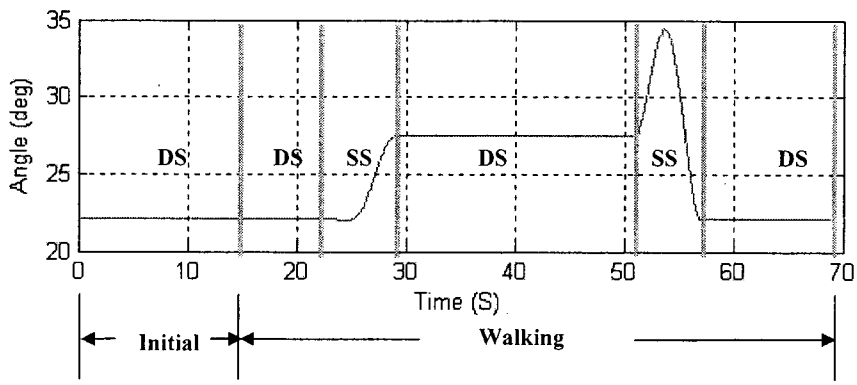

Fig. 3-16 Desired trajectory for joint variable θ_{11}

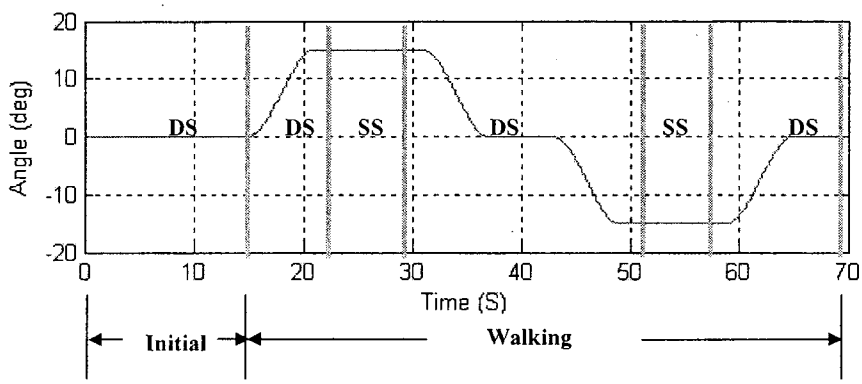

Fig. 3-17 Desired trajectory for joint variable θ_{12}

In Fig. 3-8 to Fig. 3-17, "DS" represents the double-support phase and "SS" represents the single-support phase.

3.6.2.2 The Desired Trajectories in Voltages

The desired trajectories in voltages are the actual trajectories used in software design and digital controller design. §4.1.3.1 provides the detailed procedure to convert angles in degrees to angles in voltages.

The desired trajectories in voltages are plotted in Fig. 3-18 to Fig. 3-27.

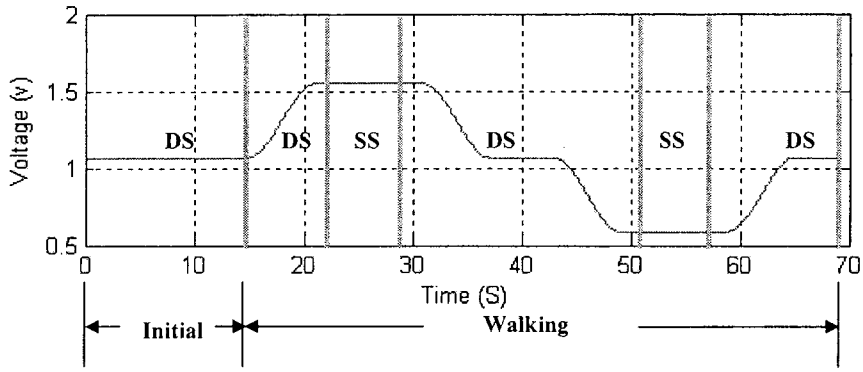

Fig. 3-18 Desired voltage for joint O_1

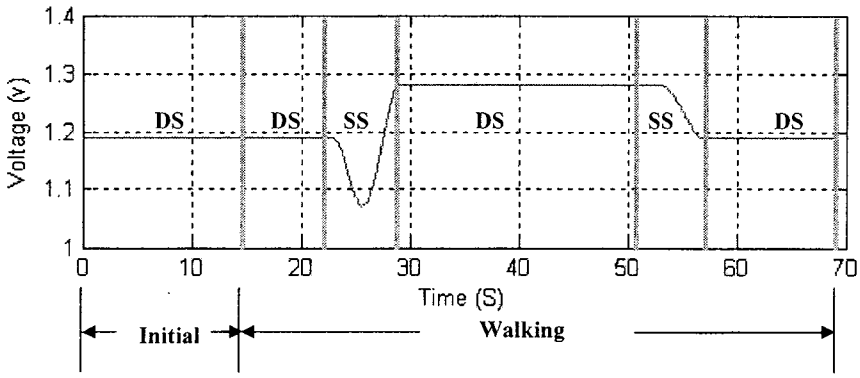

Fig. 3-19 Desired voltage for joint O_2

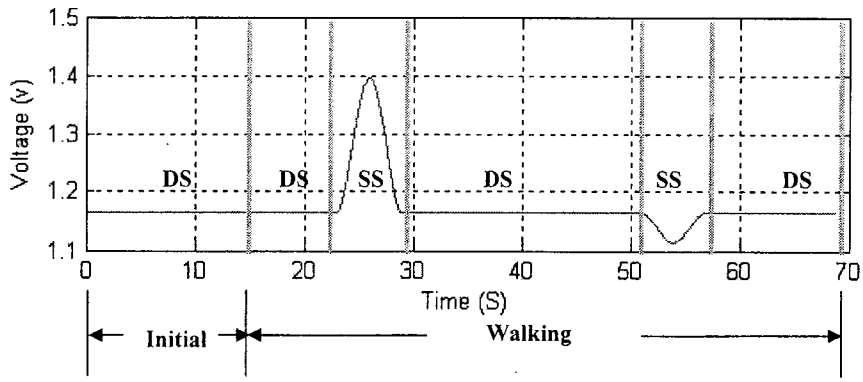

Fig. 3-20 Desired voltage for joint O_3

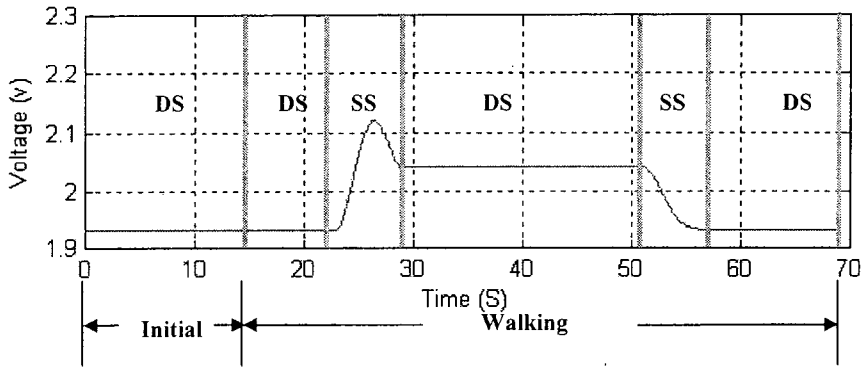

Fig. 3-21 Desired voltage for joint O_4

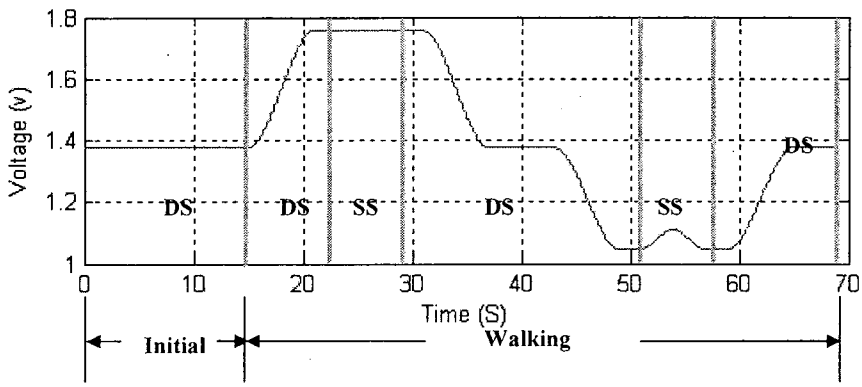

Fig. 3-22 Desired voltage for joint O_5

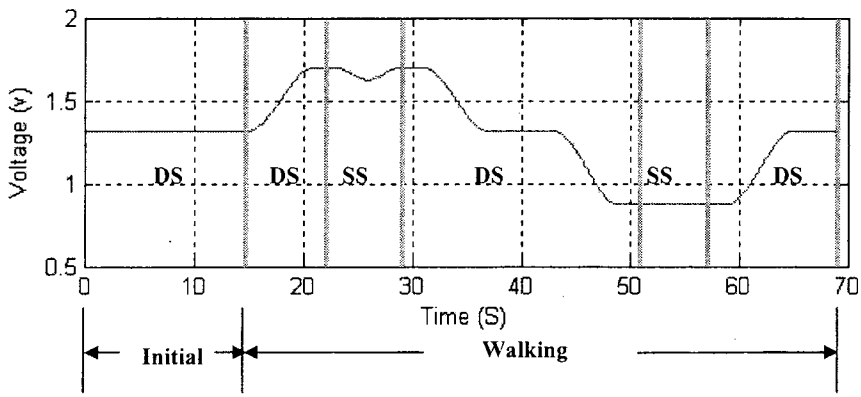

Fig. 3-23 Desired voltage for joint O_8

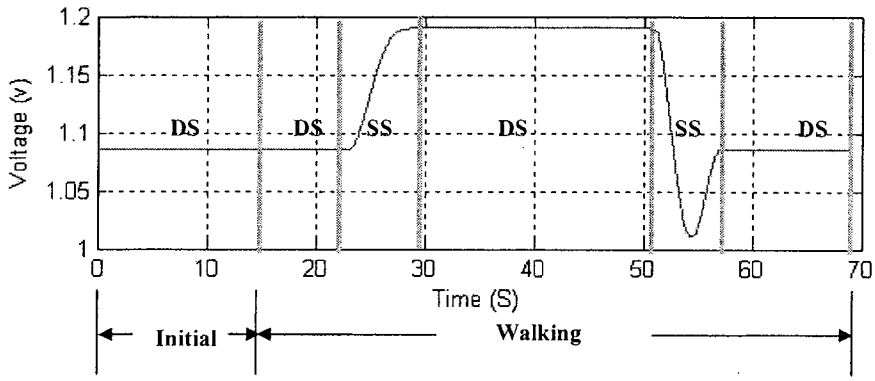

Fig. 3-24 Desired voltage for joint O_9

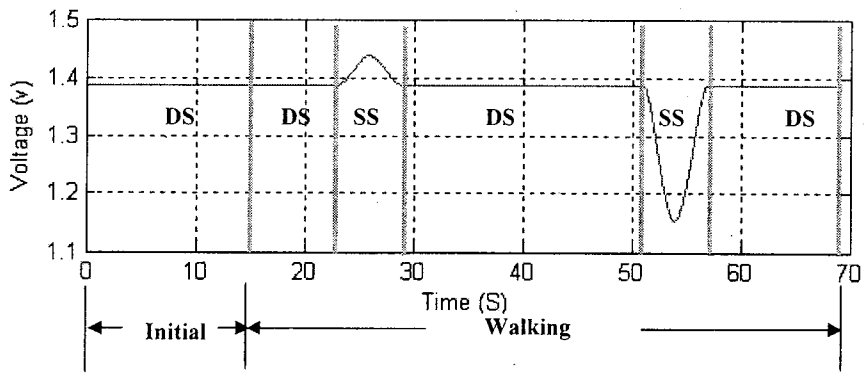

Fig. 3-25 Desired voltage for joint O_{10}

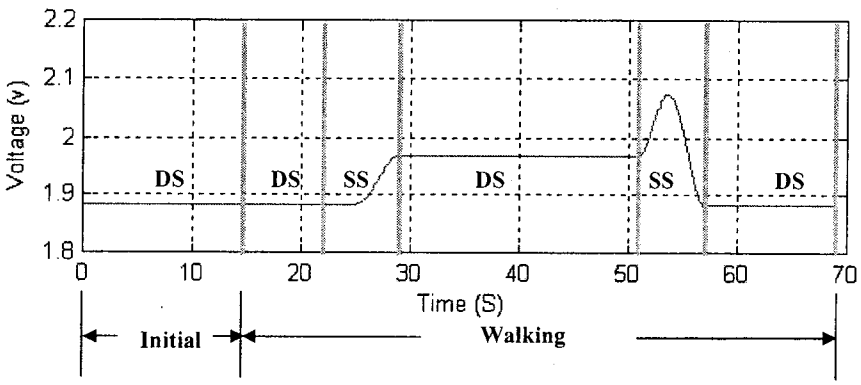

Fig. 3-26 Desired voltage for joint O_{11}

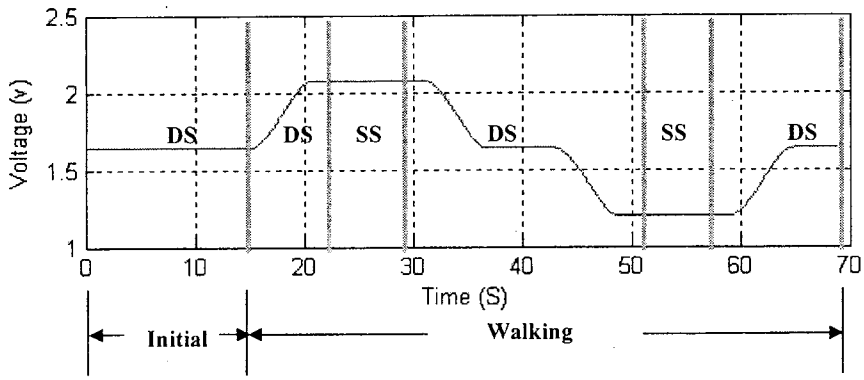

Fig. 3-27 Desired voltage for joint O_{12}

3.7 Zero Moment Point Analysis

The ZMP is defined as the point on the ground about which the sum of all the moments of the active forces equals zero. If the ZMP is within the contact area between the feet and the ground, the biped robot is able to walk. The stability margin can be large if the desired ZMP is designed near the center of the contact area. Therefore, for the balance requirement, the ZMP has to be calculated.

The first step to calculate ZMP is to compute the position, speed and acceleration for the mass center of each link. To find the position, which is the x, y and z coordinates, the forward kinematics need to be performed.

For this thesis, the ZMP is calculated for the single-support phase Fig. 3-28 indicates the approximate locations of the mass centers of the 10 DOF biped robot links.

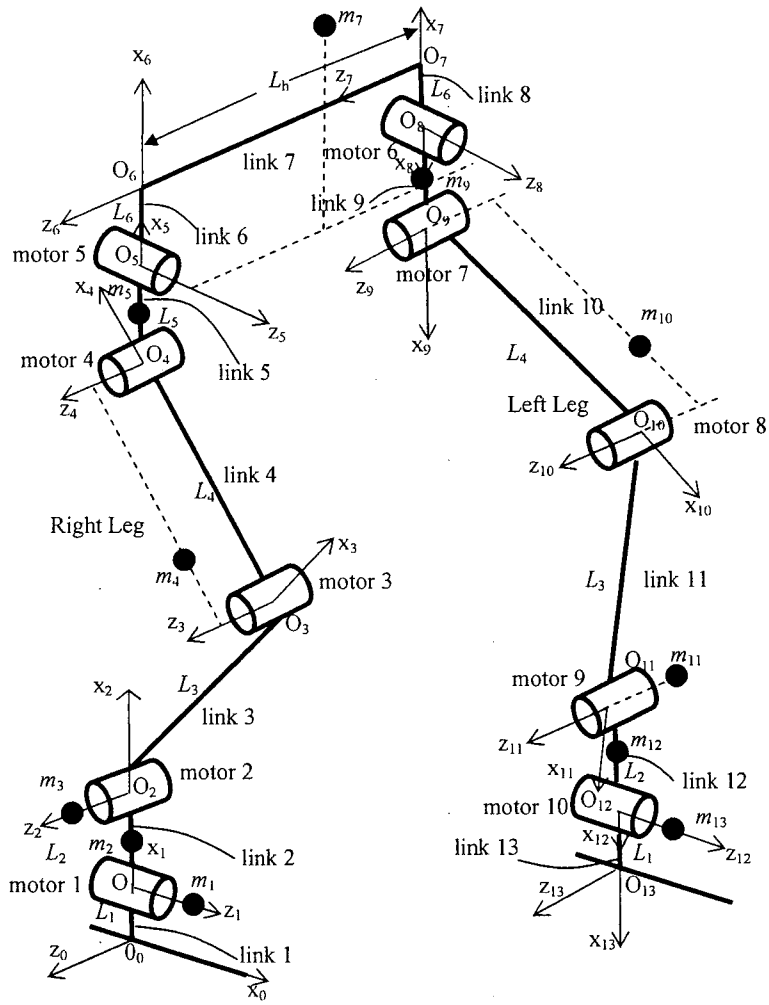

Fig. 3-28 Robot link mass center locations

3.7.1 ZMP Calculation

The ZMP is the point on the ground, which is the x-y plane as shown in Fig. 2-2. The ZMP can be computed by using the following Equations [6]

$$\hat{o}_{ZMP} = \frac{\hat{n} \times \hat{M}_o^{gi}}{\hat{R}^{gi} \cdot \hat{n}} \tag{3-18}$$

$$\hat{M}_o^{gi} = \sum_{i=1}^{n} \left[m_i \hat{O}_{Gi} \times \left(\hat{g} - \hat{a}_{Gi} \right) - \dot{\hat{H}}_{Gi} \right] \tag{3-19}$$

$$\hat{R}^{gi} = m_i \hat{g} - \sum_{i=1}^{n} m_i \hat{a}_{Gi} \tag{3-20}$$

where m_i is the mass of the link i, $\hat{O}_{Gi}$ is the position of the mass center of link i, $\hat{a}_{Gi}$ is the acceleration of $\hat{O}_{Gi}$, $\hat{n}$ is the normal vector, $\dot{\hat{H}}_{Gi}$ is the rate of angular momentum at point $\hat{O}_{Gi}$. $\dot{\hat{H}}_{Gi}$ is calculated by

$$\dot{\hat{H}}_{Gi} = R_i \left(I_{Gi} \dot{\hat{\omega}}_i - \left(I_{Gi} \hat{\omega}_i \right) \times \hat{\omega}_i \right) \tag{3-21}$$

where R_i is the rotation matrix associated to frame i, I_{Gi}, $\hat{\omega}_i$ and $\dot{\hat{\omega}}_i$ are the inertia matrix, the angular velocity and angular acceleration of the mass center of link i. The symbol "^" represents a 3-by-1 vector. The symbol "×" represents the cross product and "•" denotes the dot product.

By using the recursive computation method [20], the angular velocity $\hat{\omega}_i$ can be calculated by

$$\hat{\omega}_i = \left(R_{i-1}^i \right)^T \hat{\omega}_{i-1} + \hat{b}_i \dot{q}_i \tag{3-22}$$

where

$$\hat{b}_i = \left(R_0^i \right)^T \hat{z}_{i-1} \tag{3-23}$$

In Equation (3-22) and (3-23), R_{i-1}^i and R_0^i are the rotation matrices from frame i to frame i-1 and frame 0 respectively, the symbol "T" represents transpose matrix, $\hat{z}_{i-1}$ is given by the first three elements in the third column of the transformation matrix ${}^{i-1}_{i}T$, $\dot{q}_i$ is the angular velocity for the joint rotating angle θ_i.

The angular acceleration of the mass center of link i can be calculated by

$$\hat{\dot{\omega}}_i = \left(R_{i-1}^i\right)^T \hat{\dot{\omega}}_{i-1} + \hat{b}_i \ddot{q}_i + \hat{\omega}_i \times \hat{b}_i \dot{q}_i \tag{3-24}$$

The acceleration of the mass center of link i can be calculated by

$$\hat{a}_{Gi} = \left(R_{i-1}^i\right)^T \hat{a}_{i-1} + \hat{\dot{\omega}}_i \times \hat{r}_{i,ci} + \hat{\omega}_i \times \left(\hat{\omega}_i \times \hat{r}_{i,ci}\right) \tag{3-25}$$

where $\hat{r}_{i,ci}$ is the vector from joint i to the center of mass of link i, and $\hat{a}_{i-1}$ is the acceleration of the end of link i-1 (i.e. joint i). $\hat{a}_i$ can be calculated as

$$\hat{a}_i = \left(R_{i-1}^i\right)^T \hat{a}_{i-1} + \hat{\dot{\omega}}_i \times \hat{r}_{i,i+1} + \hat{\omega}_i \times \left(\hat{\omega}_i \times \hat{r}_{i,i+1}\right) \tag{3-26}$$

where $\hat{r}_{i,i+1}$ is the vector from joint i to joint i+1.

I_{Gi} is the inertia matrix of link i about a frame parallel to frame i, whose origin is at the center of mass of link i. For link 2, link 5, link 8 and link 12, I_{Gi} can be calculated as

$$I_{Gi} = \frac{1}{12} mL^2 \tag{3-27}$$

where m is the mass of the link and L is the length of the link.

For link 1, link 3, link 11 and link 13, I_{Gi} can be calculated as

$$I_{Gi} = \left(I_m + I_g\right) G\_R^2 \tag{3-28}$$

where I_m is the motor rotor inertia, I_g is the gearhead mass inertia and G_R is the gear ratio, of the motor 1, motor 2, motor 9 and motor 10 for link 1, link 3, link 11 and link 13, respectively.

For link 4, link 7 and link 10, I_{Gi} can be calculated by using Parallel axis theorem as

$$I_{Gi} = I^{center} + m\left[(\hat{r} \bullet \hat{r})E_3 - \hat{r}(\hat{r})^T\right] \tag{3-29}$$

where m is the mass of the link, $\hat{r}$ is the vector from the motor rotating axis to the center of mass of link i, E_3 is the 3-by-3 identity matrix. "•" represent the dot product. I^{center} is the moment of inertia about the rotating axis of motor 3 and motor 4 for link 4, motor 5 and motor 6 for link 7, and motor 7 and motor 8 for link 10. I^{center} can be calculated by using Equation (3-28).

According to the D-H model in Fig. 2-1, Table 2-2 and Fig. 3-28, the physical features of the robot links are listed in Table 3-2. The coordinates are approximately measured, due to the irregular shape of the robot links.

Table 3-2: Physical Features of the Robot Links

Link	m_i (kg)	$\hat{r}_{i,i+1}$	$\hat{r}_{i,ci}$
1	0.585	$[L_1,0,0]$	$[L_1,0,0.5L_{motor1}]$
2	0.05	$[L_2,0,0]$	$[0.5L_2,0,0]$
3	0.585	$[L_3,0,0]$	$[0,0,0.5L_{motor2}]$
4	1.147	$[L_4,0,0]$	$\left[\frac{L_4 m_{motor3}}{m_4},0,0.5L_{motor3}\right]$
5	0.05	$[L_5,0,0]$	$[0.5L_5,0,0]$
6	0	$[L_6,0,0]$	$[0.5L_6,0,0]$
7	1.181	$[0,0,-L_h]$	$[0.5H_{body},-0.5L_{motor5},-0.5L_h]$
8	0	$[L_6,0,0]$	$[0.5L_6,0,0]$
9	0.05	$[L_5,0,0]$	$[0.5L_5,0,0]$
10	1.147	$[L_4,0,0]$	$\left[L_4 - \frac{L_4 m_{motor8}}{m_{10}},0,-0.5L_{motor8}\right]$
11	0.585	$[L_3,0,0]$	$[L_3,0,-0.5L_{motor9}]$
12	0.05	$[L_2,0,0]$	$[0.5L_2,0,0]$
13	0.585	$[L_1,0,0]$	$[0,0.5L_{motor10},0]$

The masses for link 6 and link 8 are zero because their masses are added to the robot body, which is link 7. L_{motor} and m_{motor} represent the length and mass of the motor with gearhead and H_{body} denotes the body height, which is defined in Table 4-3. See Table 4-1 and Appendix G for the lengths and masses of the motors and the gearheads.

3.7.2 ZMP Simulation and Analysis

Simulations are performed with MATLAB and results are plotted in Fig. 3-29 to Fig. 3-32, where (x_{ZMP}, y_{ZMP}, 0) is the coordinates of ZMP in the reference frame with the origin at O_r.

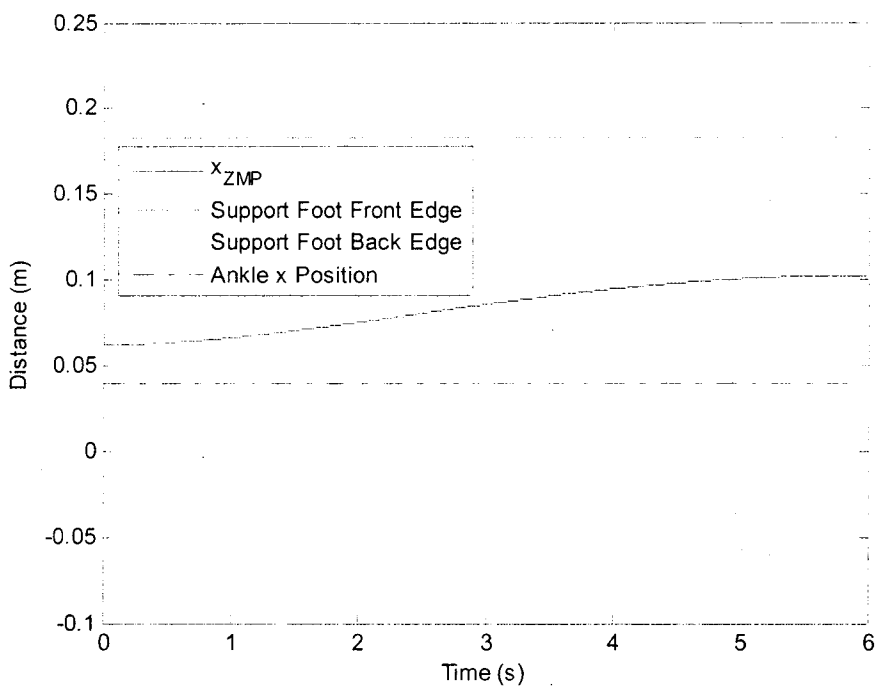

Fig.3-29 x_{ZMP} for the single-support phase with left leg support

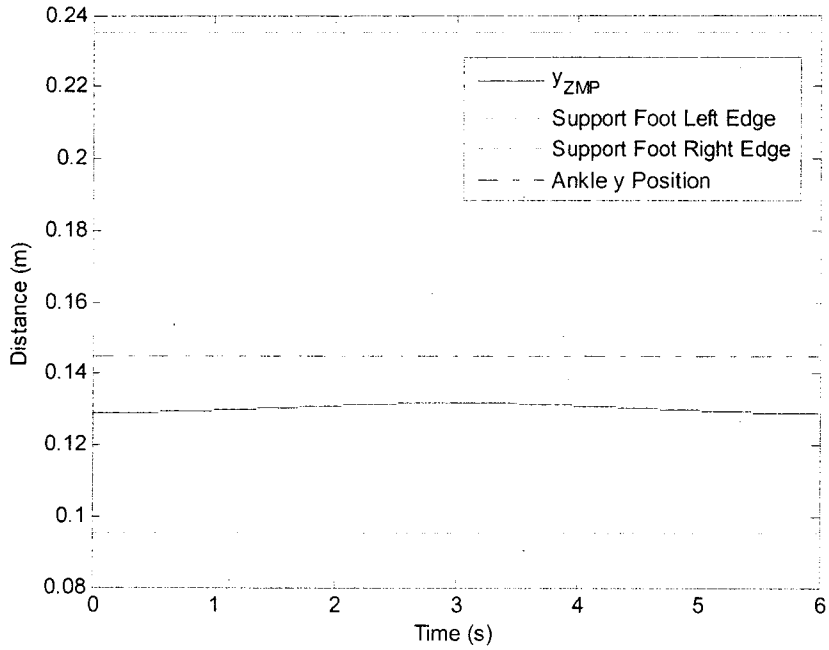

Fig.3-30 y_{ZMP} for the single-support phase with left leg support

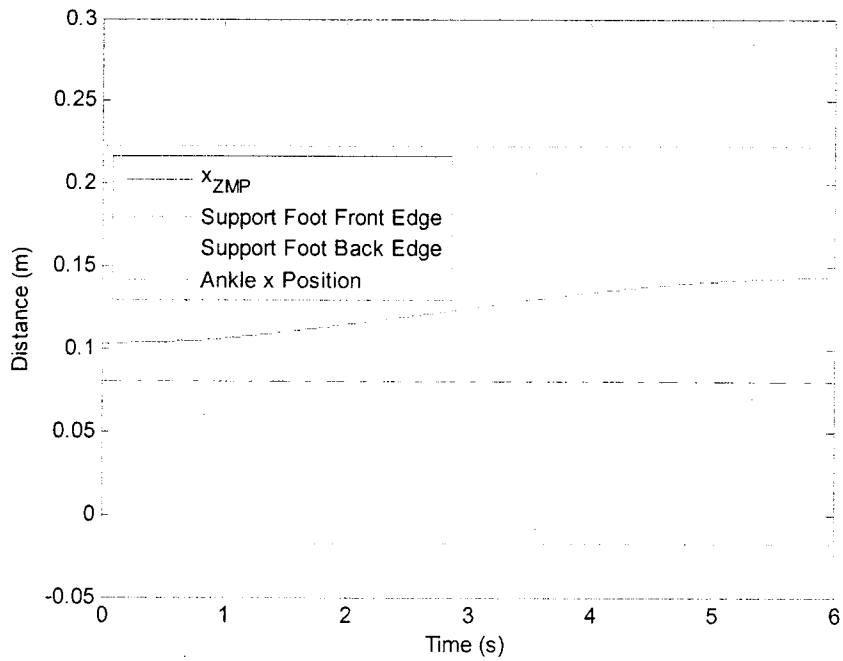

Fig.3-31 x_{ZMP} for the single-support phase with right leg support

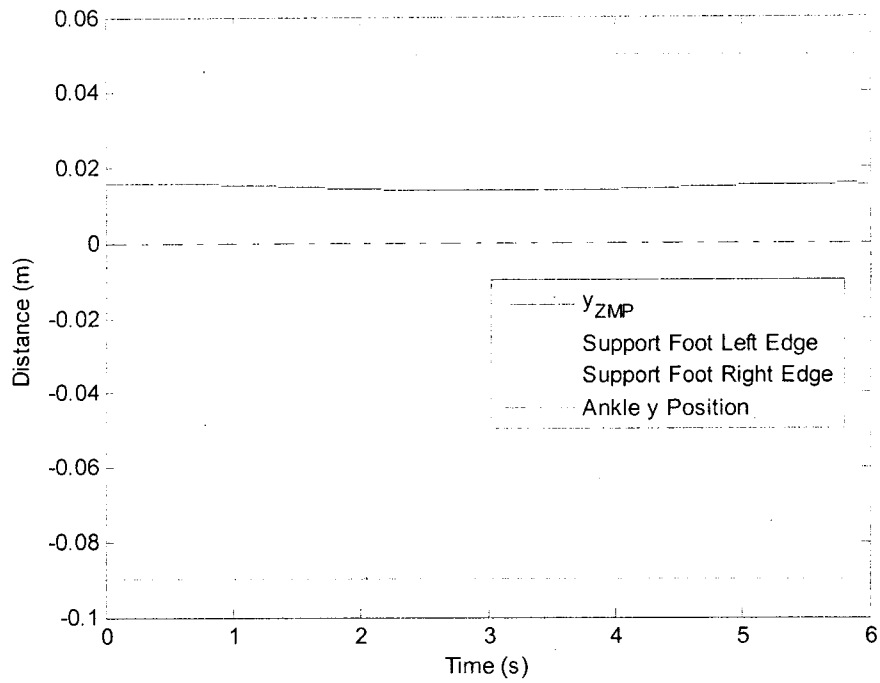

Fig.3-32 y_{ZMP} for the single-support phase with right leg support

Fig. 3-29 and Fig. 3-31 show the x coordinate of the ZMP and the x coordinates of the front and back edges of the support foot. It can be observed that x_{ZMP} is maintained within the two edges of the support foot. It can be also seen that x_{ZMP} is increasing during the walking process, which means the weight of the robot is transferred forward. Fig. 3-30 and Fig. 3-32 show the y coordinate for ZMP and the y coordinates for the left and right edges of the support foot. It is noticed that y_{ZMP} stays within the two edges of the support foot. It can be seen that the ZMP is within the contact area between the support foot and the ground and the robot is able to walk stably.

Chapter 4

Robot Prototype Design

The 10 DOF biped robot prototype is composed of mechanical design and electrical design. Fig. 4-1 shows a block diagram for the composition of the biped robot. Each function block will be explained in the following sections.

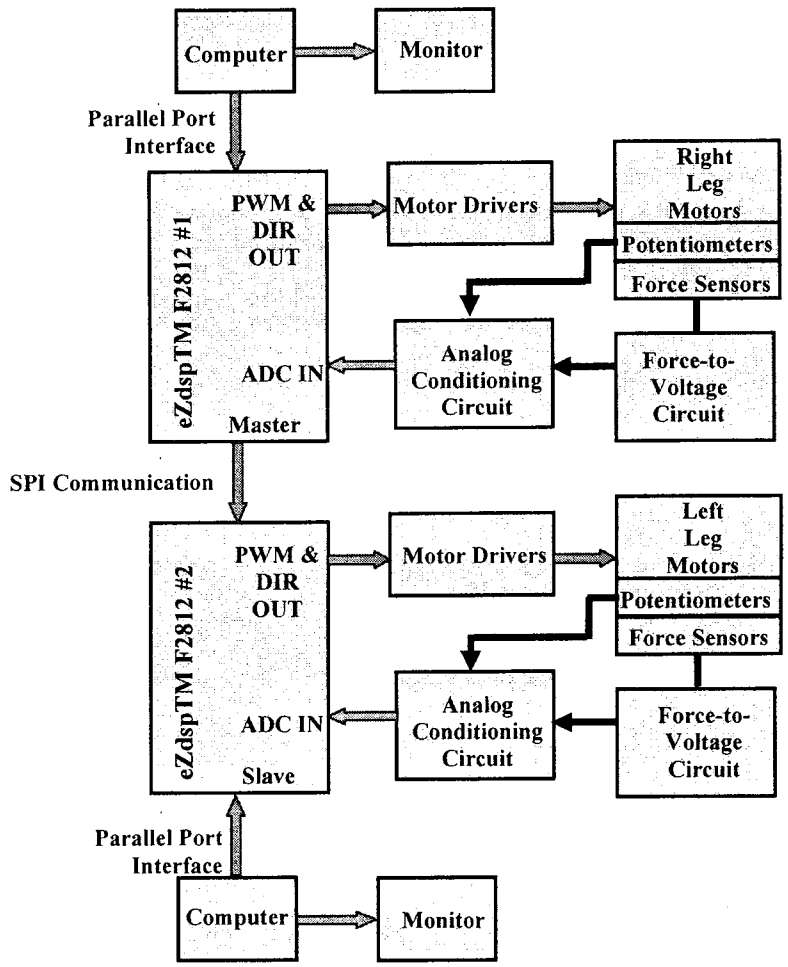

Fig. 4-1 Block diagram of the 10 DOF biped robot

4.1 Mechanical Design

4.1.1 Robot Size and Material Selection

The 10 DOF biped robot is mainly designed according to the parameters listed in Table 3-1 and Table 3-2. The structure of the robot should be simple, lightweight, easy to machine and easy to assemble. Aluminum is chosen for the material of the robot structure because it is light and easy to machine to the desired shape. Bolts and nuts are used to assemble the robot. The size of the robot body is designed so that it can hold all the control circuit boards.

AutoCAD is used to do the mechanical design of the biped robot. The robot parts are machined in the university machine shop. The height of the robot prototype is 978.65 mm, the width is 432.84 mm and the depth is 268.35 mm. See Appendix B for the detailed mechanical drawings of the robot prototype structure.

The biped robot has two legs and one body. Each leg has two ankle joints, one knee joint and two hip joints. See Fig. 4-2 and Fig. 4-3 for the overall structure of the 10 DOF biped robot.

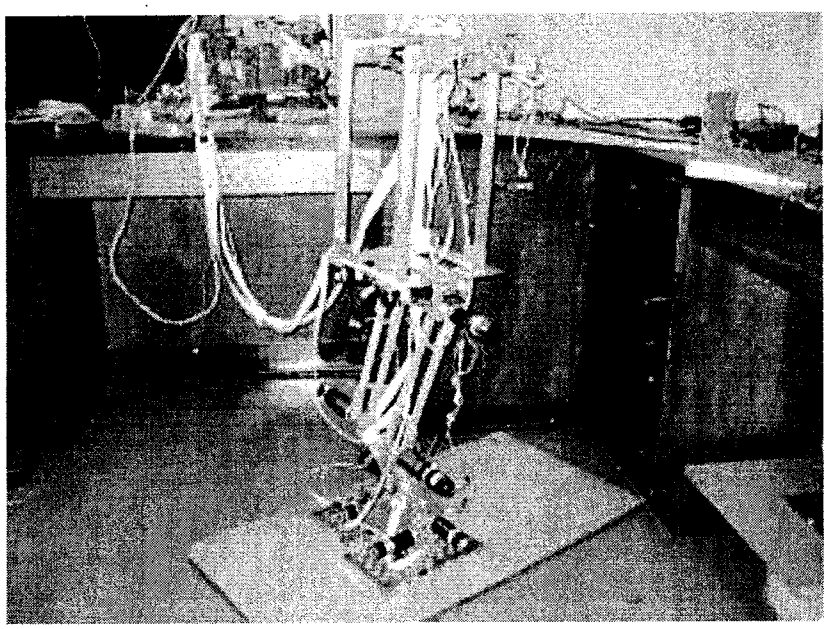

Fig. 4-2 The side view of the 10 DOF biped robot

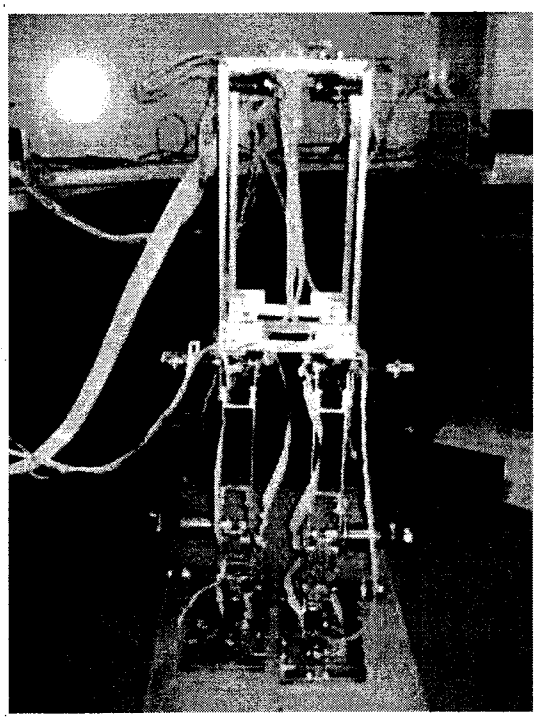

Fig. 4-3 The front view of the 10 DOF biped robot

4.1.2 Actuator Selection

There are three kinds of actuators commonly used for robots: hydraulic actuators, pneumatic actuators and electric motors. The electric motors with gearhead are chosen as the actuators because they are lighter and easier to control compared with other two kinds of actuators.

The electric motors for each joint are listed in Table 4-1.

Table 4-1 Motor Selection for the 10 DOF Biped Robot

		Gearhead		DC Motor	
		Model	**Gear Ratio**	**Model**	**Power (W)**
Hip	Pitch	Maxon Planetary Gearhead166949	246:1	Maxon RE-max 29 226788	22
	Roll	Maxon Planetary Gearhead166949	246:1	Maxon RE-max 29 226788	22
Knee	Pitch	Faulhaber Planetary Gearhead 38/2	159:1	Faulhaber 3257 024CR	83
Ankle	Pitch	Maxon Planetary Gearhead166949	246:1	Maxon RE-max 29 226788	22
	Roll	Maxon Planetary Gearhead166949	246:1	Maxon RE-max 29 226788	22

See Fig. 4-4 to Fig. 4-7 for the detailed structure of the ankle, knee and hip joints with DC motors.

See Appendix G for the DC motor and gearhead data sheets.

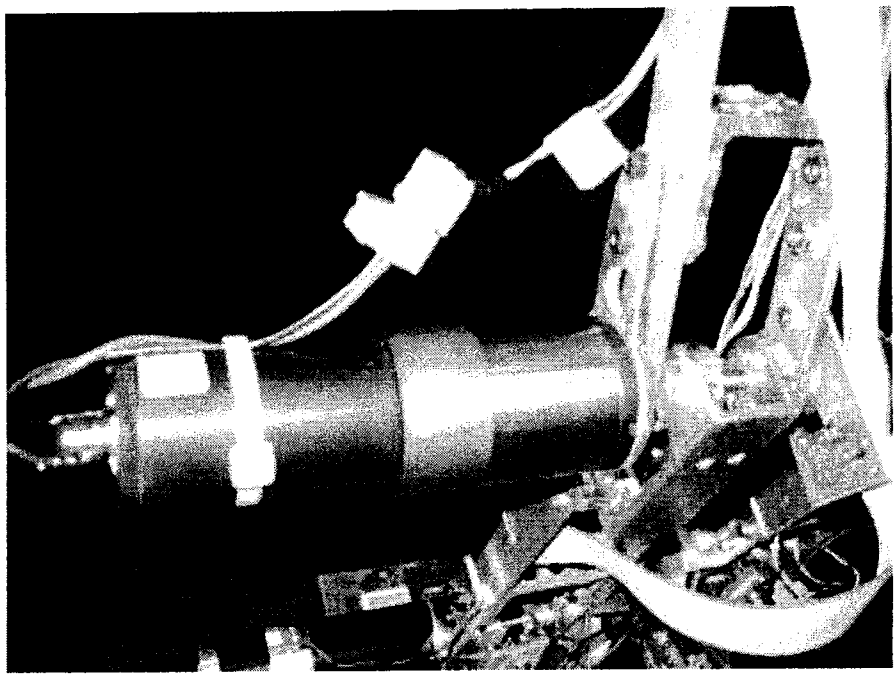

Fig. 4-4 The knee joint 1

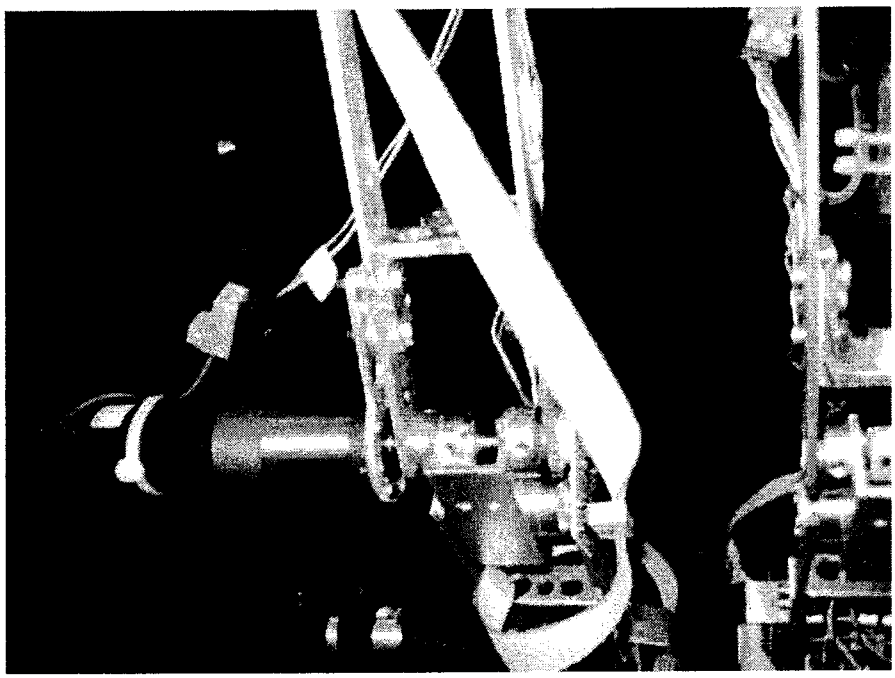

Fig. 4-5 The knee joint 2

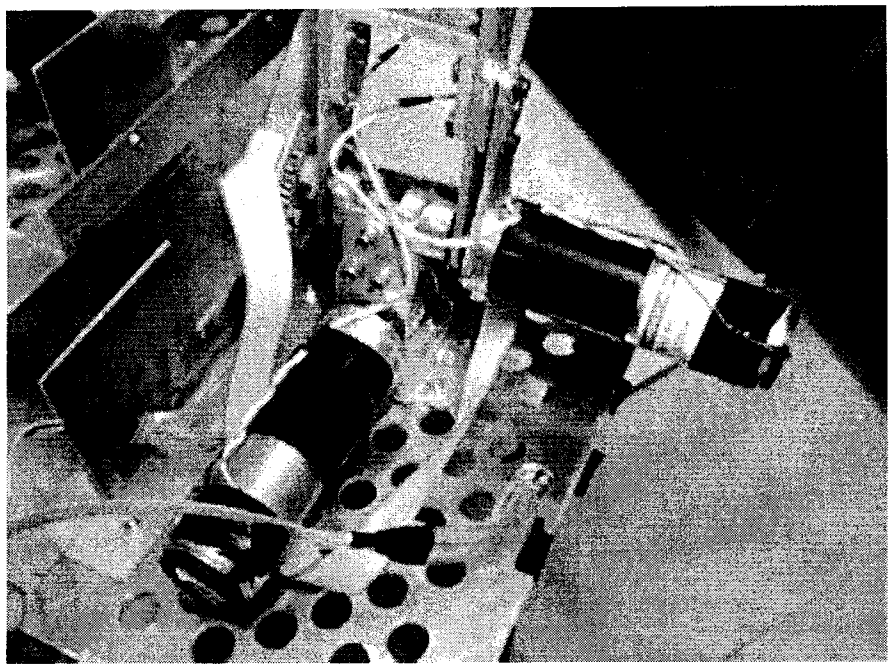

Fig. 4-6 The ankle joints

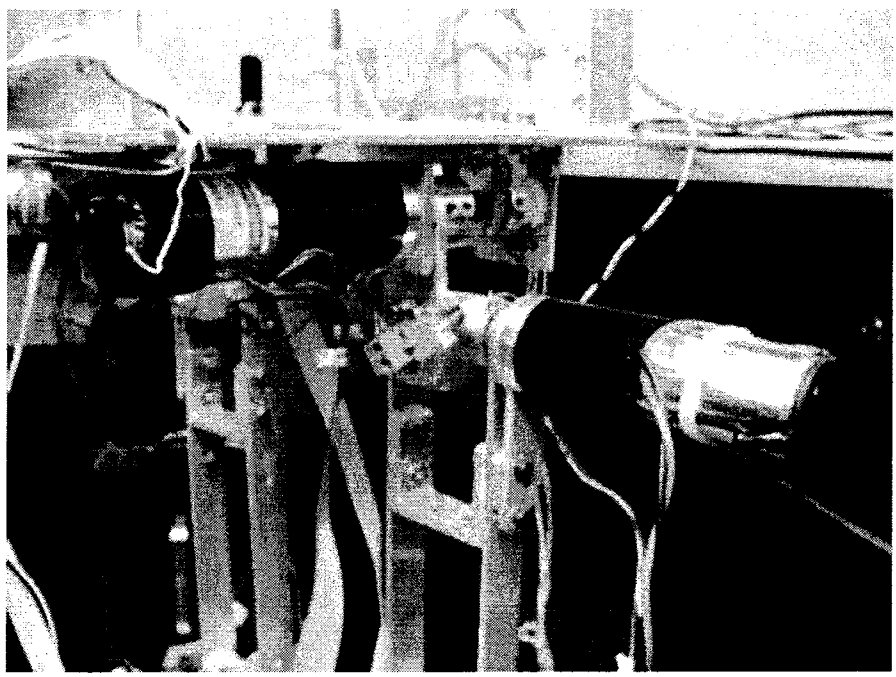

Fig. 4-7 The hip joints

4.1.3 Sensors Selection

4.1.3.1 Potentiometers

The most important information required for robot control is joint position feedback. Both potentiometers and encoders can be used to obtain this feedback signal. For this 10 DOF biped robot, the potentiometers are used. Compared to encoders, the potentiometers are cheaper, can reflect the angle position directly and don't need to set the initial value for the angle position after turning on the power.

The potentiometer (EVWAE4001B14 10K from Matsushita Electronic Components Co., Ltd., Osaka, Japan) used in the robot has very small size, lightweight, big operating range and good linearity. Fig. 4-8 shows the details about how the potentiometer is mounted to the joint.

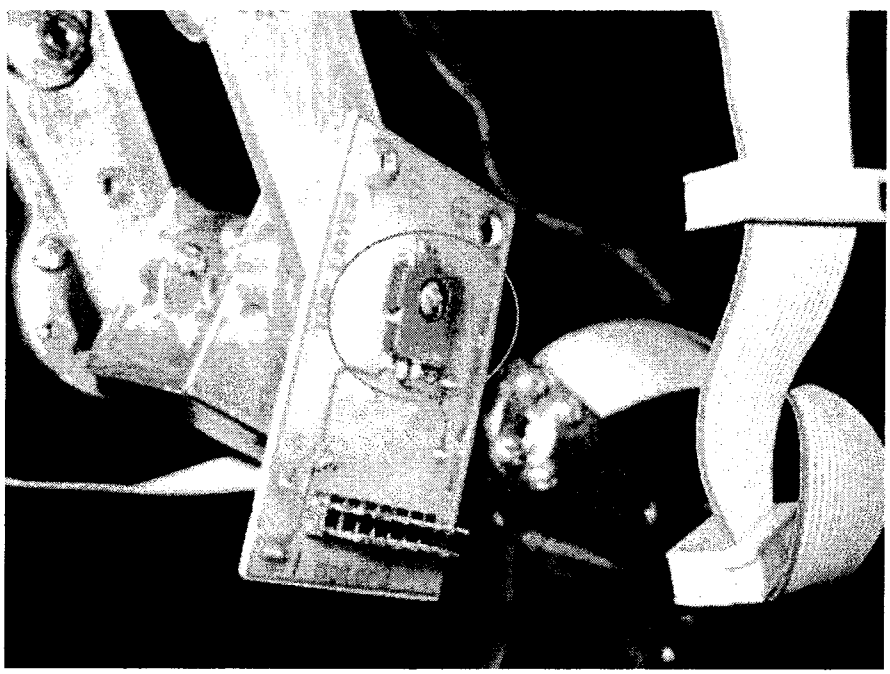

Fig. 4-8 Potentiometer structure

The desired trajectories for joint angles have the unit of degree. However, the feedback measurements from the potentiometer are voltage signals with the unit of volt. Therefore, the relationship between degree and voltage for every potentiometer has to be determined by doing the experiment. During the experiment, the voltage output value and corresponding rotating angle are recorded. The experiments were performed for all potentiometers in the range between 0 volt to 3 volt, which is the DSP board's ADC input range. About fifteen to twenty pairs of readings were taken and the MATLAB function polyfit was used to obtain the relationship of the angle in degrees and the voltage in volts. It is worth pointing out here that only slope of the relation between the angle in degrees and in voltage in volts will be used in the real system. Fig. 4-9 to Fig. 4-18 show the plots for the relationship between angles in degrees and voltages in volts. The legend "measured" represents the curve generated with the measured data while "polyfit" denotes the curve calculated with the polyfit function. It can be observed that the errors caused by the polyfit function are small.

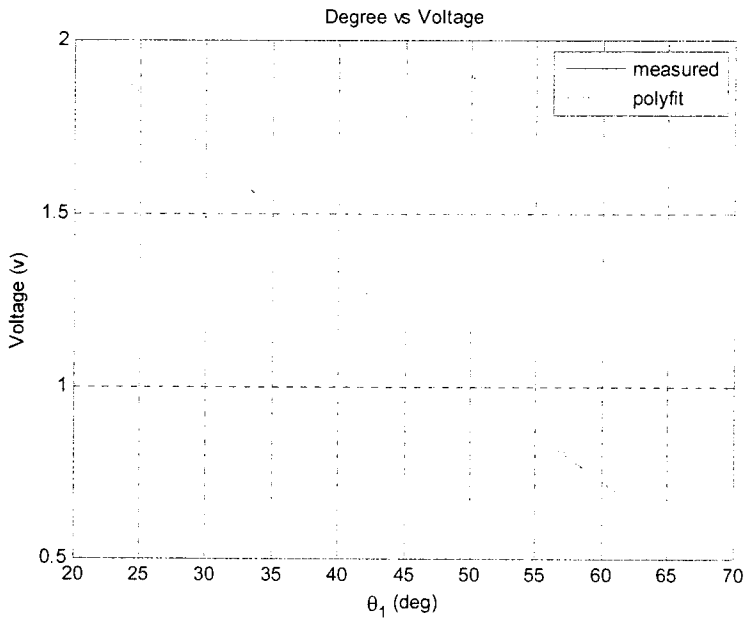

Fig. 4-9 Joint O_1 potentiometer

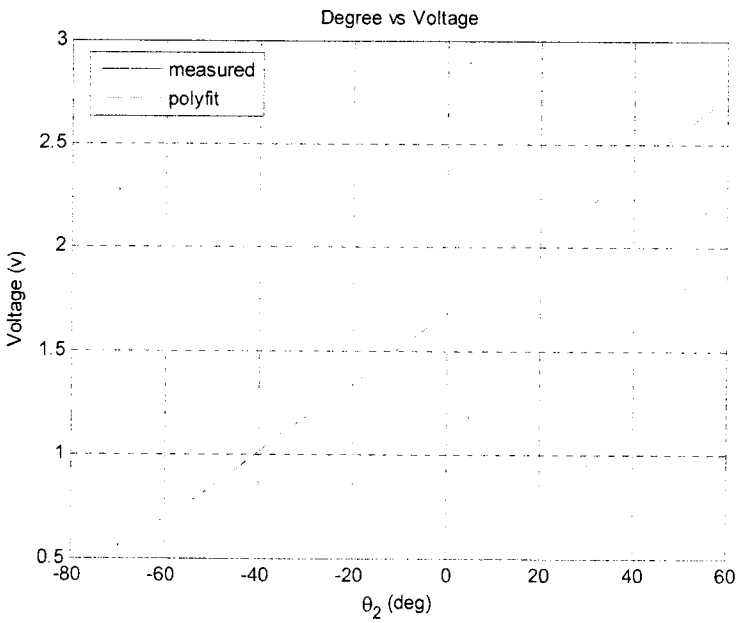

Fig. 4-10 Joint O_2 potentiometer

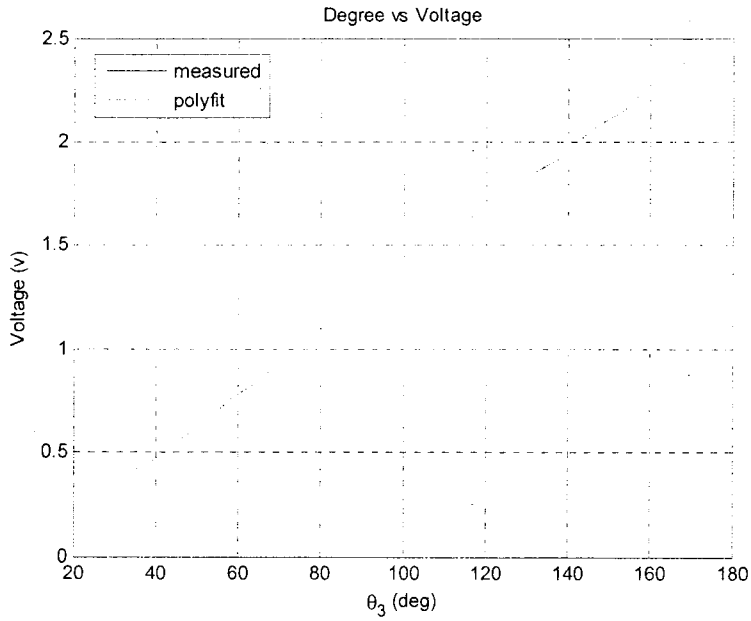

Fig. 4-11 Joint O_3 potentiometer

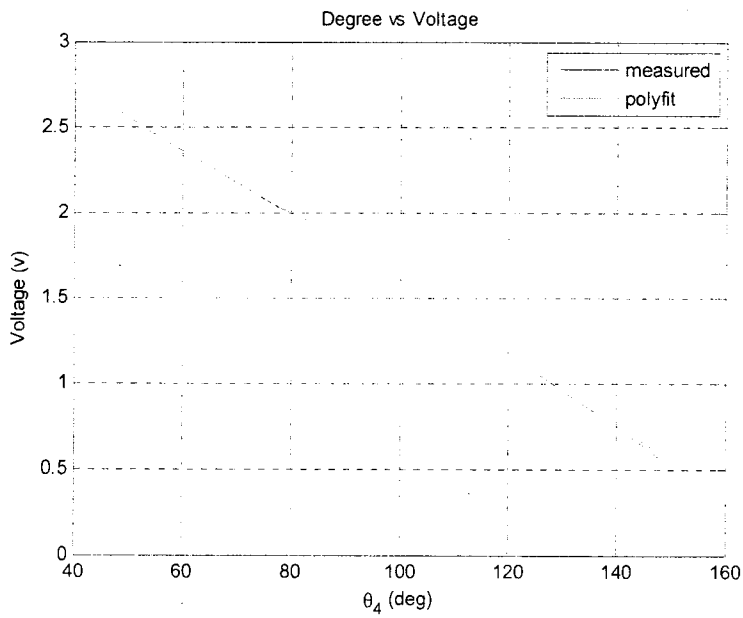

Fig. 4-12 Joint O_4 potentiometer

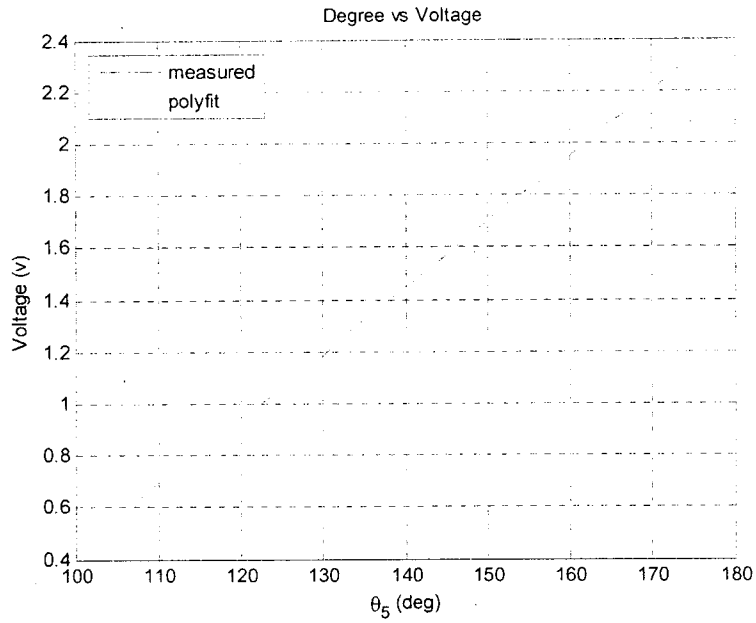

Fig. 4-13 Joint O_5 potentiometer

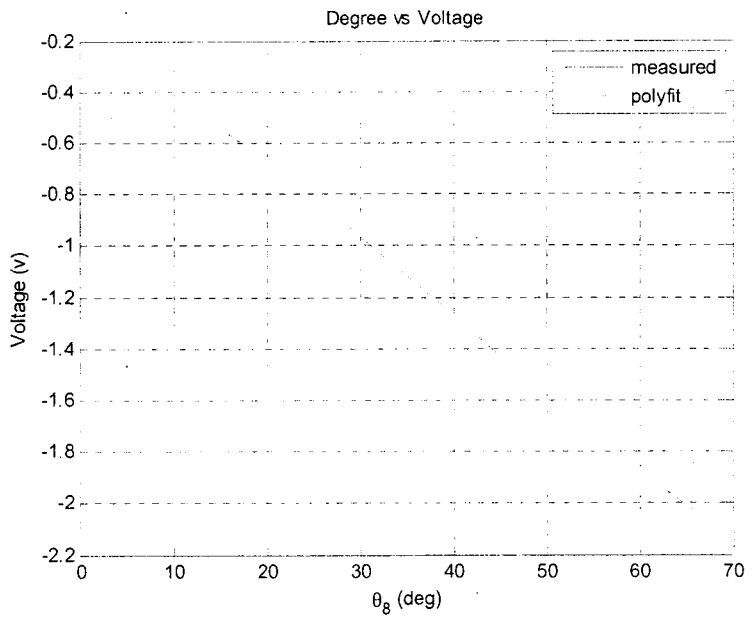

Fig. 4-14 Joint O_8 potentiometer

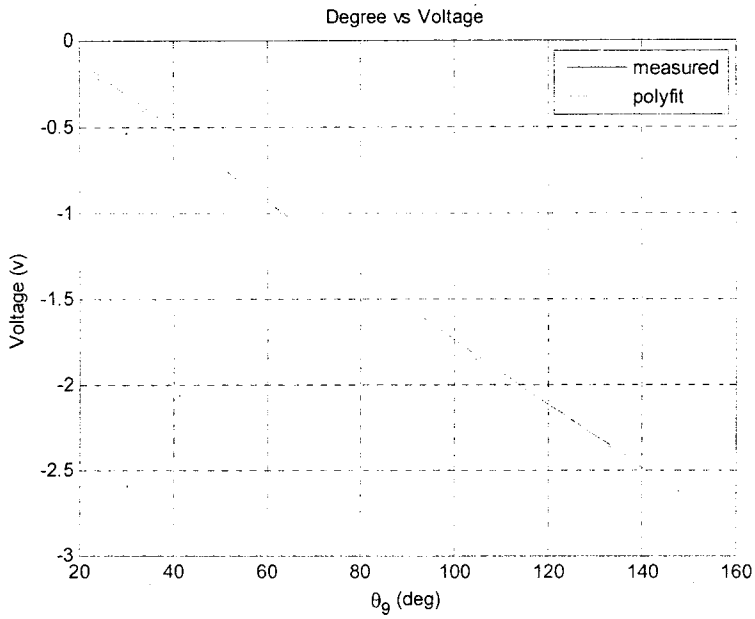

Fig. 4-15 Joint O_9 potentiometer

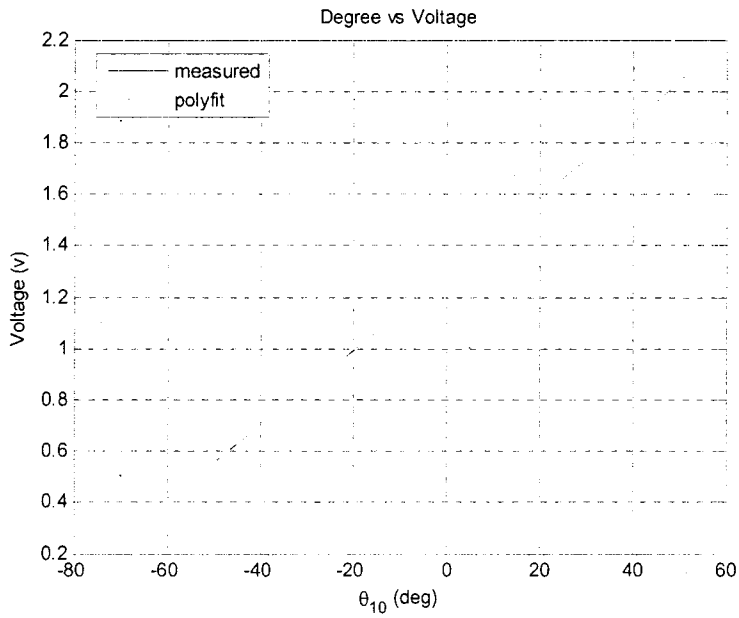

Fig. 4-16 Joint O_{10} potentiometer

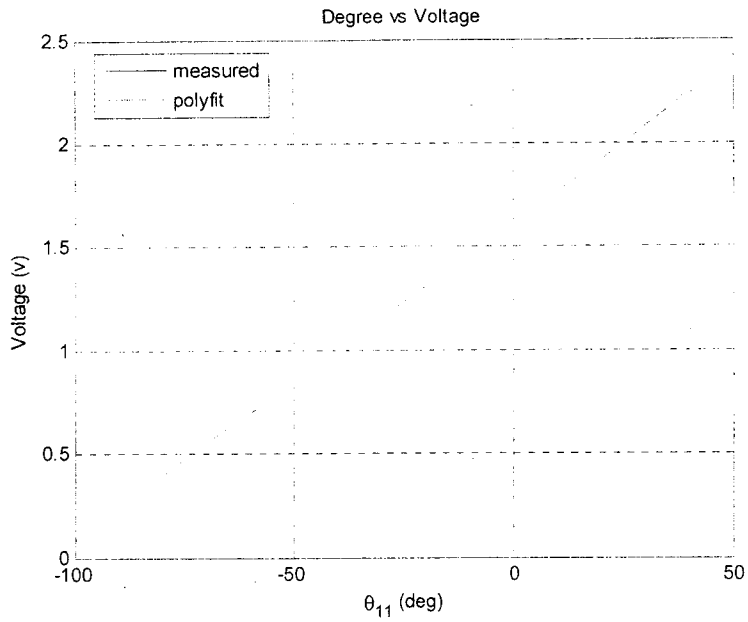

Fig. 4-17 Joint O_{11} potentiometer

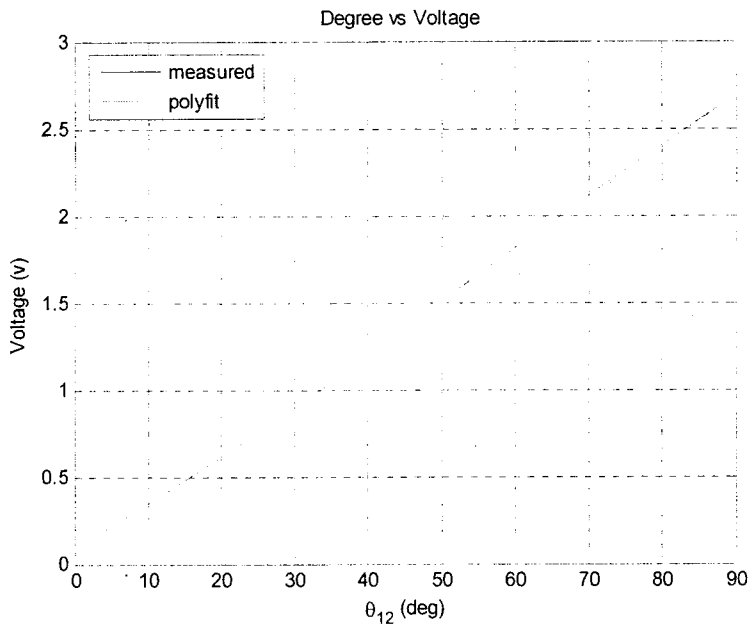

Fig. 4-18 Joint O_{12} potentiometer

The desired trajectories plotted in §3.6.2.1 are the angles in degrees against time. To convert these desired trajectories in degrees into voltages, the slope values determined from Fig. 4-9 to Fig. 4-18 are used. For the y-axis intercept, the voltages corresponding to zero degrees for each joint angle can be measured by setting all the joint angles to zero degrees and taking the voltage readings. The values of the slope and y-axis intercept for each joint variable are listed in Table 4-2.

Table 4-2 Coefficients for Conversion from Degree to Voltage

	slope_av	**intercept_av**
Joint O_1	-0.0319	1.0681
Joint O_2	0.0168	1.6509
Joint O_3	0.0148	0.5435
Joint O_4	-0.0204	1.6369
Joint O_5	0.0253	1.3766
Joint O_8	-0.0295	1.3154
Joint O_9	-0.0196	1.4737
Joint O_{10}	0.0148	2.0122
Joint O_{11}	0.0155	1.5414
Joint O_{12}	0.0295	1.6369

According to Table 4-2, the relation between voltage and degree is:

$$Voltage = \text{slope\_av} \times Degree + \text{intercept\_av} \qquad (4\text{-}1)$$

From Equation (4-1), the trajectories designed in Chapter 3 can be converted from degree to voltage. The voltage trajectories are the actual trajectories used in software design and digital controller design.

See Fig. 3-18 to Fig. 3-27 in §3.6.2.2 for the desired voltage trajectories.

4.1.3.2 Force Sensor

Another important information is the force information on the foot. In this robot design, four force sensors (Tekscan's FlexiForce Sensors A201-25) are installed on each foot sole. The loading force range is 0 lb to 25 lb (111.2 N). The conductance (1/R) between two leads of the force sensor will change linearly, while the loading force changes. Fig. 4-19 [21] shows the curve of force and conductance.

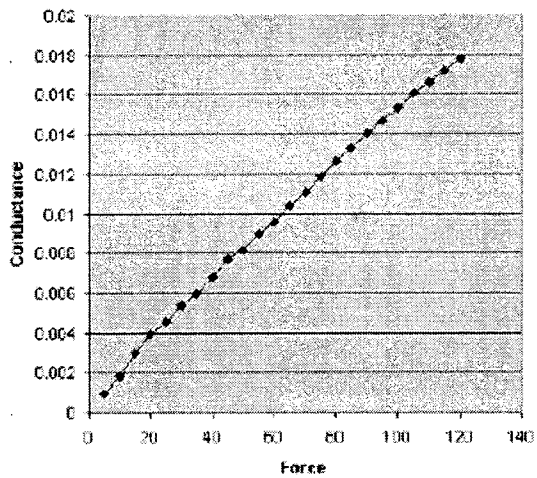

Fig. 4-19 Force vs. conductance for FlexiForce sensor

Force sensors will detect the contact force between the foot soles and the ground. The measurements could be used to determine the ZMP of the robot. The ZMP information is required to perform active balance control for the biped robot. The robot will adjust its ZMP actively to keep balance during the walking process.

For this robot system, the force sensors are not used in control algorithm, but they are installed onto the robot feet. The electric circuit for force sensors is also designed for the future use.

4.1.4 Limit Switch Protection

For each joint, a limit switch is installed to protect the motor and the joint. All the limit switches are connected in series. If any one of the limit switches is triggered, the power to the biped robot will be cut off. The limit switch used in the biped robot is Panasonic Detector Switch ESE 24. It is very small and easy to mount. A plastic plate is glued to each joint to trigger the limit switch.

See Fig. 4-20 for the detailed structure for the limit switch.

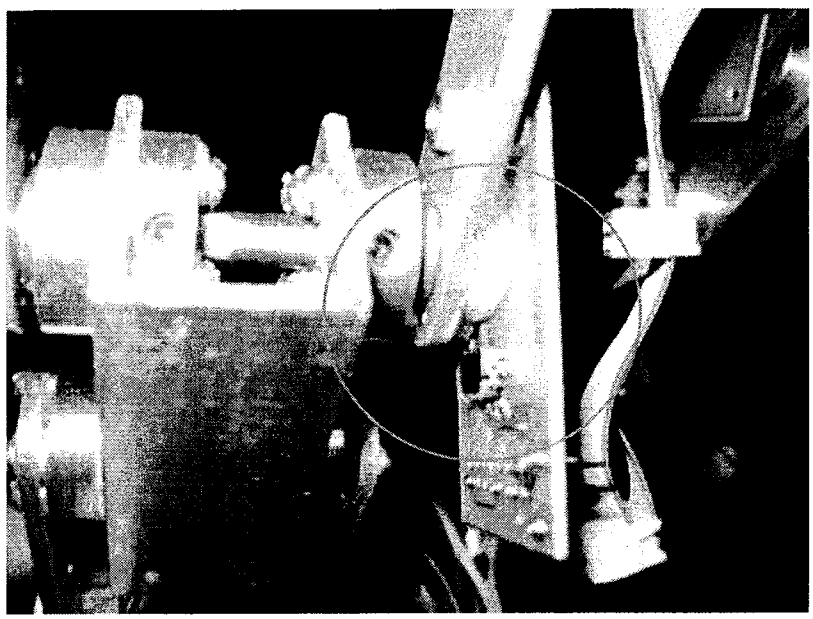

Fig. 4-20 Limit switch structure

4.1.5 Foot Structure and Force Sensor Installation

The foot of the robot is made with a 140 mm-by-240 mm aluminum plate. There are many holes drilled on the plate, to reduce the weight of the foot. Rubber pieces are installed on each corner of the footplate to increase the friction between the sole and the ground and absorb impact when the foot contacts the floor. A force sensor is installed under each rubber piece.

See Fig. 4-21 and Fig. 4-22 for the details of the foot structure and force sensor installation.

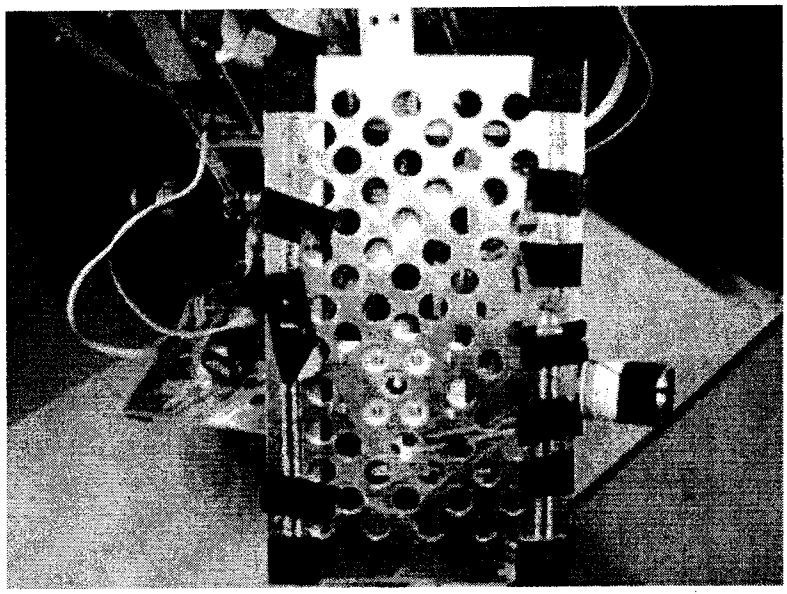

Fig. 4-21 Foot plate structure

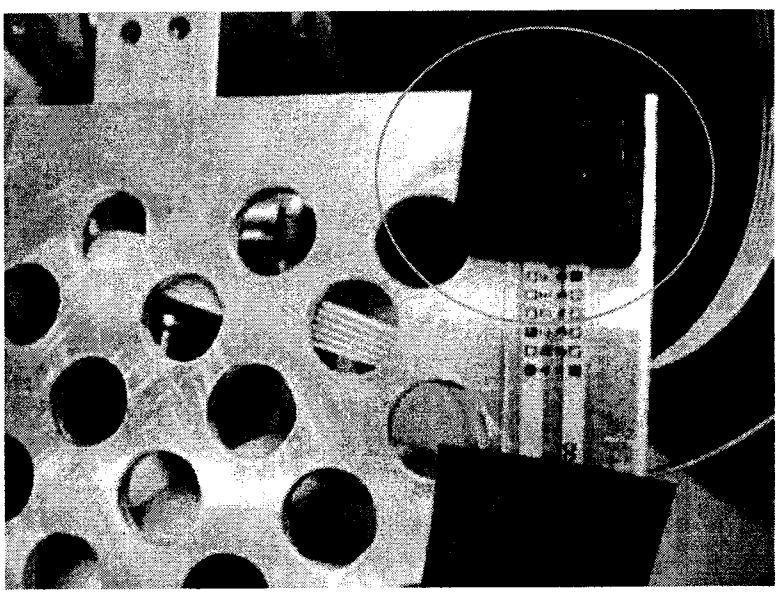

Fig. 4-22 Force sensor structure

4.1.6 Final Robot Prototype

Table 4-3 lists the parameters of the10 DOF biped robot prototype.

Table 4-3 Parameters of the 10 DOF Biped Robot

Weight		6941 g
Dimensions	Height	978.65 mm
	Width	432.84 mm
	Depth	268.35 mm
	Length of Shin	190 mm
	Length of Thigh	270 mm
	Height of Body	390.38 mm
DOF	Ankle	2 x 2
	Knee	1 x 2
	Hip	2 x 2
	Total	10 DOF

4.2 Electrical Design

4.2.1 Control Hardware

Two eZdspTMF2812 develop boards from Spectrum Digital Inc, based on TMS320F2812 Digital Signal Processor (DSP) from Texas Instruments, are used to control the biped robot. Each leg is controlled by one eZdspTMF2812. It reads feedback signals, calculates the desired trajectories and the error signals, and generates the control signals. This DSP board has following key features [22]:

Motor Control Peripherals

Two Event Managers (EVA, EVB) can drive up to 10 motors.

Serial Port Peripherals

Serial Peripheral Interface (SPI) is used to communicate between two DSP boards.

Serial Communications Interface (SCI) is used to communicate between DSP board and computer.

12-Bit Analog-to-Digital Converter (ADC)

The board has 16 ADC channels. The feedback signals from the joint potentiometers and force sensors are connected to ADC inputs on the DSP board.

Up to 56 General Purpose I/O (GPIO) Pins

The direction signals for motor drivers and the relay signal to turn on the system power are connected to some of the GPIO pins.

On board 3.3V output

The DSP board can provide 3.3V, which is used as the power supply for electronics circuits.

A table summarizing the system connections on DSP board is shown in Table 4-4.

Table 4-4 System Connections on DSP Board

	Feedback	ADC	PWM	Direction	Activation
DSP #1 Master Right Leg	O_1	ADCINA0	PWM1	GPIO A9	GPIO A8
	O_2	ADCINA1	PWM3	GPIO A10	
	O_3	ADCINA2	PWM5	GPIO A11	
	O_4	ADCINA3	PWM7	GPIO A12	
	O_5	ADCINA4	PWM9	GPIO A13	
	FS1	ADCINA6			
	FS2	ADCINA7			
	FS3	ADCINB0			
	FS4	ADCINB1			
DSP #2 Slave Left Leg	O_8	ADCINA0	PWM1	GPIO A9	GPIO A8
	O_9	ADCINA1	PWM3	GPIO A10	
	O_{10}	ADCINA2	PWM5	GPIO A11	
	O_{11}	ADCINA3	PWM7	GPIO A12	
	O_{12}	ADCINA4	PWM9	GPIO A13	
	FS1	ADCINA6			
	FS2	ADCINA7			
	FS3	ADCINB0			
	FS4	ADCINB1			

In the table, "FS" stands for Force Sensor. See §4.2.4 for detailed connections between two DSP board by using SPI communication.

See Appendix C for the block diagram and layout schematics of eZdspTMF2812 DSP board [23].

4.2.2 Analog Signal Conditioning

There are 10 potentiometers connected with motor shafts to provide the voltage feedback signals. A voltage of 3.3V is connected to those potentiometers, so the voltage feedback readings will vary from 0 to 3.3V.

The voltage feedback signals can be directly connected to DSP ADC inputs, because the input voltage range for DSP is also from 0 to 3V. However, the range of the

feedback signals from the potentiometers is much less than the range from 0 to 3.3V. In order to improve the control accuracy, a differential amplifier circuit as shown in Fig. 4-23 is used to amplify the feedback signals before connected to DSP board ADC inputs.

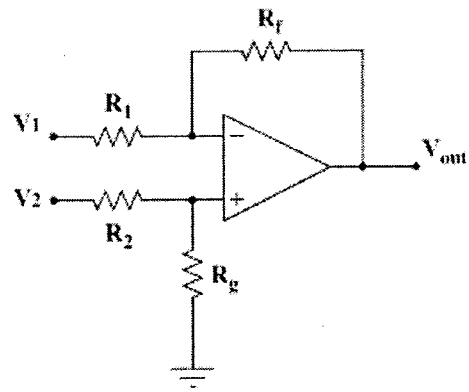

Fig. 4-23 Differential amplifier

The output voltage from this amplifier can be calculated as

$$V_{out} = V_2(\frac{(R_f + R_1)R_g}{(R_g + R_2)R_1}) - V_1\frac{R_f}{R_1} \tag{4-2}$$

In the Fig. 4-23 V_1 is considered as the reference voltage V_r. V_2 is the feedback voltage V_{in}. The maximum and minimum values of V_{in} can be measured from the potentiometer output denoted as V_{in_max} and V_{in_min}. Let V_{o1} and V_{o2} denote the output voltages for the inputs of V_{in_max} and V_{in_min} respectively, and set R_g=R_2 and G=R_f/R_1. Then, it follows from Equation (4-2) that

$$\begin{cases} V_{o1} = (G+1)V_{in\_min}/2 - GV_r \\ V_{o2} = (G+1)V_{in\_max}/2 - GV_r \end{cases} \tag{4-3}$$

from which, the gain G and the reference voltage V_r can be calculated as

$$\begin{cases} G = \dfrac{V_{o1} - V_{o2}}{V_{in\_\min}/2 - V_{in\_\max}/2} - 1 \\ V_r = \dfrac{(G+1)(V_{in\_\min}/2) - V_{o1}}{G} \end{cases} \tag{4-4}$$

OP295 dual CBCMOS operational amplifier is used because it can operate with single supply from 3V to 36V. Each chip contains two operational amplifiers. In this analog signal conditioning circuit, one operational amplifier is used as a voltage follower to avoid loading effect. Another one is used as a differential amplifier. Each DSP board has 16 ADC channels; therefore, there are 16 OP295s on the analog signal conditioning board.

See Appendix D for the analog signal conditioning schematics.

4.2.3 Motor Driver

H-bridge LMD18200 is used as a motor driver. It can deliver up to 3A continuous current and operates at a supply voltage up to 55V. It is controlled by two inputs, direction and pulse-width modulation (PWM). Fig. 4-24 [24] shows the relation between the output voltage and the DIRECTION and PWM. It can be seen from Fig. 4-24 that the duty-cycle of PWM is used to control the output voltage. On the other hand, DIRECTION is used to control the direction of the output current, i.e. the direction of motor rotation. The larger the duty-cycle the higher the output voltage and the bigger the output current. Furthermore, the sign changes from 1 to 0 will reverse the direction of the rotation of the motor.

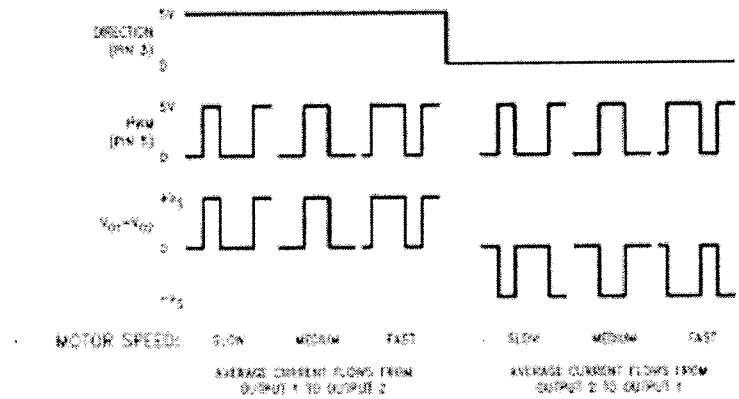

Fig. 4-24 Sign/magnitude PWM control

DIRECTION and PWM from LMD18200 are connected to the DSP board. The BRAKE input on the LMD18200 is always connected to a logic "low" signal to enable the H-bridge.

To replace the H-bridge easily, a small adaptor board is designed and implemented for each H-bridge.

See Appendix D for the motor driver and H-bridge adaptor schematics.

4.2.4 Communication

There are five motors for each leg of the robot. Two DSP boards are used, one for each leg. The Serial Peripheral Interface (SPI) is used to transfer data between two DSP boards. The SPI is a high-speed synchronous serial I/O port, which allows a serial bit stream of programmed length (one to sixteen bits) to be shifted into and out of the device at a programmable bit-transfer rate. Normally, the SPI is used for communications between the DSP controller and external peripherals or another processor. Its typical applications include external I/O or peripheral expansion through devices such as shift registers, display drivers, and ADCs. Multi-device communications are supported by the master/slave operation of the SPI. The DSP board for the right leg is set to be the master

board while the DSP board for the left leg is used as the slave board. Fig. 4-25 shows the connections between two DSP boards.

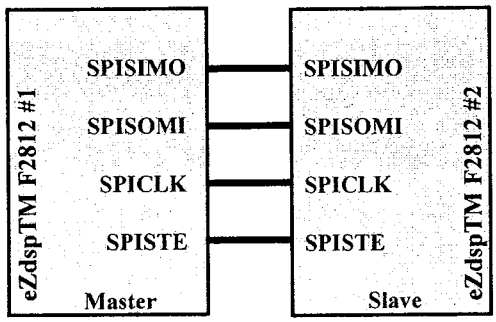

Fig. 4-25 SPI communication between two DSP boards

The Serial Communications Interface (SCI) is used for transferring data between DSP boards and PC computers. The SCI is a two-wire asynchronous serial port. The communication is implemented by EIA-232 driver MAX232.

See Appendix D for the communication circuit schematics.

4.2.5 Potentiometer Feedback and Limit Switch

The 3.3V power supply coming from the DSP boards is connected to one lead of the 10K potentiometer. The voltage feedback is taken from the middle lead. The third lead is connected to the ground.

There are three leads on a limit switch. The middle one is connected to 3.3V, which is used to generate logic "high" signal. The other two leads are connected to ground. Therefore, the output from the limit switch is normally logic "high". It will switch to logic "low" when the limit switch is triggered.

The potentiometer and limit switch are mounted on a small circuit board. The small circuit boards are attached to the motor shaft.

See Appendix D for the potentiometer feedback and limit switch schematics.

4.2.6 System Activation and Protection

The system activation and protection circuit is built with logic gates and relays (Omron General-Purpose Relay SPDT LY1-0). If there is a logic "high" fed to the relay circuit, the relay will close and the system will be powered on. Otherwise, there is no power for the system.

For activation, after running the control program, the system will wait three second, and then DSP will send a logic "low" out to turn on the system power.

For protection, the relay will open if there is a logic "low" coming from the limit switches. For each joint, there will be a limit switch to prevent the motor from overturning, which may damage the gears or other mechanical parts of the joint. All the limit switches are connected in series. If any one of the limit switches is triggered, the power will be cut off for the whole system. The signal from limit switches is normally "high", and it becomes "low" as soon as it is triggered.

Fig. 4-26 shows the logic gate schematics for activation and protection signal, which is fed to the relay circuit.

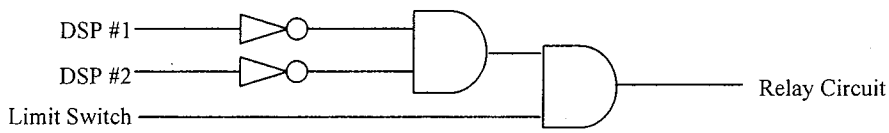

Fig. 4-26 Logic gate schematic for activation and protection circuit

See Appendix D for the activation and protection circuit schematics.

4.2.7 Force to Voltage Converter

The FlexiForce sensor is a force-sensitive resistor. Therefore, to integrate the force sensor into an application, a force-to-voltage circuit is used.

Fig. 4-27 shows the schematics for force-to-voltage circuit.

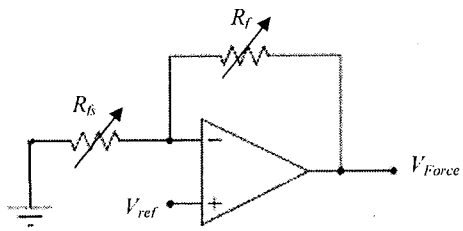

Fig. 4-27 Force-to-voltage conversion circuit

The output of the force-to-voltage circuit is given by

$$V_{Force} = \left(1 + \frac{R_f}{R_{fs}}\right) V_{ref} \tag{4-5}$$

where R_f is the feedback resistance, V_{ref} is the reference voltage. R_{fs} represents the resistance feedback from the force sensor.

The voltage signals from the force-to-voltage circuit will be fed to the analog signal conditioning circuit designed in §4.2.2.

See Appendix D for the force-to-voltage circuit schematics.

4.3 PCB Design, Fabricate and Assembly

The software called ExpressPCB (version 6.1.4) is used to design the Printed Circuit Board (PCB). It is a free software (refer to http://www.expresspcb.com/index.htm for details). The software package contains two part: ExpressSCH and ExpressPCB.

ExpressSCH is ued to draw the schematic diagram and ExpressPCB is used to draw the PCB layout. These two parts can link to each other, which makes it easier to draw connection lines in the PCB layout.

The PCBs are designed as double-sided. The boards are fabricated in the University Electrical Lab.

The components are assembled on this double-sided PCB. The PCB did not have copper plated through holes, so some component pins have to be soldered on both sides of the board. Although the ICs can be soldered directly into the PCB, the sockets for the IC chips are used, because it is easy for troubleshooting and replacement. All the via holes are fitted with short pieces of wire.

See Appendix E for the PCB art work and components layout diagrams.

The size of the PCB are designed in a way that it can fit into the robot body. All the boards, including DSP boards, are mounted together by the 25 mm plastic standoff. It will provide enough space for inter-wiring.

Fig. 4-28 shows the details for the structure of the system circuit board.

See Appendix H for the I/O ports description for each board and Appendix I for the electric circuit boards inter-wiring schematics.

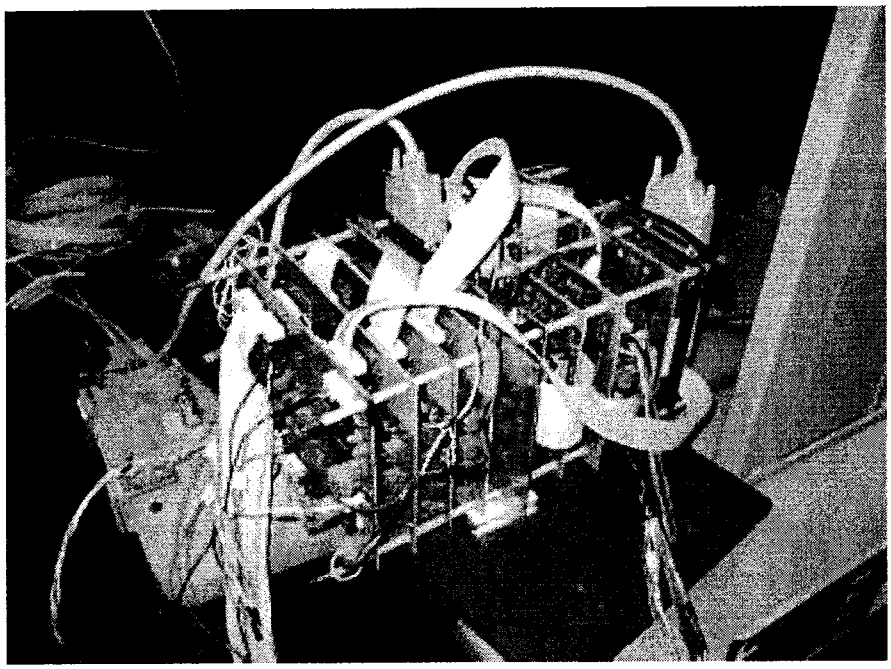

Fig. 4-28 System circuit boards structure

Chapter 5

Control Program Design

Two eZdspTMF2812 DSP boards are used to control the biped robot, one for each leg. Fig. 5-1 shows the flow chart of the control program for each leg. Each function block in the flow chart will be explained in details in the following sections. The software used to perform the robot control is MATLAB Simulink. See Appendix F for Simulink programs.

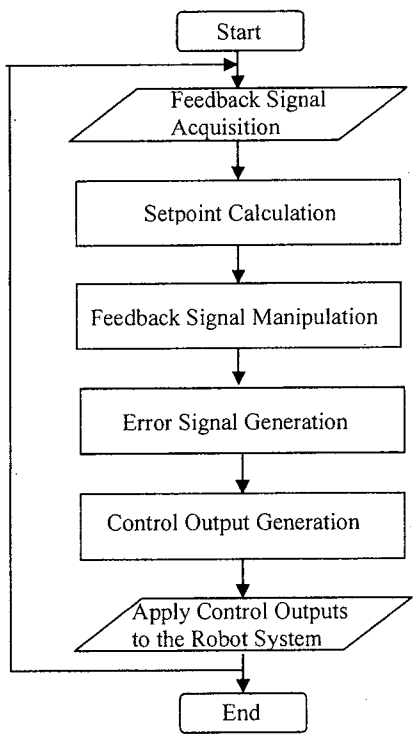

Fig. 5-1 The flow chart of the control program

5.1 Setpoint Calculation

The setpoint is the instantaneous desired joint angle for each joint variable during the biped robot walking. The setpoints for the joint angles are calculated at every sampling time. The sampling rate for the robot control program is set to 0.001 second.

For the joints O_1, O_5, O_8 and O_{12}, the setpoints for the periods of weight shifting are calculated by using Equation (3-2). The weight shifting periods include the period that the robot shifts the weight to the support leg and the period that the robot shift weight back. The duration of the weight shifting period is the value of T_c_SW in Table 3-1.

For the joints O_2, O_3, O_4, O_9, O_{10} and O_{11}, the setpoints for the single-support phase are calculated by Equation (3-2). The single-support phase includes both single support phases with left leg support and right leg support. The duration of the single-support phase is the value of T_c in Table 3-1.

The following constraints should be satisfied while calculating the setpoints for the joints:

$$V(t)=\begin{cases} v_{11}=V(t_1), & t=t_1 \\ v_{12}=V(t_2), & t=t_2 \\ v_{13}=V(t_3), & t=t_3 \end{cases} \tag{5-1}$$

In Equation (5-1) t_1 is the time instant when the weight shifting phase or the single-support phase starts, t_3 denotes the time instant when the weight shifting phase or the single-support phase ends, and $t_2=(t_1+t_3)/2$. The values for t_1, t_2 and t_3 are read from Fig. 3-18 to Fig. 3-27, and v_{11}, v_{12} and v_{13} are the voltages corresponding to t_1, t_2 and t_3. Table 5-1 lists the time and the corresponding voltages for the joints O_1, O_5, O_8 and O_{12}, and

Table 5-2 lists the time and the corresponding voltages for the joints O_2, O_3, O_4, O_5, O_8, O_9, O_{10} and O_{11}.

Table 5-1 Time and Corresponding Voltages for Joints O_1, O_5, O_8 and O_{12}

Joint		Shift Weight to the Left Leg	Shift Weight Back	Shift Weight to the Right Leg	Shift Weight Back
	t_1 (s)	15	31	43	59
	t_2 (s)	18	34	46	62
	t_3 (s)	21	37	49	65
O_1	v_{11} (v)	1.0681	1.5466	1.0681	0.5896
	v_{12} (v)	1.3074	1.3074	0.8289	0.8289
	v_{13} (v)	1.5466	1.0681	0.5896	1.0681
O_5	v_{11} (v)	1.3766	1.7561	1.3766	1.0477
	v_{12} (v)	1.5663	1.5663	1.2122	1.2122
	v_{13} (v)	1.7561	1.3766	1.0477	1.3766
O_8	v_{11} (v)	1.3154	1.6989	1.3154	0.8729
	v_{12} (v)	1.5071	1.5071	1.0942	1.0942
	v_{13} (v)	1.6989	1.3154	0.8729	1.3154
O_{12}	v_{11} (v)	1.6369	2.0794	1.6369	1.1944
	v_{12} (v)	1.8582	1.8582	1.4157	1.4157
	v_{13} (v)	2.0794	1.6369	1.1944	1.6369

Table 5-2 Time and Corresponding Voltages for Joints O_2, O_3, O_4, O_5, O_8, O_9, O_{10} and O_{11}

Joint		Single-Support Phase with Left Leg Support	Single-Support Phase with Right Leg Support
	t_1 (s)	23	51
	t_2 (s)	26	54
	t_3 (s)	29	57
O_2	v_{11} (v)	1.1896	1.2690
	v_{12} (v)	1.0756	1.2388
	v_{13} (v)	1.2690	1.1896
O_3	v_{11} (v)	1.1644	1.1662
	v_{12} (v)	1.3955	1.1279
	v_{13} (v)	1.1662	1.1644
O_4	v_{11} (v)	1.9327	2.0315
	v_{12} (v)	2.1127	1.9421
	v_{13} (v)	2.0315	1.9327
O_5	v_{11} (v)	1.7561	1.0477
	v_{12} (v)	1.7561	1.111
	v_{13} (v)	1.7561	1.0477
O_8	v_{11} (v)	1.6989	0.8729
	v_{12} (v)	1.6251	0.8729
	v_{13} (v)	1.6989	0.8729
O_9	v_{11} (v)	1.0851	1.1452
	v_{12} (v)	1.1640	1.0165
	v_{13} (v)	1.1452	1.0851
O_{10}	v_{11} (v)	1.3871	1.3823
	v_{12} (v)	1.4376	1.1544
	v_{13} (v)	1.3823	1.3871
O_{11}	v_{11} (v)	1.8844	1.9369
	v_{12} (v)	1.8942	2.0721
	v_{13} (v)	1.9369	1.8844

From Equation (5-1), Table 5-1 and Table 5-2, the coefficients (c_1 c_2 .... c_8) can be determined by using the third-order spline interpolation method described in §3.1. The desired trajectories in voltages can be calculated by using Equation (3-2), that is,

$$\begin{cases} p_1(t) = c_1 + c_2(t-t_1) + c_3(t-t_1)^2 + c_4(t-t_1)^3, & t_1 \le t \le t_2 \\ p_2(t) = c_5 + c_6(t-t_2) + c_7(t-t_2)^2 + c_8(t-t_2)^3, & t_2 \le t \le t_3 \end{cases}$$

The setpoints for joints O_1 and O_{12} are kept constant if the biped robot is not in the weight shifting phase. The setpoints for joints O_5, O_8 are kept constant if the biped robot is neither in the weight shifting phase nor in the single-support phase. Moreover, the setpoints for joints O_2, O_3, O_4, O_9, O_{10} and O_{11} are kept constant if the biped robot is not in the single-support phase. The constant setpoints for the joints are listed in Table 5-3, Table 5-4, Table 5-5 and Table 5-6.

Table 5-3 Constant Setpoints for Joints O_1 and O_{12}

Joint	Before 15 Second	21 - 31 Second	37 - 43 Second	49 - 59 Second	65 - 69 Second
Setpoint for O_1 (v)	1.0681	1.5466	1.0681	0.5896	1.0681
Setpoint for O_{12} (v)	1.6369	2.0794	1.6369	1.1944	1.6369

Table 5-4 Constant Setpoints for Joint O_5

Joint	Before 15 Second	21 - 31 Second	37 - 43 Second	49 - 51 and 57 - 59 Second	65 - 69 Second
Setpoint for O_5 (v)	1.3766	1.7561	1.3766	1.0477	1.3766

Table 5-5 Constant Setpoints for Joint O_8

Joint	Before 15 Second	21 - 23 and 29 - 31 Second	37 - 43 Second	49 - 59 Second	65 - 69 Second
Setpoint for O_8 (v)	1.3154	1.6989	1.3154	0.8729	1.3154

Table 5-6 Constant Setpoints for Joints O_2, O_3, O_4, O_9, O_{10} and O_{11}

Joint	Before 23 Second	29 - 51 Second	57 - 69 Second
Setpoint for O_2 (v)	1.1896	1.2690	1.1896
Setpoint for O_3 (v)	1.1644	1.1662	1.1644
Setpoint for O_4 (v)	1.9327	2.0315	1.9327
Setpoint for O_9 (v)	1.0851	1.1452	1.0851
Setpoint for O_{10} (v)	1.3871	1.3823	1.3871
Setpoint for O_{11} (v)	1.8844	1.9369	1.8844

5.2 Feedback Signal Acquisition and Manipulation

For each leg, the feedback signals from the biped robot include five signals from the joint potentiometers and four signals from the force sensors. Those signals are fed to ADC inputs of eZdspTMF2812. eZdspTMF2812 has 16 channels of 12-bit analog-to-digital converters, so the output of ADC is a number in the range from 0 to 4095 (FFF in hex). On the other hand, the voltage input to ADC ranges from 0 to 3V. Therefore, the ADC output needs to multiply a scaling factor of 3/4095 to get the corresponding voltage value.

The readings from the ADC outputs can not be used directly for controller design because they are corrupted with noise. A first order digital low pass filter with a cutoff frequency of about 3.3Hz is used to filter out the unnecessary noise and make the signal more stable. The digital filter is implemented by

$$y_k = \frac{T_s}{\tau + T_s}\left(\frac{3}{4095}x_k\right) + \frac{\tau}{\tau + T_s}y_{k-1} \tag{5-2}$$

where $\tau = 0.3$, $T_s = 0.001$, x_k is the reading from the ADC output at the k-th sampling time, y_k is the output signal of the filter at the k-th sampling time, and y_{k-1} is the output signal of the filter at the $(k\text{-}1)^{th}$ sampling time.

5.3 Control Output Calculation

5.3.1 PD Control plus Gravity Compensation

The Proportional-Derivative (PD) controller is widely used in industrial robot control and is very simple to implement, so PD control is used to control the biped robot. The main control strategy is PD control plus gravity compensation (PWM Offset), where gravity compensation is used to cancel the effect of gravity force. The controller is applied to each joint independently. The control outputs from the controller are PWM and direction signals. Fig. 5-2 is the block diagram for the biped robot controller.

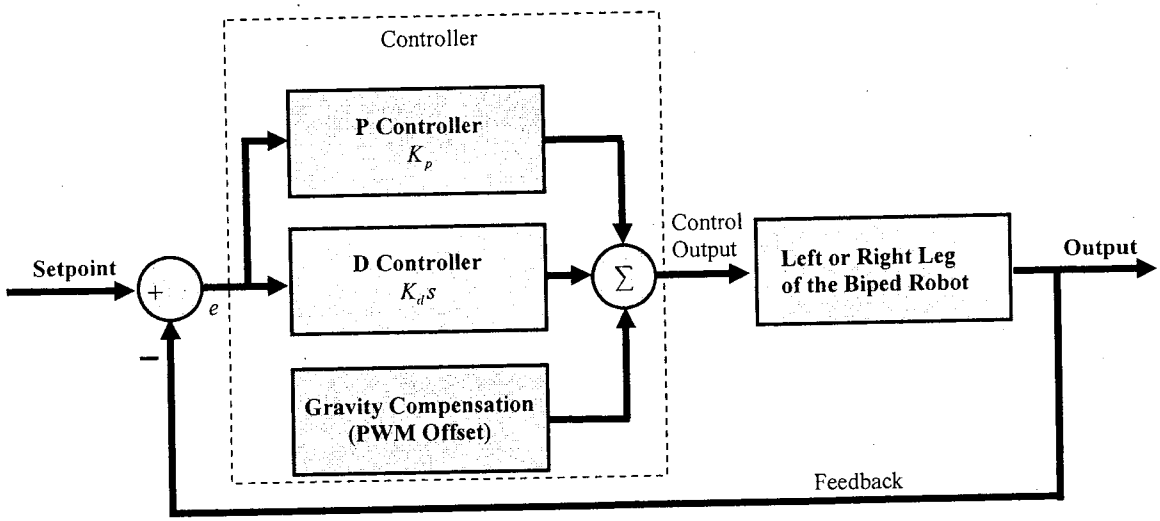

Fig.5-2 Block diagram for the biped robot controller

The transfer function of the practical PD controller is given by

$$C(s) = K_p + K_d \frac{s}{1+\tau s} \tag{5-3}$$

with the proportional gain K_p and the derivative gain K_d. After transforming Equation (5-3) to its discrete time counterpart with the sampling time T_s, the control output from the PD controller can be written as

$$u_k = K_p e_k + K_d \dot{e}_k \tag{5-4}$$

where $\dot{e}_k = \frac{1}{\tau + T_s}(\tau \dot{e}_{k-1} + e_k - e_{k-1})$ with the time constant $\tau = 0.3$ and the sampling time $T_s = 0.001$. In Equation (5-4), u_k is the controller output signal at the k-th sampling time, e_k is the error signal at the k-th sampling time, which is the difference between the setpoint signal and feedback signal at the k-th sampling time, e_{k-1} is the error signal at the $(k\text{-}1)^{th}$ sampling time.

The control signal, which is applied to the biped robot, is the PD controller output plus the PWM offset. The overall controller output is calculated by

$$PWM_k = u_k + PWM\_OS_k \tag{5-5}$$

where PWM_k represents the duty-cycle of the PWM signal at the k-th sampling time, which is the signal for the motor driver (the H-bridge LMD18200) and PWM_OS_k denotes the PWM offset at the k-th sampling time.

As indicated in §4.2.3, the motor driver requires two input signals, PWM and DIRECTION. The direction signal is a digital signal that provides the information about which way the motor will rotate. This signal depends on the polarity of PWM_k. If PWM_k is positive, the direction signal is logic "high"; if PWM_k is negative, the direction signal is logic "low".

The control signal PWM_k and direction signal are applied to every joint independently.

5.3.2 Control Parameter Tuning

For each joint, the proportional gain (K_p), the derivative gain (K_d) and PWM offset (*PWM_OS*) are different. These control parameters are also different in different timing periods, such as the single-support phase with left leg support or the weight shifting phase. The values for K_p, K_d and *PWM_OS* are determined by experiments. The dynamic modeling is not performed for this robot, because the exact mass center and the moment of inertia for each link are unknown. Therefore, the trial-and-error method is used to tune the values of K_p, K_d and *PWM_OS*. After each experiment, according to the control performance, the K_p, K_d and *PWM_OS* are tuned. The tuning process is repeated until a satisfactory control performance is achieved. In the end, the best control parameter combinations for all joint variables are obtained. Fig. 5-3 to Fig. 5-32 show the tuning results for K_p, K_d and *PWM_OS*.

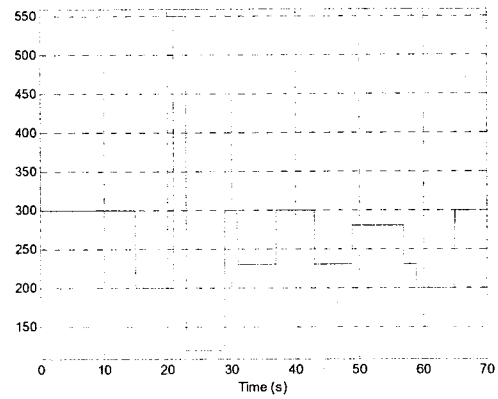

Fig. 5-3 P gain for joint O_{12}

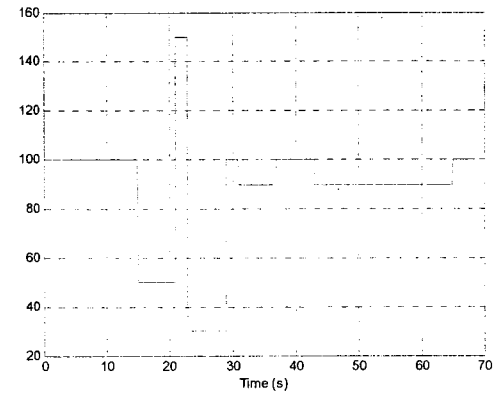

Fig. 5-4 D gain for joint O_{12}

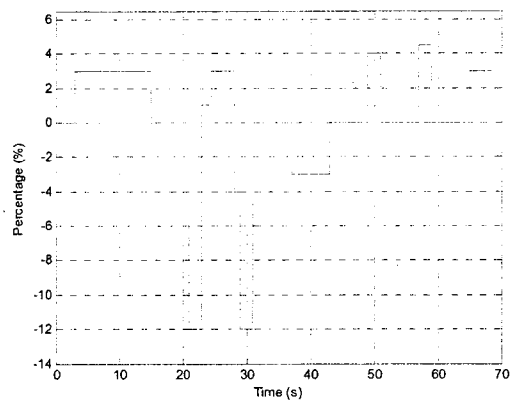

Fig. 5-5 PWM offset for joint O_{12}

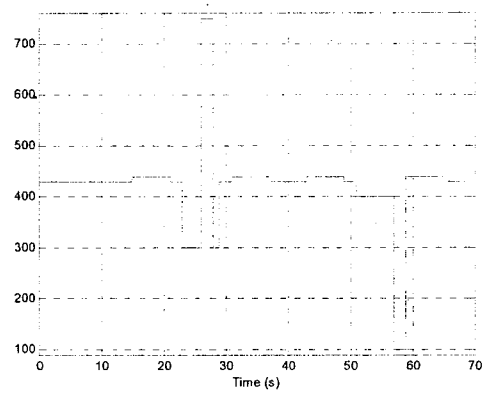

Fig. 5-6 P gain for joint O_{11}

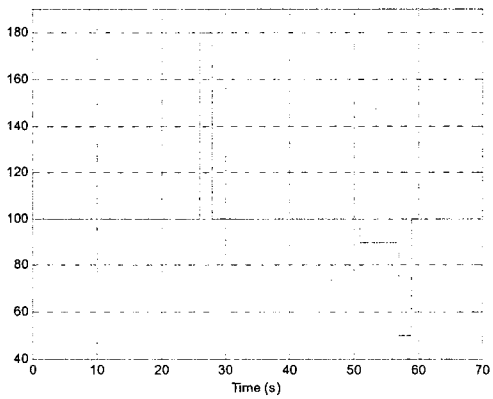

Fig. 5-7 D gain for joint O_{11}

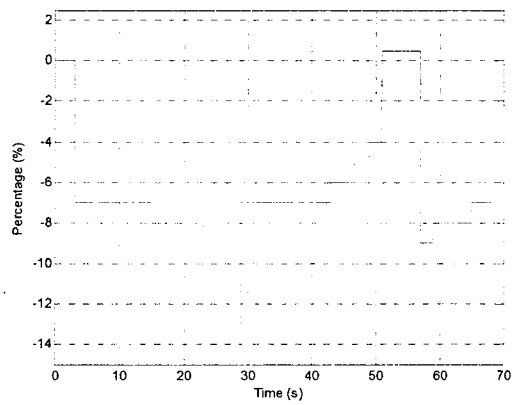

Fig. 5-8 PWM offset for joint O_{11}

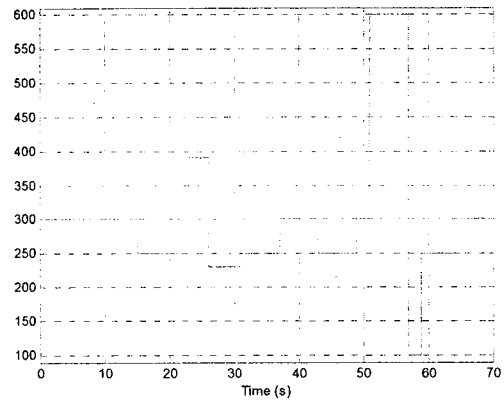

Fig. 5-9 P gain for joint O_{10}

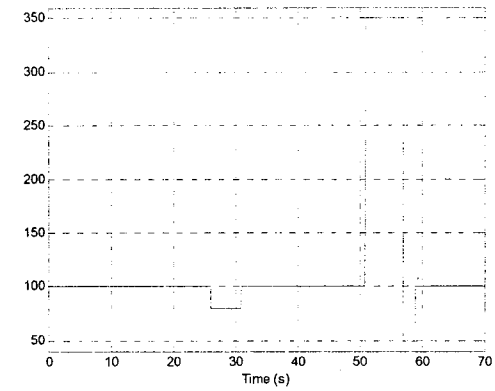

Fig. 5-10 D gain for joint O_{10}

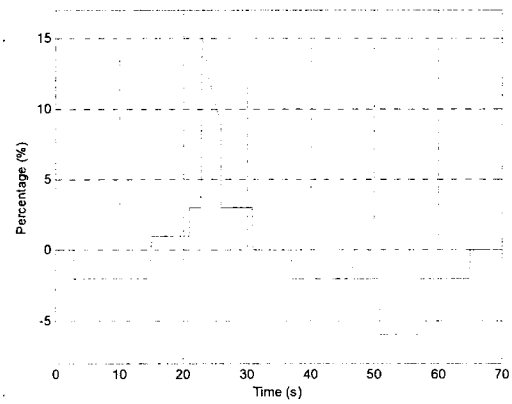

Fig. 5-11 PWM offset for joint O_{10}

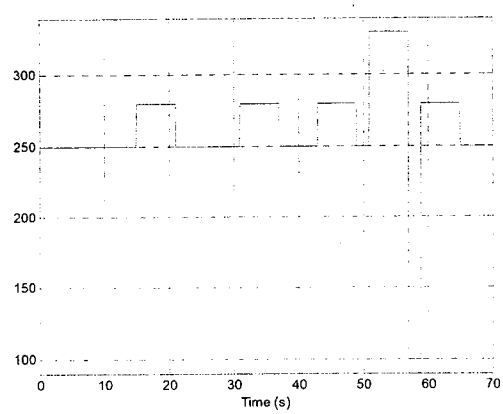

Fig. 5-12 P gain for joint O_9

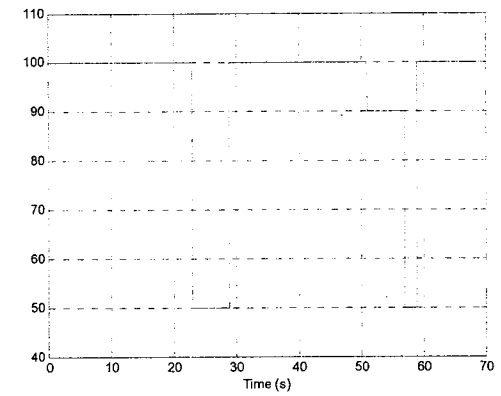

Fig. 5-13 D gain for joint O_9

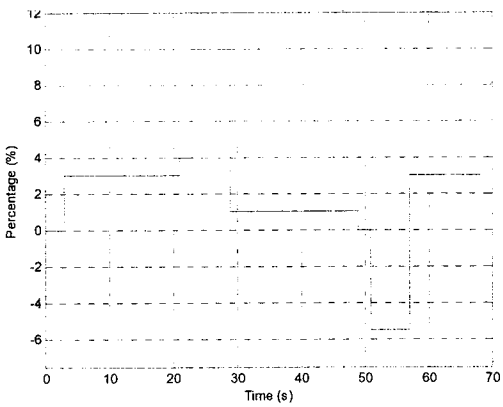

Fig. 5-14 PWM offset for joint O_9

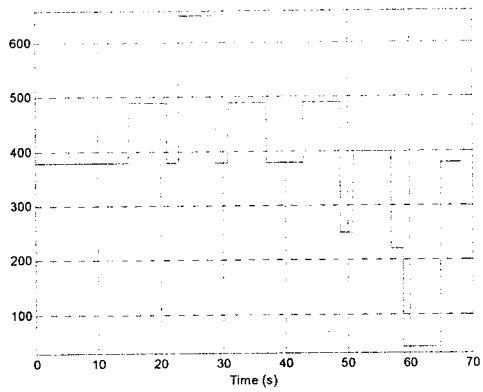

Fig. 5-15 P gain for joint O_8

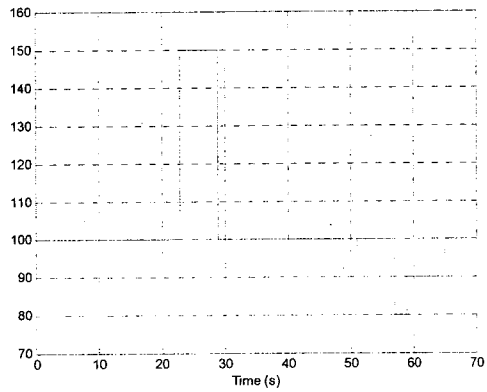

Fig. 5-16 D gain for joint O_8

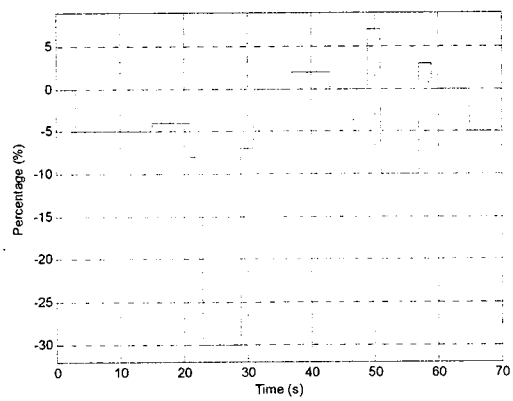

Fig. 5-17 PWM offset for joint O_8

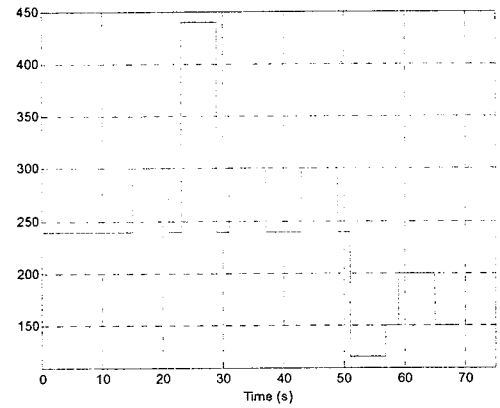

Fig. 5-18 P gain for joint O_1

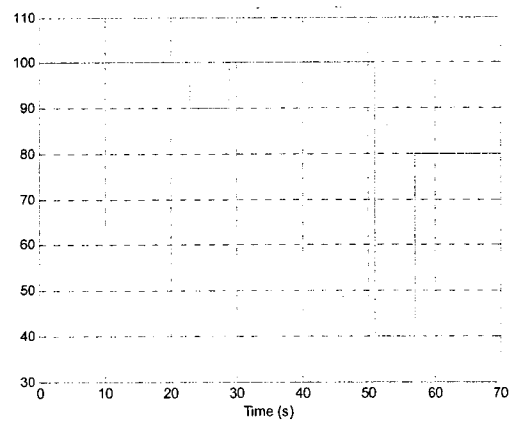

Fig. 5-19 D gain for joint O_1

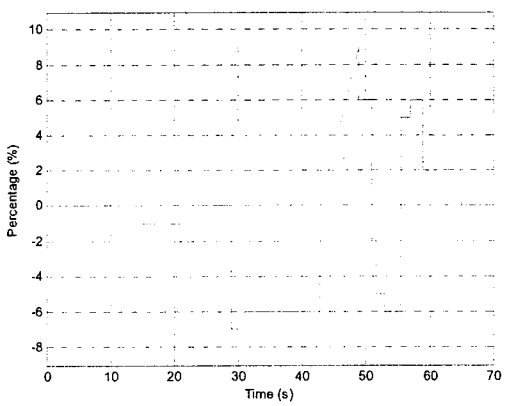

Fig. 5-20 PWM offset for joint O_1

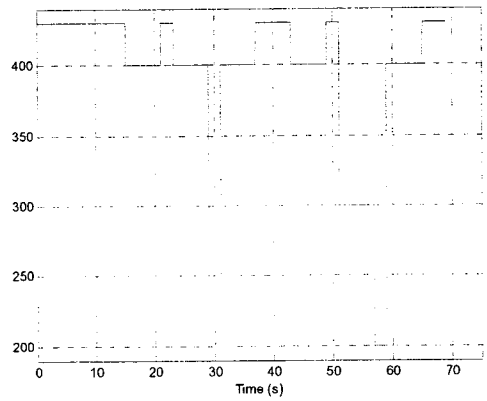

Fig. 5-21 P gain for joint O_2

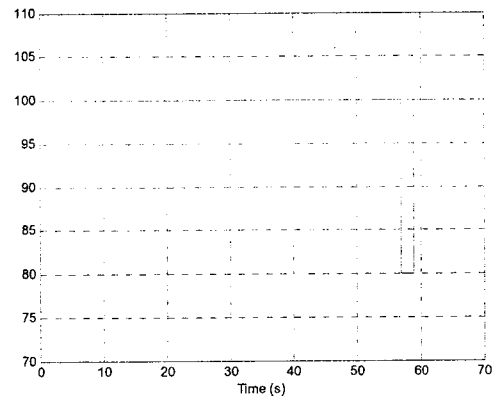

Fig.5-22 D gain for joint O_2

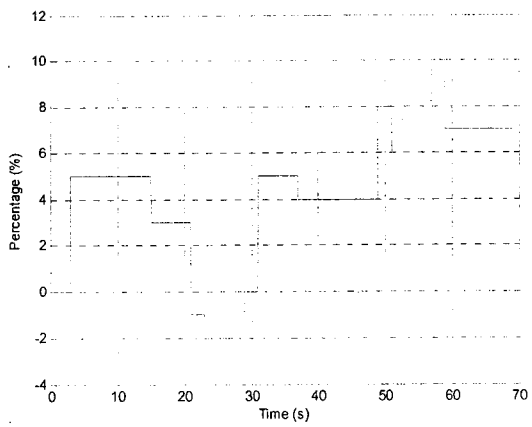

Fig. 5-23 PWM offset for joint O_2

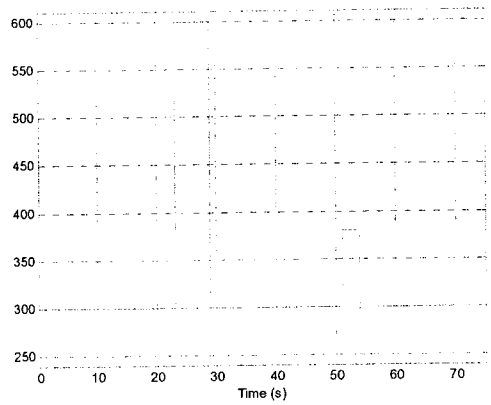

Fig. 5-24 P gain for joint O_3

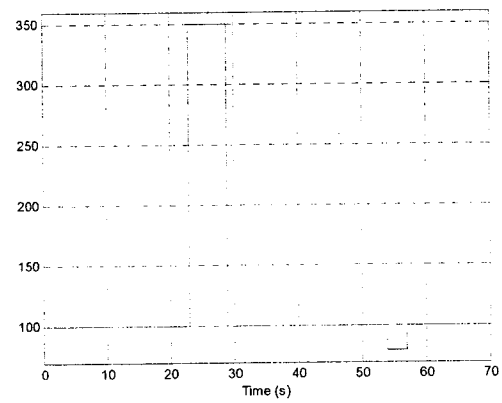

Fig. 5-25 D gain for joint O_3

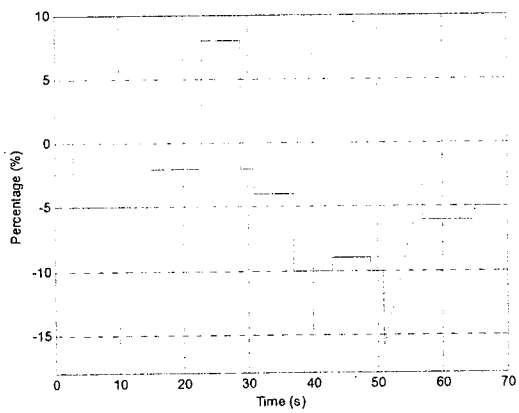

Fig. 5-26 PWM offset for joint O_3

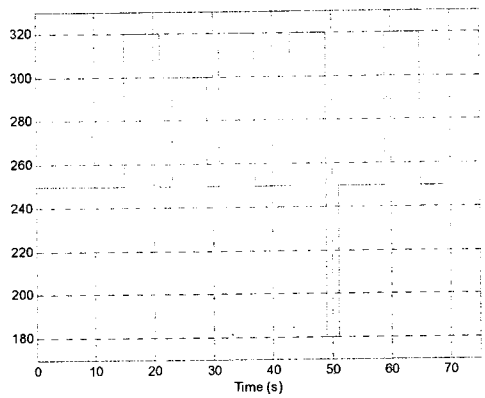

Fig. 5-27 P gain for joint O_4

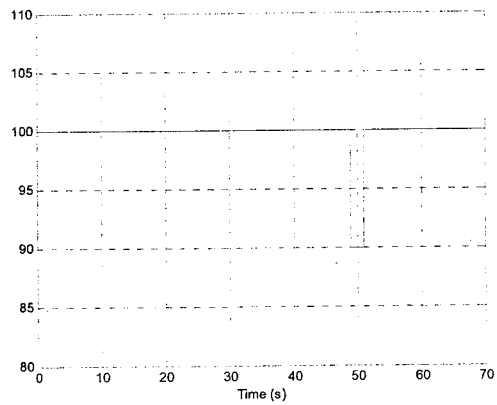

Fig. 5-28 D gain for joint O_4

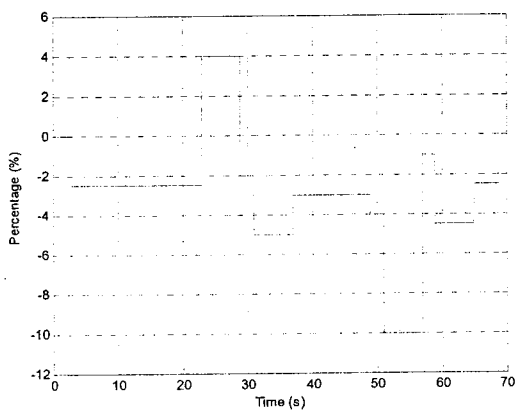

Fig. 5-29 PWM offset for joint O_4

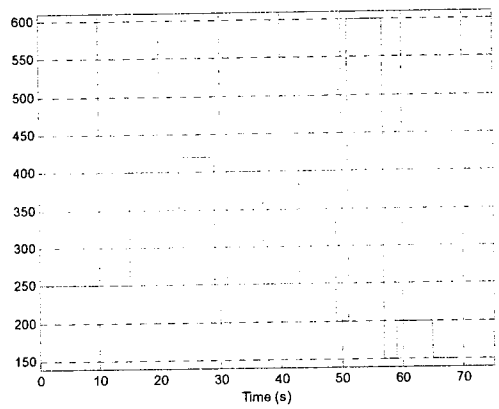

Fig. 5-30 P gain for joint O_5

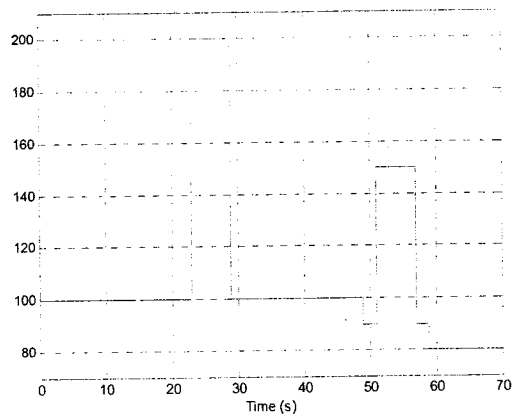

Fig. 5-31 D gain for joint O_5

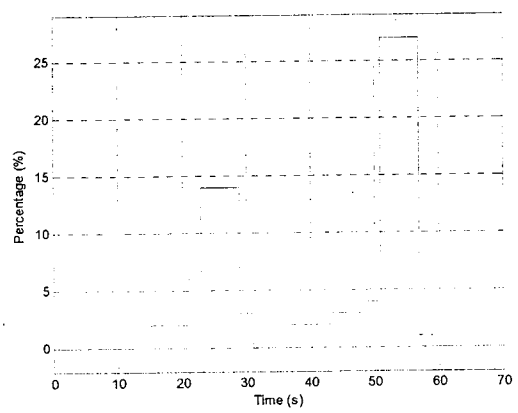

Fig. 5-32 PWM offset for joint O_5

Chapter 6

Experiment Results

The walking experiments have been done on the 10 DOF biped robot built for this thesis. The biped robot prototype is described in Chapter 4. The controller is the PD controller plus gravity compensation described in Chapter 5. The whole walking cycle starts from the home position and is composed of shifting weight to the left leg, swinging the right foot forward, shifting weight back to the home position, shifting weight to the right leg, swinging the left foot forward, and shifting weight back to the home position. It takes 69 seconds to finish the whole process.

6.1 Experiment Results

Fig. 6-1 to Fig. 6-30 are the plots for experiment results. There are three figures for each rotating joint, which are the desired and actual trajectories, tracking errors and the corresponding duty-cycle of PWM.

It can be observed from the error plots that the tracking errors are controlled within ±2.5 degrees. In this error range, the 10 DOF biped robot is able to walk on the flat surface stably by following the desired trajectories.

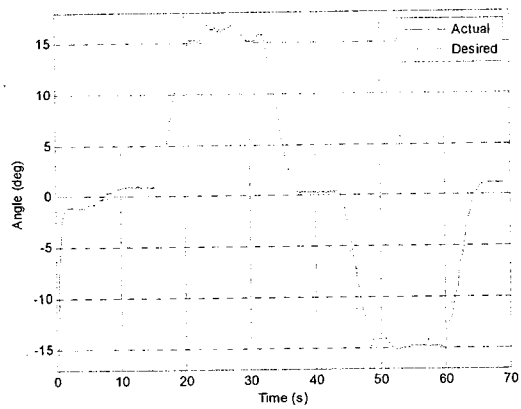

Fig. 6-1 Tracking control performance for joint O_{12}

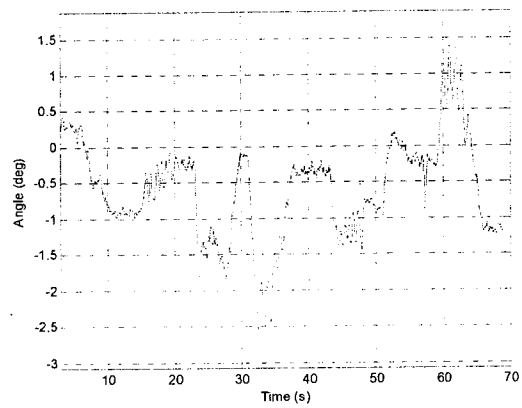

Fig. 6-2 Tracking error for joint O_{12}

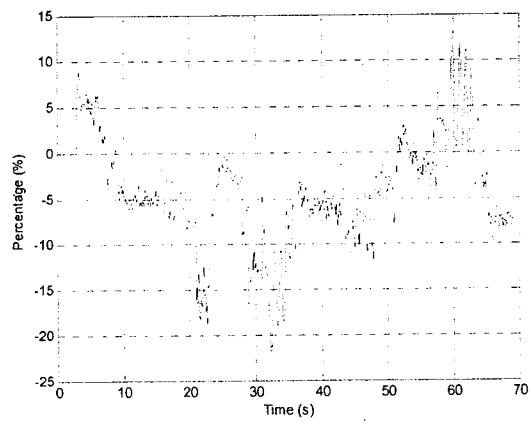

Fig. 6-3 PWM for joint O_{12}

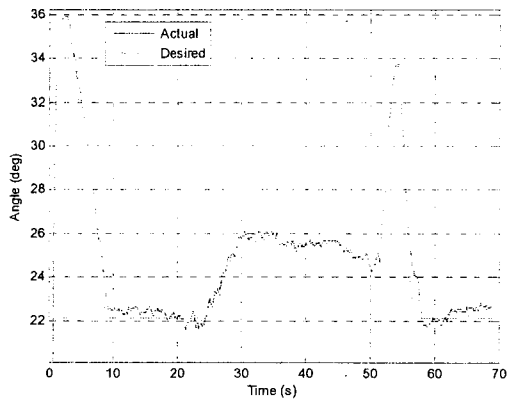

Fig. 6-4 Tracking control performance for joint O_{11}

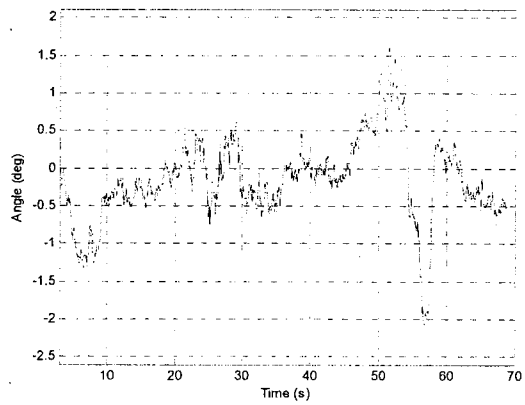

Fig. 6-5 Tracking error for joint O_{11}

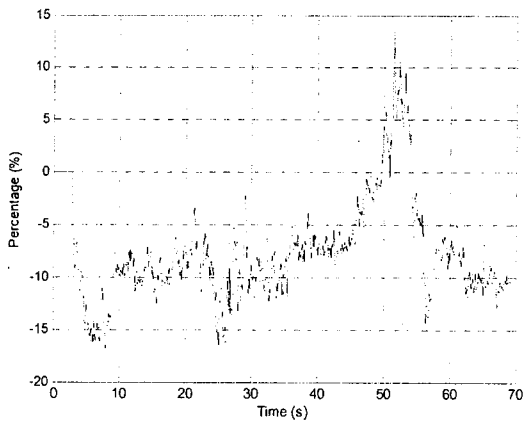

Fig. 6-6 PWM for joint O_{11}

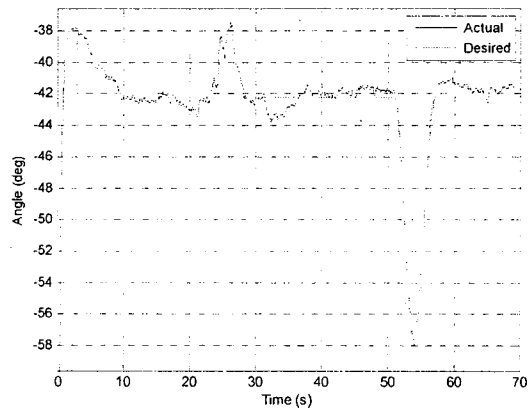

Fig. 6-7 Tracking control performance for joint O_{10}

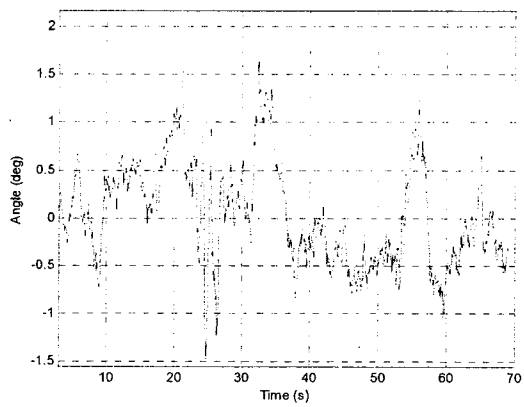

Fig. 6-8 Tracking error for joint O_{10}

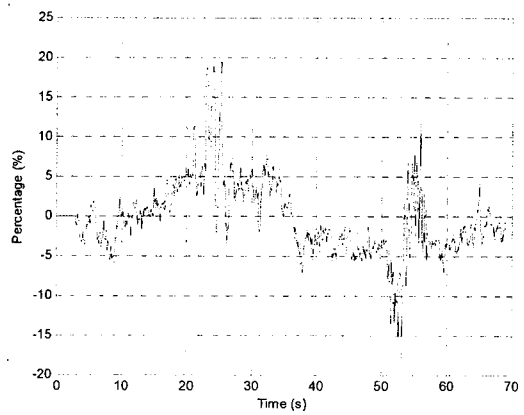

Fig. 6-9 PWM for joint O_{10}

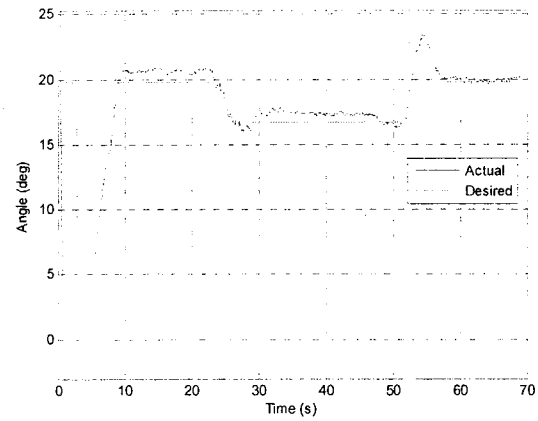

Fig. 6-10 Tracking control performance for joint O_9

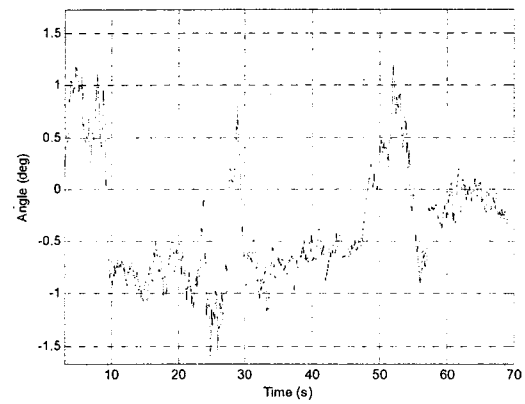

Fig. 6-11 Tracking error for joint O_9

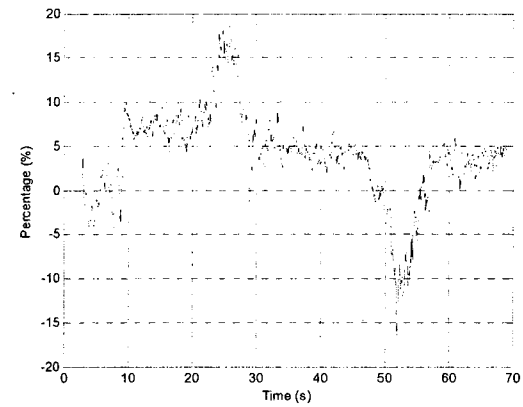

Fig. 6-12 PWM for joint O_9

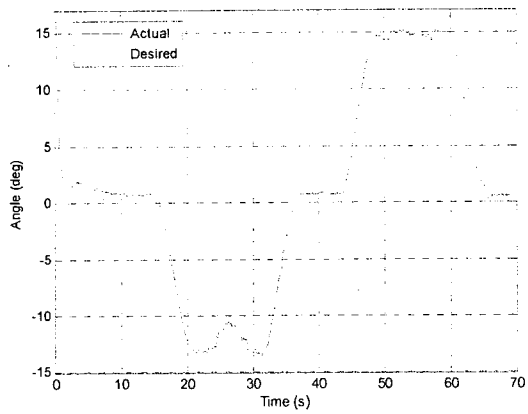

Fig. 6-13 Tracking control performance for joint O_8

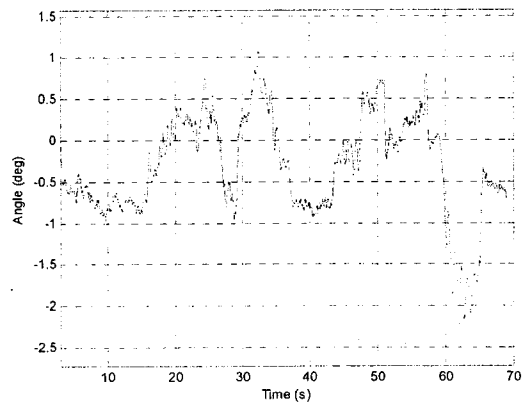

Fig. 6-14 Tracking error for joint O_8

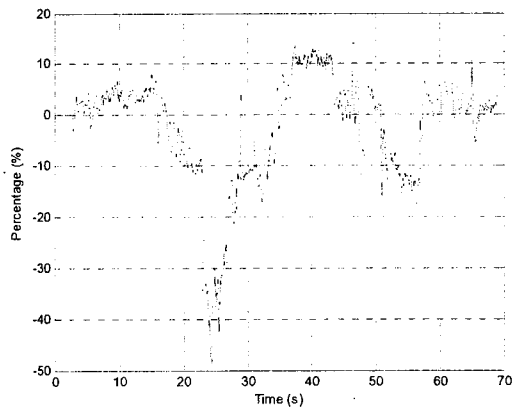

Fig. 6-15 PWM for joint O_8

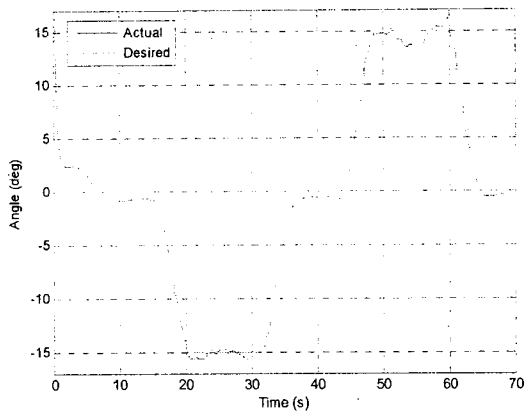

Fig. 6-16 Tracking control performance for joint O_1

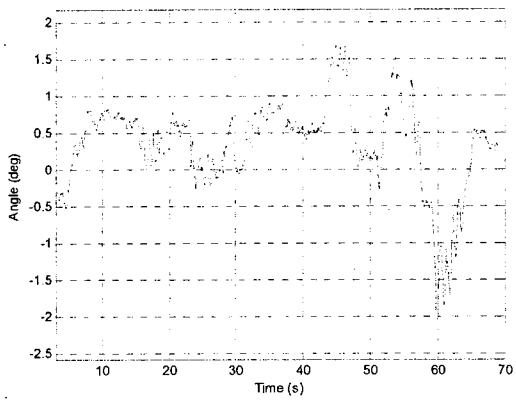

Fig. 6-17 Tracking error for joint O_1

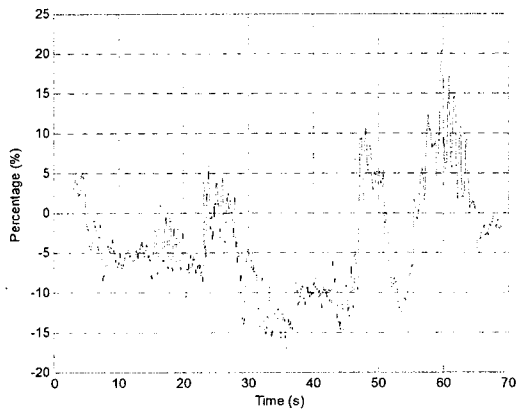

Fig. 6-18 PWM for joint O_1

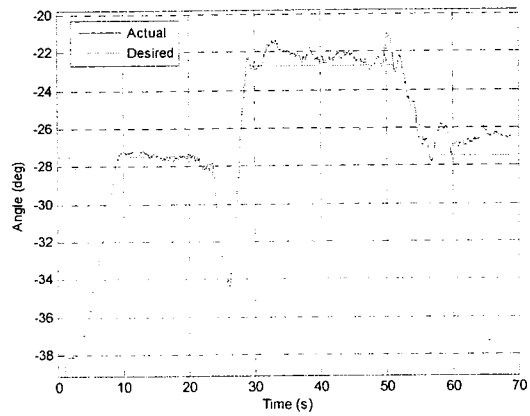

Fig. 6-19 Tracking control performance for joint O_2

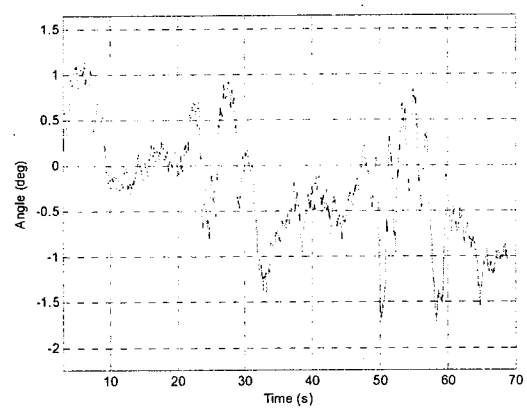

Fig. 6-20 Tracking error for joint O_2

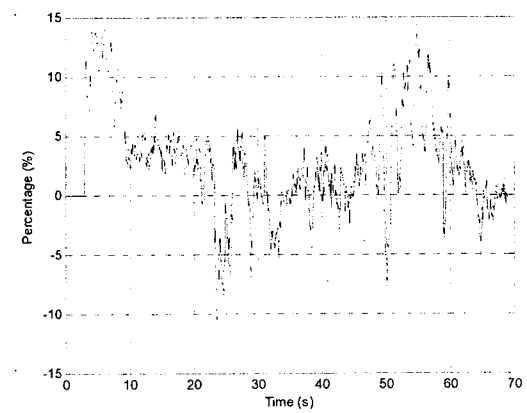

Fig. 6-21 PWM for joint O_2

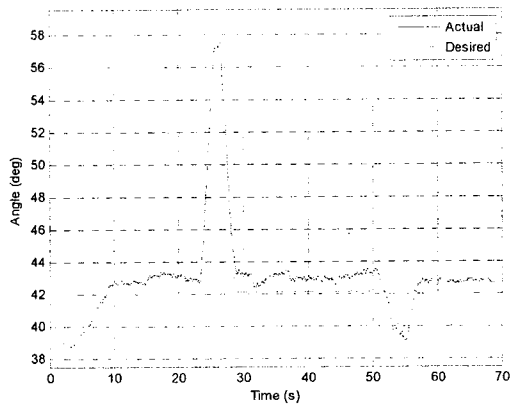

Fig. 6-22 Tracking control performance for joint O_3

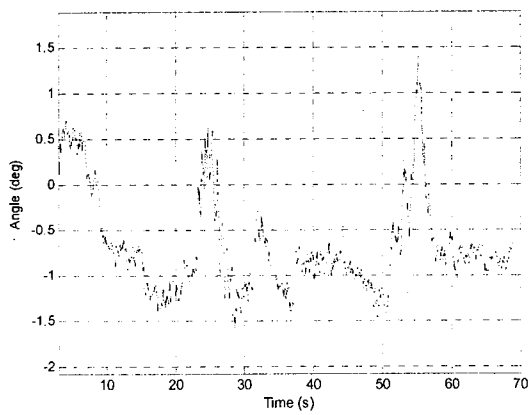

Fig. 6-23 Tracking error for joint O_3

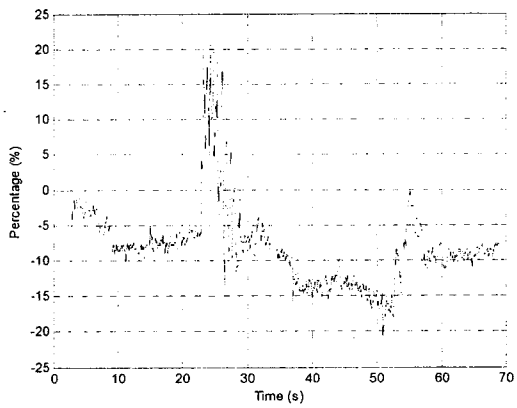

Fig. 6-24 PWM for joint O_3

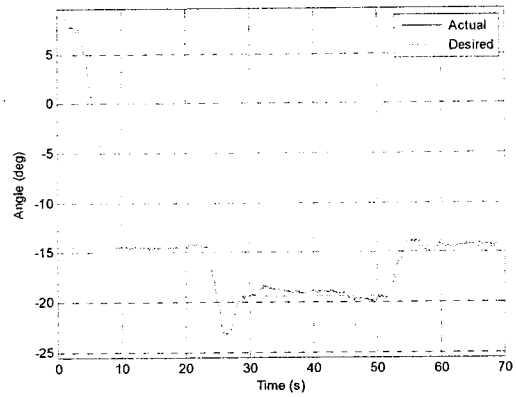

Fig. 6-25 Tracking control performance for joint O_4

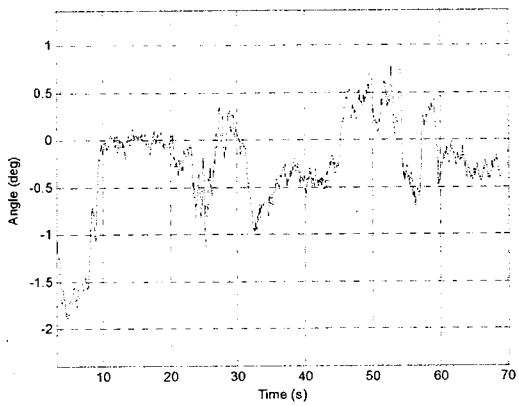

Fig. 6-26 Tracking error for joint O_4

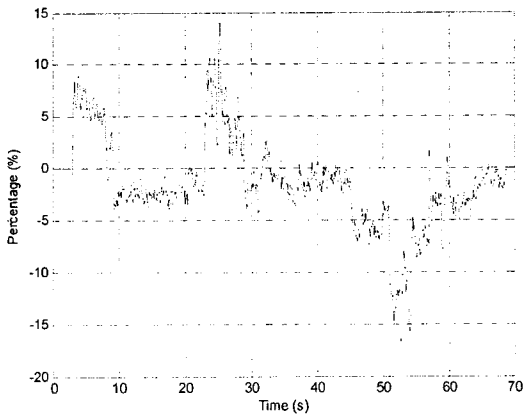

Fig. 6-27 PWM for joint O_4

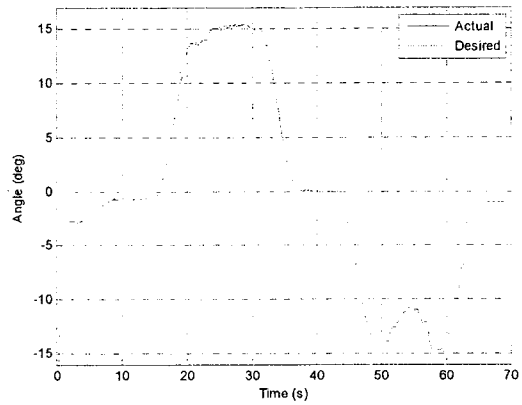

Fig. 6-28 Tracking control performance for joint O_5

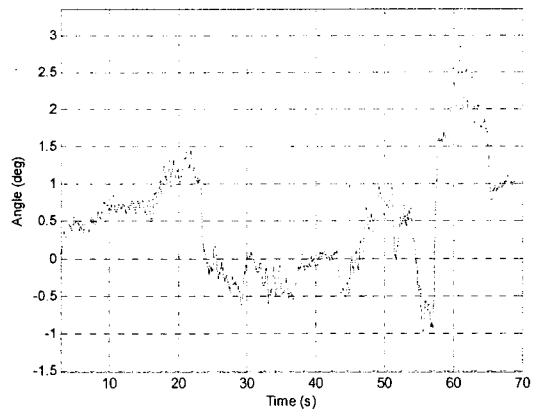

Fig. 6-29 Tracking error for joint O_5

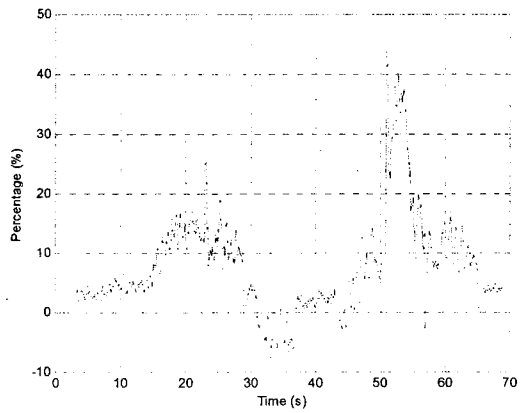

Fig. 6-30 PWM for joint O_5

6.2 Home Position Adjustment

The power supply to the motor drivers is turned on 3 seconds after the main control program starts. As soon as the power is on, the PD controller starts to bring the biped robot to its predefined home position from the initial position. In general, there are some differences between the home position and the initial position, which may cause some oscillations because of derivative control. This problem is solved by generating a linear trajectory between the home position and initial position using the linear interpolation method. Mathematically, the linear trajectory is calculated by

$$V_i = \begin{cases} \dfrac{V_i^{\text{Home}} - V_i^{Initial}}{6}(t-3) + V_i^{Initial}, & 3 < t \le 9 \\ V_i^{\text{Home}}, & 9 < t \le 15 \end{cases} \tag{6-1}$$

where i=1, 2, 3, 4, 5, 8, 9, 10, 11, 12 denotes the joint number, $V_i^{Initial}$ is the voltage for joint i, which is the voltage reading at t equals 3 second, V_i^{Home} represents the voltage corresponding to the home position for joint i. It takes 12 seconds for the biped robot to implement the home position adjustment.

Chapter 7

Conclusions and Future Work

7.1 Conclusions

The objective of this research is to design and control a 10 DOF biped robot. At this point the robot is able to walk stably on the flat ground by itself. The goal has been achieved successfully.

The forward kinematics and inverse kinematics have been performed for the robot system. The desired trajectories for the joint variables have been designed by the third-order spline interpolation method. The ZMP has been also analyzed to ensure that it is inside the stable region.

The robot prototype has been designed and built with aluminum material. DC motors are chosen as the actuators and the potentiometers are mounted to each joint to get the feedback signals. The potentiometers are calibrated to find the relationship between the degree and voltage. eZdspTM F2812 DSP boards are used as control hardware. The electrical circuits, including analog signal conditioning, motor driver, communication, feedback and limit switch, system activation and protection, have been designed and PCBs have been fabricated.

The MATLAB Simulink program is employed as the software platform for this robot research. The controller for the robot system is PD control plus gravity compensation. The control parameters have been tuned by using the trial-and-error

method from the experiments. The control results show that the biped robot is able to follow the desired trajectories.

Force sensors have been used to detect the contact forces between the foot soles and the ground, which can be used to determine the ZMP and perform active balance control for the biped robot. The force sensors have not been used in control algorithm for this research, but force sensors have been installed on the robot prototype and the appropriate electrical circuit has been designed for the future use.

7.2 Future Work

By controlling the joint variables to follow the desired trajectories, the 10 DOF biped robot in this thesis is able to walk on the flat floor. In order to design and build a more advanced biped robot. The following work should be done in the future.

1. Improve the current robot structure design and change the way to mount the DC motor. The structure should be stronger, lighter and easier to assemble. The DC motors should be mounted inside the leg to improve the left-right balance control.
2. All the circuit boards need to be mounted on the robot body and more powerful motors are needed.
3. Because the trial-and-error method is not an efficient way to tune the controller parameters, dynamic modeling for the biped robot system should be done so that some advanced control methods based on dynamic models can be used to design a controller. On the other hand, some other control design methods, such as fuzzy logic and neural network, can also be used for the controller design.
4. The walking speed of the robot in this thesis is very slow. To make the robot walk faster, an advanced controller needs to be designed.
5. Active balance control needs to be done by using force feedback from either force sensors or load cells and altitude feedback from gyroscopes and accelerometers. A more advanced controller should be designed to be able to adjust the zero moment point for active balance control so that the biped robot will be able to walk on rough or slope surface.

References

[1] http://www.humanoid.waseda.ac.jp/booklet/kato_4.html

[2] http://world.honda.com/ASIMO/history/

[3] http://www.communistrobot.com/robots/7

[4] http://www.communistrobot.com/robots/6

[5] M. Vukobratovic and J. Stepanenko, "Mathematical Models of General Anthropomorphic Systems," *Mathematical Biosciences,* Vol. 17, pp.191-242, 1973.

[6] P. Sardain and G. Bessonnet, "Forces Acting on a Biped Robot. Center of Pressure—Zero Moment Point," *IEEE Transactions on Systems, Man, and Cybernetics – Part A: Systems and Humans*, Vol. 34, No. 5, pp. 630-638, September 2004.

[7] P. Sardain and G. Bessonnet, "Zero Moment Point—Measurements From a Human Walker Wearing Robot Feet as Shoes," *IEEE Transactions on Systems, Man, and Cybernetics – Part A: Systems and Humans*, Vol. 34, No. 5, pp. 638-648, September 2004.

[8] M. Vukobratovic and B. Borovac, "Zero-Moment Point – Thirty Five Years of its Life," *International Journal of Humanoid Robotics*, Vol. 1, No. 1, pp. 157–173, 2004.

[9] S. Kajita, F. Kahehiro, K. Kaneko, K. Fujiwara, K. Harada, K. Yokoi, and H. Hirukawa, "Biped Walking Pattern Generation using Preview Control of the Zero-Moment-Point," *Proceedings of IEEE International Conference on Robotics and Automation*, Vol. 2, pp. 1620 - 1626, Taipei, Taiwan, September 2003.

[10] O. Kurt and K. Erbatur, "Robot Reference Generation with Natural ZMP Trajectories," *9th IEEE International Workshop on Advanced Motion Control*, pp. 403-410, 2006.

[11] Q. Huang, K. Yokoi, S. Kajita, K. Kaneko, H. Arai, N. Koyachi, and K. Taine, "Planning Walking Patterns for a Biped Robot," *IEEE Transactions on Robotics and Automation*, Vol. 17, No. 3, pp. 280-289, June 2001.

[12] Z. Tang, C. Zhou, and Z. Sun, "Trajectory Planning for Smooth Transition of a Biped Robot," *Proceedings of IEEE International Conference on Robotics & Automation*, pp. 2455-2460, Taipei, Taiwan, September, 2003.

[13] J. Aoki and K. Watanabe, "Control for Robust Standing of a Bipedal Robot by Sole Pressure," *SICE Annual Conference*, pp. 627-630, Kagawa University, Japan, September 2007.

[14] V. Prahlad, G. Dip, and C. Meng-Hwee, "Disturbance Rejection by Online ZMP Compensation," *Robotica*, 26: 9-17, Cambridge University Press, 2007.

[15] S. Ito, H. Kawasaki, K. Morikiand, and M. Sasaki, "Robot Experiment of Torque Learning for Biped Balance with respect to Periodic External Force," *Proceedings of 12th International Conference on Advanced Robotics*, pp. 418-423, 2005.

[16] J. KIM and J. OH, "Realization of Dynamic Walking for the Humanoid Robot Platform KHR-1," *Advanced Robotics*, Vol. 18, No. 7, pp. 749 - 768, 2004.

[17] C. Shih and W. A. Gruver, "Control of a Biped Robot in the Double-Support Phase," *IEEE Transactions on Systems, Man, and Cybernetics*, Vol. 22, No 4. July/August 1992.

[18] C. Azevedo, B. Espiau, B. Amblard, and C. Assaiante, "Bipedal locomotion: toward unified concepts in robotics and neuroscience," *Biological Cybernetics*, 2006.

[19] Y. Hurmuzlu, F. Genot, and B. Brogliato, "Modelling, stability and control of biped robots-a general framework," *Automatica*, Vol.40, pp.1647-1664, 2004.

[20] M.W. Spong and M. Vidyasagar, "Robot Dynamics and Control," John Wiley & Sons, 1989.

[21] http://www.tekscan.com/pdfs/FlexiforceUserManual.pdf, *FlexiForce® Force Sensors User Manual Rev. F*, September, 2005.

[22] http://focus.ti.com/lit/ds/symlink/tms320f2812.pdf, *TMS320F2810, TMS320F2811, TMS320F2812, TMS320C2810, TMS320C2811, TMS320C2812 Digital Signal Processors Data Manual*, 2006.

[23] http://c2000.spectrumdigital.com/ezf2812/docs/ezf2812_techref.pdf, *eZdspF2812 Technical Reference Rev. F*, 2003.

[24] http://www.national.com/ds/LM/LMD18200.pdf, *LMD18200 - 3A, 55V H-Bridge Data Sheet*, April, 2005.

Appendix A

Forward Kinematics for the Single Support Phase with Right Leg Support

The following matrices are the homogeneous transformation matrices for the biped robot in the single support phase with right leg support, see Fig. 2-1 and Table 2-2, with the assumption that θ_1, θ_5, θ_8 and θ_{12} are zero.

$$A_1 = \begin{bmatrix} 0 & 0 & 1 & 0 \\ 1 & 0 & 0 & L_1 \\ 0 & 1 & 0 & 0 \\ 0 & 0 & 0 & 1 \end{bmatrix} \tag{A-1}$$

$$A_2 = \begin{bmatrix} \cos\theta_1 & 0 & -\sin\theta_1 & L_2\cos\theta_1 \\ \sin\theta_1 & 0 & \cos\theta_1 & L_2\sin\theta_1 \\ 0 & -1 & 0 & 0 \\ 0 & 0 & 0 & 1 \end{bmatrix}$$

$$= \begin{bmatrix} \cos 0 & 0 & -\sin 0 & L_2\cos 0 \\ \sin 0 & 0 & \cos 0 & L_2\sin 0 \\ 0 & -1 & 0 & 0 \\ 0 & 0 & 0 & 1 \end{bmatrix} = \begin{bmatrix} 1 & 0 & 0 & L_2 \\ 0 & 0 & 1 & 0 \\ 0 & -1 & 0 & 0 \\ 0 & 0 & 0 & 1 \end{bmatrix} \tag{A-2}$$

$$A_3 = \begin{bmatrix} \cos\theta_2 & -\sin\theta_2 & 0 & L_3\cos\theta_2 \\ \sin\theta_2 & \cos\theta_2 & 0 & L_3\sin\theta_2 \\ 0 & 0 & 1 & 0 \\ 0 & 0 & 0 & 1 \end{bmatrix} \tag{A-3}$$

$$A_4 = \begin{bmatrix} \cos\theta_3 & -\sin\theta_3 & 0 & L_4\cos\theta_3 \\ \sin\theta_3 & \cos\theta_3 & 0 & L_4\sin\theta_3 \\ 0 & 0 & 1 & 0 \\ 0 & 0 & 0 & 1 \end{bmatrix} \tag{A-4}$$

$$A_5 = \begin{bmatrix} \cos\theta_4 & 0 & \sin\theta_4 & L_5\cos\theta_4 \\ \sin\theta_4 & 0 & -\cos\theta_4 & L_5\sin\theta_4 \\ 0 & 1 & 0 & 0 \\ 0 & 0 & 0 & 1 \end{bmatrix} \tag{A-5}$$

$$A_6 = \begin{bmatrix} \cos\theta_5 & 0 & -\sin\theta_5 & L_6\cos\theta_5 \\ \sin\theta_5 & 0 & \cos\theta_5 & L_6\sin\theta_5 \\ 0 & -1 & 0 & 0 \\ 0 & 0 & 0 & 1 \end{bmatrix}$$

$$= \begin{bmatrix} \cos 0 & 0 & -\sin 0 & L_6\cos 0 \\ \sin 0 & 0 & \cos 0 & L_6\sin 0 \\ 0 & -1 & 0 & 0 \\ 0 & 0 & 0 & 1 \end{bmatrix} = \begin{bmatrix} 1 & 0 & 0 & L_6 \\ 0 & 0 & 1 & 0 \\ 0 & -1 & 0 & 0 \\ 0 & 0 & 0 & 1 \end{bmatrix} \tag{A-6}$$

$$A_7 = \begin{bmatrix} 1 & 0 & 0 & 0 \\ 0 & 1 & 0 & 0 \\ 0 & 0 & 1 & -L_h \\ 0 & 0 & 0 & 1 \end{bmatrix} \tag{A-7}$$

$$A_8 = \begin{bmatrix} -1 & 0 & 0 & -L_6 \\ 0 & 0 & -1 & 0 \\ 0 & -1 & 0 & 0 \\ 0 & 0 & 0 & 1 \end{bmatrix} \tag{A-8}$$

$$A_9 = \begin{bmatrix} \cos\theta_8 & 0 & \sin\theta_8 & L_5\cos\theta_8 \\ \sin\theta_8 & 0 & -\cos\theta_8 & L_5\sin\theta_8 \\ 0 & 1 & 0 & 0 \\ 0 & 0 & 0 & 1 \end{bmatrix}$$

$$= \begin{bmatrix} \cos 0 & 0 & \sin 0 & L_5\cos 0 \\ \sin 0 & 0 & -\cos 0 & L_5\sin 0 \\ 0 & 1 & 0 & 0 \\ 0 & 0 & 0 & 1 \end{bmatrix} = \begin{bmatrix} 1 & 0 & 0 & L_5 \\ 0 & 0 & -1 & 0 \\ 0 & 1 & 0 & 0 \\ 0 & 0 & 0 & 1 \end{bmatrix} \tag{A-9}$$

$$A_{10} = \begin{bmatrix} \cos\theta_9 & -\sin\theta_9 & 0 & L_4\cos\theta_9 \\ \sin\theta_9 & \cos\theta_9 & 0 & L_4\sin\theta_9 \\ 0 & 0 & 1 & 0 \\ 0 & 0 & 0 & 1 \end{bmatrix} \tag{A-10}$$

$$A_{11}=\begin{bmatrix}\cos\theta_{10} & -\sin\theta_{10} & 0 & L_3\cos\theta_{10}\\ \sin\theta_{10} & \cos\theta_{10} & 0 & L_3\sin\theta_{10}\\ 0 & 0 & 1 & 0\\ 0 & 0 & 0 & 1\end{bmatrix} \tag{A-11}$$

$$A_{12}=\begin{bmatrix}\cos\theta_{11} & 0 & -\sin\theta_{11} & L_2\cos\theta_{11}\\ \sin\theta_{11} & 0 & \cos\theta_{11} & L_2\sin\theta_{11}\\ 0 & -1 & 0 & 0\\ 0 & 0 & 0 & 1\end{bmatrix} \tag{A-12}$$

$$A_{13}=\begin{bmatrix}\cos\theta_{12} & 0 & \sin\theta_{12} & L_1\cos\theta_{12}\\ \sin\theta_{12} & 0 & -\cos\theta_{12} & L_1\sin\theta_{12}\\ 0 & 1 & 0 & 0\\ 0 & 0 & 0 & 1\end{bmatrix}$$

$$=\begin{bmatrix}\cos 0 & 0 & \sin 0 & L_1\cos 0\\ \sin 0 & 0 & -\cos 0 & L_1\sin 0\\ 0 & 1 & 0 & 0\\ 0 & 0 & 0 & 1\end{bmatrix}=\begin{bmatrix}1 & 0 & 0 & L_1\\ 0 & 0 & -1 & 0\\ 0 & 1 & 0 & 0\\ 0 & 0 & 0 & 1\end{bmatrix} \tag{A-13}$$

The following matrices are the transformation matrices for the biped robot in the single support phase with right leg support with the assumption that θ_1, θ_5, θ_8 and θ_{12} are zero.

$${}^{0}_{r}T=\begin{bmatrix}1 & 0 & 0 & x_{aR}\\ 0 & 0 & -1 & y_{aR}\\ 0 & 1 & 0 & 0\\ 0 & 0 & 0 & 1\end{bmatrix} \tag{A-14}$$

$${}^{1}_{r}T={}^{0}_{r}TA_1=\begin{bmatrix}1 & 0 & 0 & x_{aR}\\ 0 & 0 & -1 & y_{aR}\\ 0 & 1 & 0 & 0\\ 0 & 0 & 0 & 1\end{bmatrix}\begin{bmatrix}0 & 0 & 1 & 0\\ 1 & 0 & 0 & L_1\\ 0 & 1 & 0 & 0\\ 0 & 0 & 0 & 1\end{bmatrix}=\begin{bmatrix}0 & 0 & 1 & x_{aR}\\ 0 & -1 & 0 & y_{aR}\\ 1 & 0 & 0 & L_1\\ 0 & 0 & 0 & 1\end{bmatrix} \tag{A-15}$$

$${}^{2}_{r}T={}^{1}_{r}TA_2=\begin{bmatrix}0 & 0 & 1 & x_{aR}\\ 0 & -1 & 0 & y_{aR}\\ 1 & 0 & 0 & L_1\\ 0 & 0 & 0 & 1\end{bmatrix}\begin{bmatrix}1 & 0 & 0 & L_2\\ 0 & 0 & 1 & 0\\ 0 & -1 & 0 & 0\\ 0 & 0 & 0 & 1\end{bmatrix}=\begin{bmatrix}0 & -1 & 0 & x_{aR}\\ 0 & 0 & -1 & y_{aR}\\ 1 & 0 & 0 & L_1+L_2\\ 0 & 0 & 0 & 1\end{bmatrix} \tag{A-16}$$

$$
{}^{3}_{r}T = {}^{2}_{r}TA_3 = \begin{bmatrix} 0 & -1 & 0 & x_{aR} \\ 0 & 0 & -1 & y_{aR} \\ 1 & 0 & 0 & L_1 + L_2 \\ 0 & 0 & 0 & 1 \end{bmatrix} \begin{bmatrix} \cos\theta_2 & -\sin\theta_2 & 0 & L_3\cos\theta_2 \\ \sin\theta_2 & \cos\theta_2 & 0 & L_3\sin\theta_2 \\ 0 & 0 & 1 & 0 \\ 0 & 0 & 0 & 1 \end{bmatrix}
$$

$$
= \begin{bmatrix} -\sin\theta_2 & -\cos\theta_2 & 0 & x_{aR} - L_3\sin\theta_2 \\ 0 & 0 & -1 & y_{aR} \\ \cos\theta_2 & -\sin\theta_2 & 0 & L_1 + L_2 + L_3\cos\theta_2 \\ 0 & 0 & 0 & 1 \end{bmatrix}
$$

$$
= \begin{bmatrix} -\sin\theta_2 & -\cos\theta_2 & 0 & G_{3\_1} \\ 0 & 0 & -1 & y_{aR} \\ \cos\theta_2 & -\sin\theta_2 & 0 & G_{3\_2} \\ 0 & 0 & 0 & 1 \end{bmatrix} \qquad \text{(A-17)}
$$

$$
{}^{4}_{r}T = {}^{3}_{r}TA_4 = \begin{bmatrix} -\sin\theta_2 & -\cos\theta_2 & 0 & G_{3\_1} \\ 0 & 0 & -1 & y_{aR} \\ \cos\theta_2 & -\sin\theta_2 & 0 & G_{3\_2} \\ 0 & 0 & 0 & 1 \end{bmatrix} \begin{bmatrix} \cos\theta_3 & -\sin\theta_3 & 0 & L_4\cos\theta_3 \\ \sin\theta_3 & \cos\theta_3 & 0 & L_4\sin\theta_3 \\ 0 & 0 & 1 & 0 \\ 0 & 0 & 0 & 1 \end{bmatrix}
$$

$$
= \begin{bmatrix} -\sin(\theta_2+\theta_3) & -\cos(\theta_2+\theta_3) & 0 & G_{3\_1} - L_4\sin(\theta_2+\theta_3) \\ 0 & 0 & -1 & y_{aR} \\ \cos(\theta_2+\theta_3) & -\sin(\theta_2+\theta_3) & 0 & G_{3\_2} + L_4\cos(\theta_2+\theta_3) \\ 0 & 0 & 0 & 1 \end{bmatrix}
$$

$$
= \begin{bmatrix} -\sin(\theta_2+\theta_3) & -\cos(\theta_2+\theta_3) & 0 & G_{4\_1} \\ 0 & 0 & -1 & y_{aR} \\ \cos(\theta_2+\theta_3) & -\sin(\theta_2+\theta_3) & 0 & G_{4\_2} \\ 0 & 0 & 0 & 1 \end{bmatrix} \qquad \text{(A-18)}
$$

$$
{}^{5}_{r}T = {}^{4}_{r}TA_5 = \begin{bmatrix} -\sin(\theta_2+\theta_3) & -\cos(\theta_2+\theta_3) & 0 & G_{4\_1} \\ 0 & 0 & -1 & y_{aR} \\ \cos(\theta_2+\theta_3) & -\sin(\theta_2+\theta_3) & 0 & G_{4\_2} \\ 0 & 0 & 0 & 1 \end{bmatrix} \begin{bmatrix} \cos\theta_4 & 0 & \sin\theta_4 & L_5\cos\theta_4 \\ \sin\theta_4 & 0 & -\cos\theta_4 & L_5\sin\theta_4 \\ 0 & 1 & 0 & 0 \\ 0 & 0 & 0 & 1 \end{bmatrix}
$$

$$
= \begin{bmatrix} -\sin(\theta_2+\theta_3+\theta_4) & 0 & \cos(\theta_2+\theta_3+\theta_4) & G_{4\_1} - L_5\sin(\theta_2+\theta_3+\theta_4) \\ 0 & -1 & 0 & y_{aR} \\ \cos(\theta_2+\theta_3+\theta_4) & 0 & \sin(\theta_2+\theta_3+\theta_4) & G_{4\_2} + L_5\cos(\theta_2+\theta_3+\theta_4) \\ 0 & 0 & 0 & 1 \end{bmatrix}
$$

$$
= \begin{bmatrix} -\sin(\theta_2+\theta_3+\theta_4) & 0 & \cos(\theta_2+\theta_3+\theta_4) & G_{5\_1} \\ 0 & -1 & 0 & y_{aR} \\ \cos(\theta_2+\theta_3+\theta_4) & 0 & \sin(\theta_2+\theta_3+\theta_4) & G_{5\_2} \\ 0 & 0 & 0 & 1 \end{bmatrix} \qquad \text{(A-19)}
$$

$$
{}^{6}_{r}T = {}^{5}_{r}TA_6 = \begin{bmatrix} -\sin(\theta_2+\theta_3+\theta_4) & 0 & \cos(\theta_2+\theta_3+\theta_4) & G_{5\_1} \\ 0 & -1 & 0 & y_{aR} \\ \cos(\theta_2+\theta_3+\theta_4) & 0 & \sin(\theta_2+\theta_3+\theta_4) & G_{5\_2} \\ 0 & 0 & 0 & 1 \end{bmatrix} \begin{bmatrix} 1 & 0 & 0 & L_6 \\ 0 & 0 & 1 & 0 \\ 0 & -1 & 0 & 0 \\ 0 & 0 & 0 & 1 \end{bmatrix}
$$

$$
= \begin{bmatrix} -\sin(\theta_2+\theta_3+\theta_4) & -\cos(\theta_2+\theta_3+\theta_4) & 0 & G_{5\_1} - L_6\sin(\theta_2+\theta_3+\theta_4) \\ 0 & 0 & -1 & y_{aR} \\ \cos(\theta_2+\theta_3+\theta_4) & -\sin(\theta_2+\theta_3+\theta_4) & 0 & G_{5\_2} + L_6\cos(\theta_2+\theta_3+\theta_4) \\ 0 & 0 & 0 & 1 \end{bmatrix}
$$

$$
= \begin{bmatrix} -\sin(\theta_2+\theta_3+\theta_4) & -\cos(\theta_2+\theta_3+\theta_4) & 0 & G_{6\_1} \\ 0 & 0 & -1 & y_{aR} \\ \cos(\theta_2+\theta_3+\theta_4) & -\sin(\theta_2+\theta_3+\theta_4) & 0 & G_{6\_2} \\ 0 & 0 & 0 & 1 \end{bmatrix} \qquad \text{(A-20)}
$$

$$
{}^{7}_{r}T = {}^{6}_{r}TA_7 = \begin{bmatrix} -\sin(\theta_2+\theta_3+\theta_4) & -\cos(\theta_2+\theta_3+\theta_4) & 0 & G_{6\_1} \\ 0 & 0 & -1 & y_{aR} \\ \cos(\theta_2+\theta_3+\theta_4) & -\sin(\theta_2+\theta_3+\theta_4) & 0 & G_{6\_2} \\ 0 & 0 & 0 & 1 \end{bmatrix} \begin{bmatrix} 1 & 0 & 0 & 0 \\ 0 & 1 & 0 & 0 \\ 0 & 0 & 1 & -L_h \\ 0 & 0 & 0 & 1 \end{bmatrix}
$$

$$
= \begin{bmatrix} -\sin(\theta_2+\theta_3+\theta_4) & -\cos(\theta_2+\theta_3+\theta_4) & 0 & G_{6\_1} \\ 0 & 0 & -1 & y_{aR}+L_h \\ \cos(\theta_2+\theta_3+\theta_4) & -\sin(\theta_2+\theta_3+\theta_4) & 0 & G_{6\_2} \\ 0 & 0 & 0 & 1 \end{bmatrix} \qquad \text{(A-21)}
$$

$$
{}^{8}_{r}T = {}^{7}_{r}TA_8 = \begin{bmatrix} -\sin(\theta_2+\theta_3+\theta_4) & -\cos(\theta_2+\theta_3+\theta_4) & 0 & G_{6\_1} \\ 0 & 0 & -1 & y_{aR}+L_h \\ \cos(\theta_2+\theta_3+\theta_4) & -\sin(\theta_2+\theta_3+\theta_4) & 0 & G_{6\_2} \\ 0 & 0 & 0 & 1 \end{bmatrix} \begin{bmatrix} -1 & 0 & 0 & -L_6 \\ 0 & 0 & -1 & 0 \\ 0 & -1 & 0 & 0 \\ 0 & 0 & 0 & 1 \end{bmatrix}
$$

$$
= \begin{bmatrix} \sin(\theta_2+\theta_3+\theta_4) & 0 & \cos(\theta_2+\theta_3+\theta_4) & G_{6\_1} + L_6\sin(\theta_2+\theta_3+\theta_4) \\ 0 & 1 & 0 & y_{aR}+L_h \\ -\cos(\theta_2+\theta_3+\theta_4) & 0 & \sin(\theta_2+\theta_3+\theta_4) & G_{6\_2} - L_6\cos(\theta_2+\theta_3+\theta_4) \\ 0 & 0 & 0 & 1 \end{bmatrix}
$$

$$
= \begin{bmatrix} \sin(\theta_2+\theta_3+\theta_4) & 0 & \cos(\theta_2+\theta_3+\theta_4) & G_{5\_1} \\ 0 & 1 & 0 & y_{aR}+L_h \\ -\cos(\theta_2+\theta_3+\theta_4) & 0 & \sin(\theta_2+\theta_3+\theta_4) & G_{5\_2} \\ 0 & 0 & 0 & 1 \end{bmatrix} \qquad \text{(A-22)}
$$

$$
{}^{9}_{r}T = {}^{8}_{r}TA_{9} = \begin{bmatrix} \sin(\theta_2+\theta_3+\theta_4) & 0 & \cos(\theta_2+\theta_3+\theta_4) & G_{5\_1} \\ 0 & 1 & 0 & y_{aR}+L_h \\ -\cos(\theta_2+\theta_3+\theta_4) & 0 & \sin(\theta_2+\theta_3+\theta_4) & G_{5\_2} \\ 0 & 0 & 0 & 1 \end{bmatrix} \begin{bmatrix} 1 & 0 & 0 & L_5 \\ 0 & 0 & -1 & 0 \\ 0 & 1 & 0 & 0 \\ 0 & 0 & 0 & 1 \end{bmatrix}
$$

$$
= \begin{bmatrix} \sin(\theta_2+\theta_3+\theta_4) & \cos(\theta_2+\theta_3+\theta_4) & 0 & G_{5\_1}+L_5\sin(\theta_2+\theta_3+\theta_4) \\ 0 & 0 & -1 & y_{aR}+L_h \\ -\cos(\theta_2+\theta_3+\theta_4) & \sin(\theta_2+\theta_3+\theta_4) & 0 & G_{5\_2}-L_5\cos(\theta_2+\theta_3+\theta_4) \\ 0 & 0 & 0 & 1 \end{bmatrix}
$$

$$
= \begin{bmatrix} \sin(\theta_2+\theta_3+\theta_4) & \cos(\theta_2+\theta_3+\theta_4) & 0 & G_{4\_1} \\ 0 & 0 & -1 & y_{aR}+L_h \\ -\cos(\theta_2+\theta_3+\theta_4) & \sin(\theta_2+\theta_3+\theta_4) & 0 & G_{4\_2} \\ 0 & 0 & 0 & 1 \end{bmatrix} \qquad \text{(A-23)}
$$

$$
{}^{10}_{r}T = {}^{9}_{r}TA_{10} = \begin{bmatrix} \sin(\theta_2+\theta_3+\theta_4) & \cos(\theta_2+\theta_3+\theta_4) & 0 & G_{4\_1} \\ 0 & 0 & -1 & y_{aR}+L_h \\ -\cos(\theta_2+\theta_3+\theta_4) & \sin(\theta_2+\theta_3+\theta_4) & 0 & G_{4\_2} \\ 0 & 0 & 0 & 1 \end{bmatrix} \begin{bmatrix} \cos\theta_9 & -\sin\theta_9 & 0 & L_4\cos\theta_9 \\ \sin\theta_9 & \cos\theta_9 & 0 & L_4\sin\theta_9 \\ 0 & 0 & 1 & 0 \\ 0 & 0 & 0 & 1 \end{bmatrix}
$$

$$
= \begin{bmatrix} \sin(\theta_2+\theta_3+\theta_4+\theta_9) & \cos(\theta_2+\theta_3+\theta_4+\theta_9) & 0 & G_{4\_1}+L_4\sin(\theta_2+\theta_3+\theta_4+\theta_9) \\ 0 & 0 & -1 & y_{aR}+L_h \\ -\cos(\theta_2+\theta_3+\theta_4+\theta_9) & \sin(\theta_2+\theta_3+\theta_4+\theta_9) & 0 & G_{4\_2}-L_4\cos(\theta_2+\theta_3+\theta_4+\theta_9) \\ 0 & 0 & 0 & 1 \end{bmatrix}
$$

$$
= \begin{bmatrix} \sin(\theta_2+\theta_3+\theta_4+\theta_9) & \cos(\theta_2+\theta_3+\theta_4+\theta_9) & 0 & G_{10\_1} \\ 0 & 0 & -1 & y_{aR}+L_h \\ -\cos(\theta_2+\theta_3+\theta_4+\theta_9) & \sin(\theta_2+\theta_3+\theta_4+\theta_9) & 0 & G_{10\_2} \\ 0 & 0 & 0 & 1 \end{bmatrix} \qquad \text{(A-24)}
$$

$$
{}^{11}_{r}T = {}^{10}_{r}TA_{11} = \begin{bmatrix} \sin(\theta_2+\theta_3+\theta_4+\theta_9) & \cos(\theta_2+\theta_3+\theta_4+\theta_9) & 0 & G_{10\_1} \\ 0 & 0 & -1 & y_{aR}+L_h \\ -\cos(\theta_2+\theta_3+\theta_4+\theta_9) & \sin(\theta_2+\theta_3+\theta_4+\theta_9) & 0 & G_{10\_2} \\ 0 & 0 & 0 & 1 \end{bmatrix} \begin{bmatrix} \cos\theta_{10} & -\sin\theta_{10} & 0 & L_3\cos\theta_{10} \\ \sin\theta_{10} & \cos\theta_{10} & 0 & L_3\sin\theta_{10} \\ 0 & 0 & 1 & 0 \\ 0 & 0 & 0 & 1 \end{bmatrix}
$$

$$
= \begin{bmatrix} \sin(\theta_2+\theta_3+\theta_4+\theta_9+\theta_{10}) & \cos(\theta_2+\theta_3+\theta_4+\theta_9+\theta_{10}) & 0 & G_{10\_1}+L_3\sin(\theta_2+\theta_3+\theta_4+\theta_9+\theta_{10}) \\ 0 & 0 & -1 & y_{aR}+L_h \\ -\cos(\theta_2+\theta_3+\theta_4+\theta_9+\theta_{10}) & \sin(\theta_2+\theta_3+\theta_4+\theta_9+\theta_{10}) & 0 & G_{10\_2}-L_3\cos(\theta_2+\theta_3+\theta_4+\theta_9+\theta_{10}) \\ 0 & 0 & 0 & 1 \end{bmatrix}
$$

$$= \begin{bmatrix} \sin(\theta_2+\theta_3+\theta_4+\theta_9+\theta_{10}) & \cos(\theta_2+\theta_3+\theta_4+\theta_9+\theta_{10}) & 0 & G_{11\_1} \\ 0 & 0 & -1 & y_{aR}+L_h \\ -\cos(\theta_2+\theta_3+\theta_4+\theta_9+\theta_{10}) & \sin(\theta_2+\theta_3+\theta_4+\theta_9+\theta_{10}) & 0 & G_{11\_2} \\ 0 & 0 & 0 & 1 \end{bmatrix} \quad \text{(A-25)}$$

$${}^{12}_{r}T = {}^{11}_{r}TA_{12}$$

$$= \begin{bmatrix} \sin(\theta_2+\theta_3+\theta_4+\theta_9+\theta_{10}) & \cos(\theta_2+\theta_3+\theta_4+\theta_9+\theta_{10}) & 0 & G_{11\_1} \\ 0 & 0 & -1 & y_{aR}+L_h \\ -\cos(\theta_2+\theta_3+\theta_4+\theta_9+\theta_{10}) & \sin(\theta_2+\theta_3+\theta_4+\theta_9+\theta_{10}) & 0 & G_{11\_2} \\ 0 & 0 & 0 & 1 \end{bmatrix} \begin{bmatrix} \cos\theta_{11} & 0 & -\sin\theta_{11} & L_2\cos\theta_{11} \\ \sin\theta_{11} & 0 & \cos\theta_{11} & L_2\sin\theta_{11} \\ 0 & -1 & 0 & 0 \\ 0 & 0 & 0 & 1 \end{bmatrix}$$

$$= \begin{bmatrix} \sin(\theta_2+\theta_3+\theta_4+\theta_9+\theta_{10}+\theta_{11}) & 0 & \cos(\theta_2+\theta_3+\theta_4+\theta_9+\theta_{10}+\theta_{11}) & G_{11\_1}+L_2\sin(\theta_2+\theta_3+\theta_4+\theta_9+\theta_{10}+\theta_{11}) \\ 0 & 1 & 0 & y_{aR}+L_h \\ -\cos(\theta_2+\theta_3+\theta_4+\theta_9+\theta_{10}+\theta_{11}) & 0 & \sin(\theta_2+\theta_3+\theta_4+\theta_9+\theta_{10}+\theta_{11}) & G_{11\_2}-L_2\cos(\theta_2+\theta_3+\theta_4+\theta_9+\theta_{10}+\theta_{11}) \\ 0 & 0 & 0 & 1 \end{bmatrix}$$

$$= \begin{bmatrix} \sin(\theta_2+\theta_3+\theta_4+\theta_9+\theta_{10}+\theta_{11}) & 0 & \cos(\theta_2+\theta_3+\theta_4+\theta_9+\theta_{10}+\theta_{11}) & G_{12\_1} \\ 0 & 1 & 0 & y_{aR}+L_h \\ -\cos(\theta_2+\theta_3+\theta_4+\theta_9+\theta_{10}+\theta_{11}) & 0 & \sin(\theta_2+\theta_3+\theta_4+\theta_9+\theta_{10}+\theta_{11}) & G_{12\_2} \\ 0 & 0 & 0 & 1 \end{bmatrix} \quad \text{(A-26)}$$

$${}^{13}_{r}T = {}^{12}_{r}TA_{13}$$

$$= \begin{bmatrix} \sin(\theta_2+\theta_3+\theta_4+\theta_9+\theta_{10}+\theta_{11}) & 0 & \cos(\theta_2+\theta_3+\theta_4+\theta_9+\theta_{10}+\theta_{11}) & G_{12\_1} \\ 0 & 1 & 0 & y_{aR}+L_h \\ -\cos(\theta_2+\theta_3+\theta_4+\theta_9+\theta_{10}+\theta_{11}) & 0 & \sin(\theta_2+\theta_3+\theta_4+\theta_9+\theta_{10}+\theta_{11}) & G_{12\_2} \\ 0 & 0 & 0 & 1 \end{bmatrix} \begin{bmatrix} 1 & 0 & 0 & L_1 \\ 0 & 0 & -1 & 0 \\ 0 & 1 & 0 & 0 \\ 0 & 0 & 0 & 1 \end{bmatrix}$$

$$= \begin{bmatrix} \sin(\theta_2+\theta_3+\theta_4+\theta_9+\theta_{10}+\theta_{11}) & \cos(\theta_2+\theta_3+\theta_4+\theta_9+\theta_{10}+\theta_{11}) & 0 & G_{13\_1} \\ 0 & 0 & -1 & y_{aR}+L_h \\ -\cos(\theta_2+\theta_3+\theta_4+\theta_9+\theta_{10}+\theta_{11}) & \sin(\theta_2+\theta_3+\theta_4+\theta_9+\theta_{10}+\theta_{11}) & 0 & G_{13\_2} \\ 0 & 0 & 0 & 1 \end{bmatrix} \quad \text{(A-27)}$$

where

$G_{3\_1} = x_{aR} - L_3\sin\theta_2$

$G_{3\_2} = L_1 + L_2 + L_3\cos\theta_2$

$G_{4\_1} = G_{3\_1} - L_4\sin(\theta_2+\theta_3)$

$G_{4\_2} = G_{3\_2} + L_4\cos(\theta_2+\theta_3)$

$G_{5\_1} = G_{4\_1} - L_5\sin(\theta_2+\theta_3+\theta_4)$

$G_{5\_2} = G_{4\_2} + L_5\cos(\theta_2+\theta_3+\theta_4)$

$$G_{6\_1} = G_{5\_1} - L_6 \sin(\theta_2 + \theta_3 + \theta_4)$$
$$G_{6\_2} = G_{5\_2} + L_6 \cos(\theta_2 + \theta_3 + \theta_4)$$
$$G_{10\_1} = G_{4\_1} + L_4 \sin(\theta_2 + \theta_3 + \theta_4 + \theta_9)$$
$$G_{10\_2} = G_{4\_1} - L_4 \cos(\theta_2 + \theta_3 + \theta_4 + \theta_9)$$
$$G_{11\_1} = G_{10\_1} + L_3 \sin(\theta_2 + \theta_3 + \theta_4 + \theta_9 + \theta_{10})$$
$$G_{11\_2} = G_{10\_2} - L_3 \cos(\theta_2 + \theta_3 + \theta_4 + \theta_9 + \theta_{10})$$
$$G_{12\_1} = G_{11\_1} + L_2 \sin(\theta_2 + \theta_3 + \theta_4 + \theta_9 + \theta_{10} + \theta_{11})$$
$$G_{12\_2} = G_{11\_2} - L_2 \cos(\theta_2 + \theta_3 + \theta_4 + \theta_9 + \theta_{10} + \theta_{11})$$
$$G_{13\_1} = G_{12\_1} + L_1 \sin(\theta_2 + \theta_3 + \theta_4 + \theta_9 + \theta_{10} + \theta_{11})$$
$$G_{13\_2} = G_{12\_2} - L_1 \cos(\theta_2 + \theta_3 + \theta_4 + \theta_9 + \theta_{10} + \theta_{11})$$

The x, y and z coordinates for ankle and hip joints are given as follows.

Right Ankle:

$$\begin{cases} x_{O_2} = x_{aR} \\ y_{O_2} = y_{aR} \\ z_{O_2} = L_1 + L_2 \end{cases} \tag{A-28}$$

Right Hip:

$$\begin{cases} x_{O_4} = G_{4\_1} = x_R - L_3 \sin\theta_2 - L_4 \sin(\theta_2 + \theta_3) \\ y_{O_4} = y_{aR} \\ z_{O_4} = G_{4\_2} = L_1 + L_2 + L_3 \cos\theta_2 + L_4 \cos(\theta_2 + \theta_3) \end{cases} \tag{A-29}$$

Left Hip:

$$\begin{cases} x_{O_9} = G_{4\_1} = x_R - L_3 \sin\theta_2 - L_4 \sin(\theta_2 + \theta_3) \\ y_{O_9} = y_{aR} + L_h \\ z_{O_9} = G_{4\_2} = L_1 + L_2 + L_3 \cos\theta_2 + L_4 \cos(\theta_2 + \theta_3) \end{cases} \tag{A-30}$$

Left Ankle:

$$\begin{cases} x_{O_{11}} = G_{11\_1} = x_R - L_3 \sin\theta_2 - L_4 \sin(\theta_2 + \theta_3) + L_4 \sin(\theta_2 + \theta_3 + \theta_4 + \theta_9) + L_3 \sin(\theta_2 + \theta_3 + \theta_4 + \theta_9 + \theta_{10}) \\ y_{O_{11}} = y_{aR} + L_h \\ z_{O_{11}} = G_{11\_2} = L_1 + L_2 + L_3 \cos\theta_2 + L_4 \cos(\theta_2 + \theta_3) - L_4 \cos(\theta_2 + \theta_3 + \theta_4 + \theta_9) - L_3 \cos(\theta_2 + \theta_3 + \theta_4 + \theta_9 + \theta_{10}) \end{cases}$$

(A-31)

Appendix B

Mechanical Design of the10 DOF Biped Robot

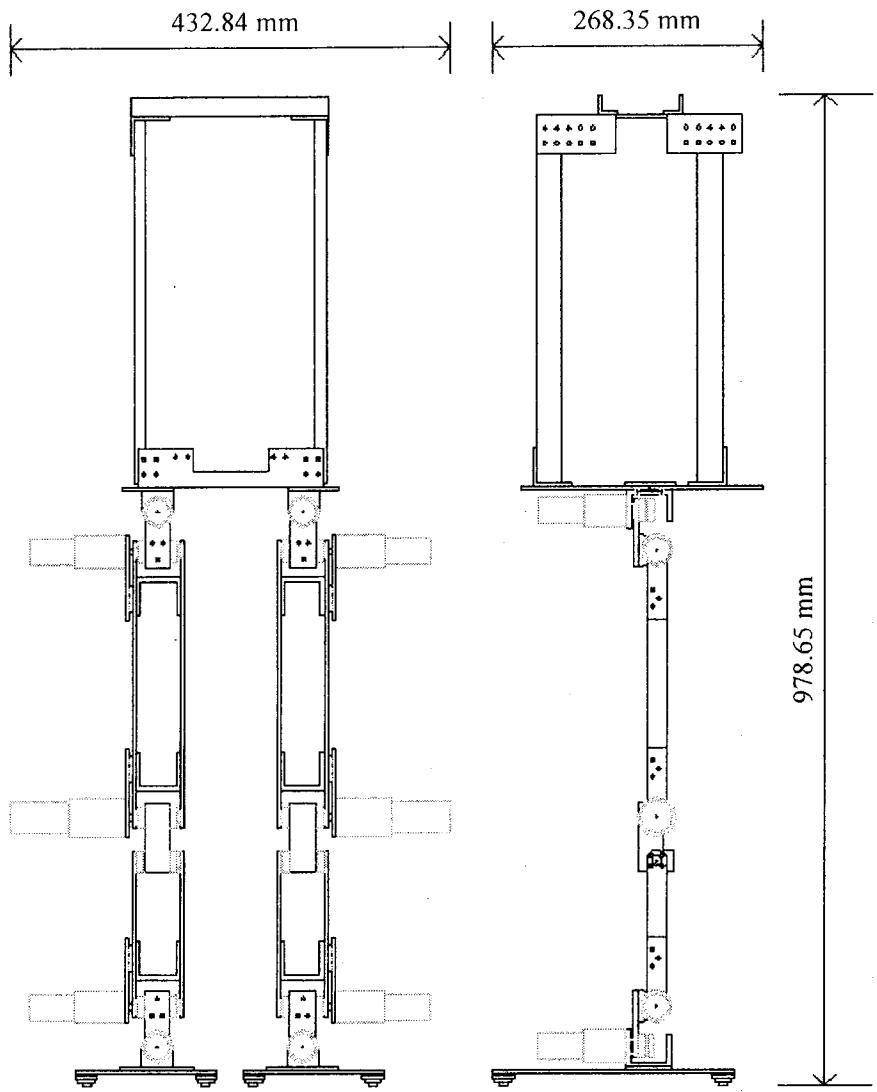

Fig. B-1 Front and side views for the 10-DOF biped robot

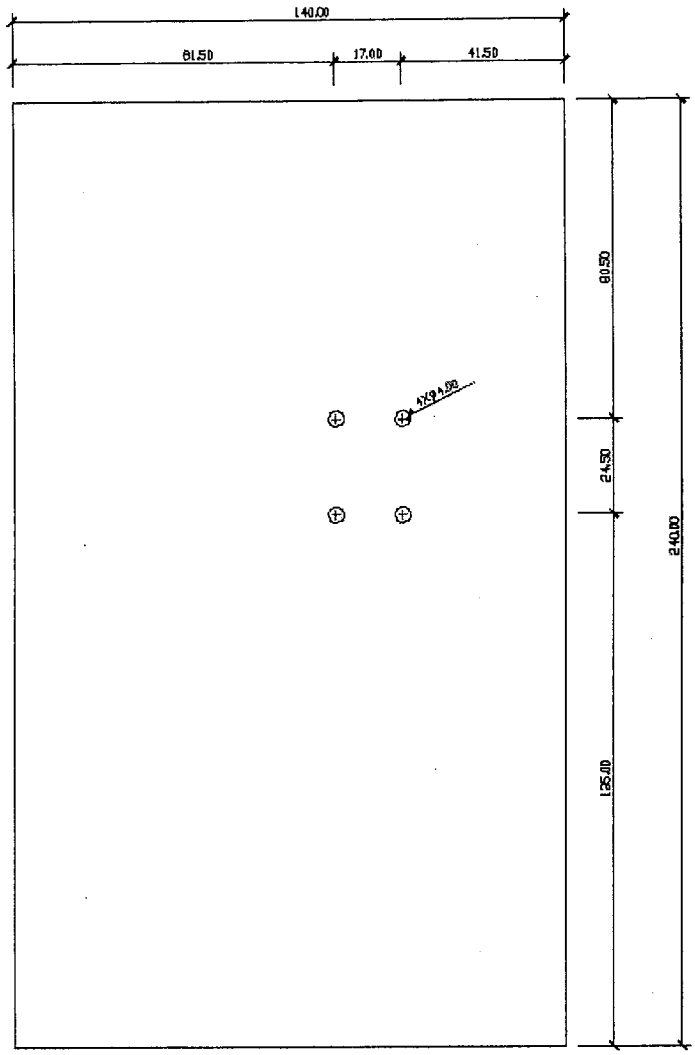

Fig. B-2 Foot plate of the biped robot

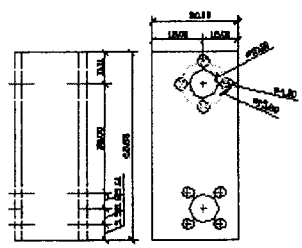

Fig. B-3 Pieces for knee

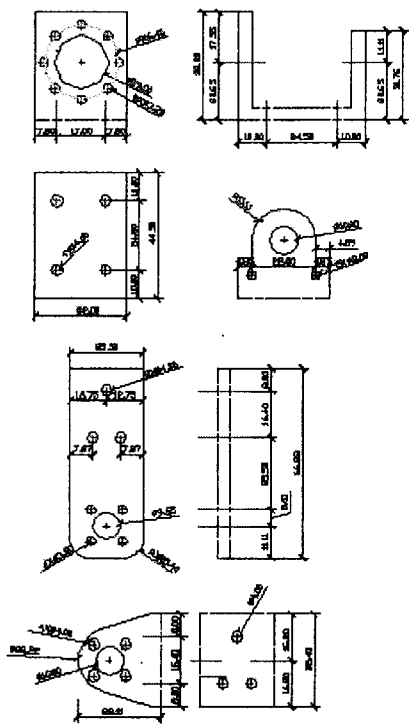

Fig. B-4 Pieces for ankle and hip

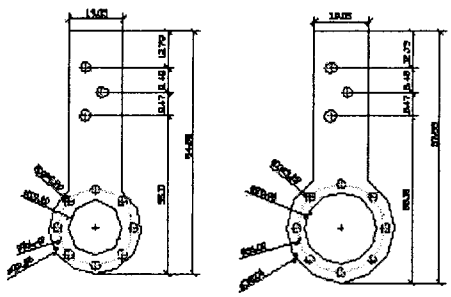

Fig. B-5 Mounting plates for DC Motor

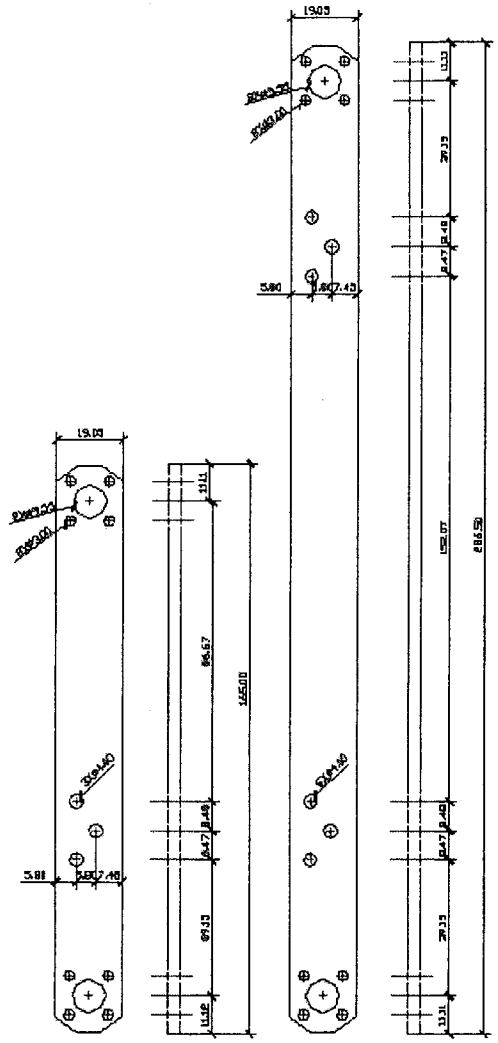

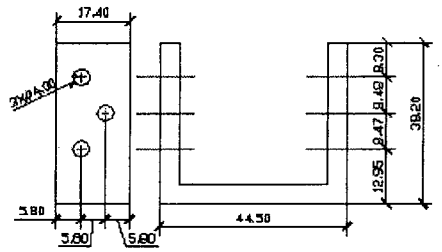

Fig. B-6 Pieces for lower leg and upper leg

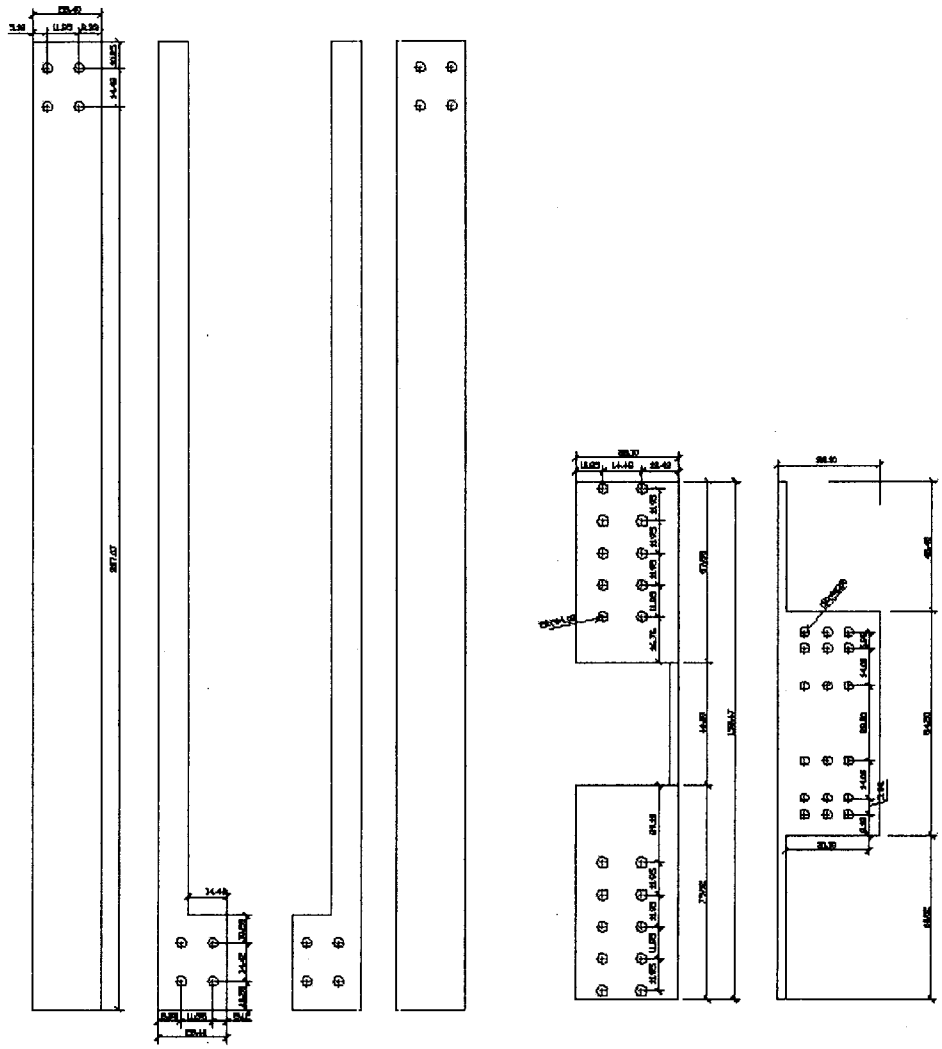

Fig. B-7 Pieces for the body of the robot 1

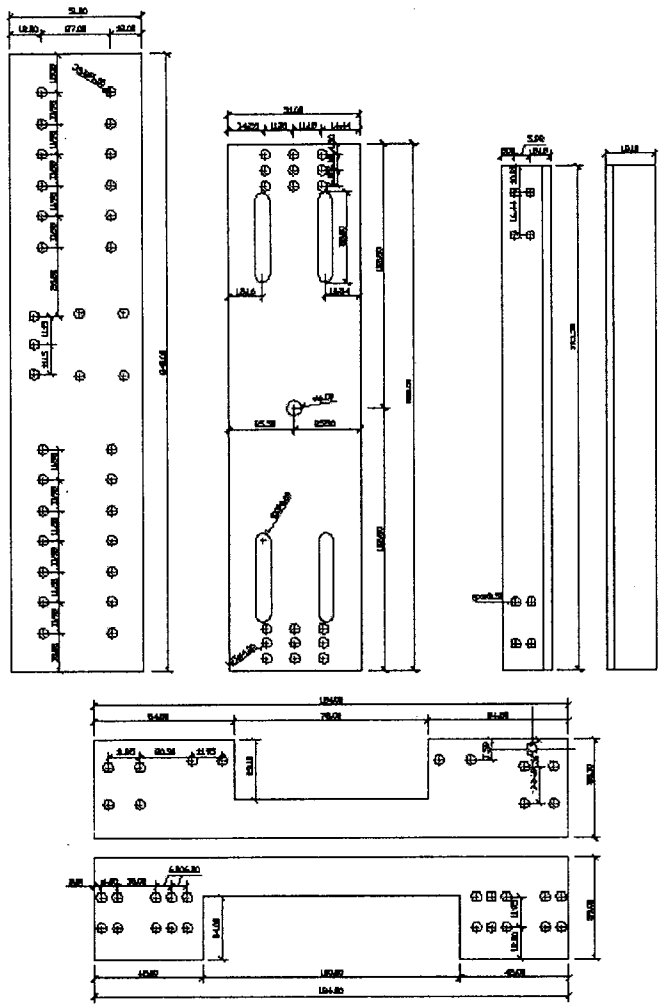

Fig. B-8 Pieces for the body of the robot 2

Appendix C

Block Diagram and Layout Schematics of eZdspTM F2812

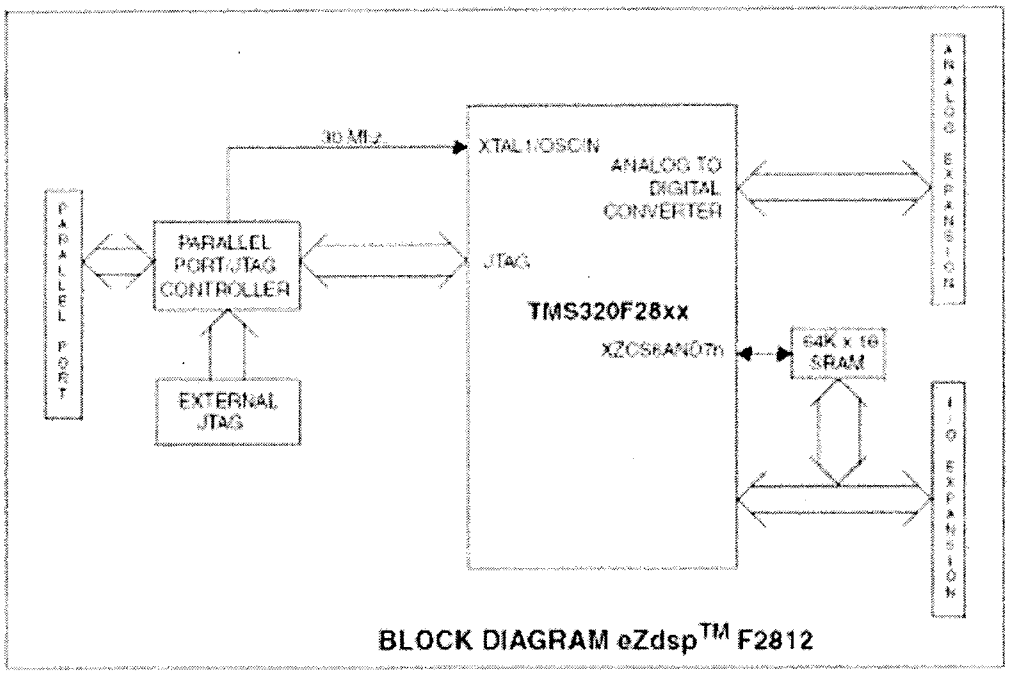

Fig. C-1 Block Diagram of the eZdspTM F2812

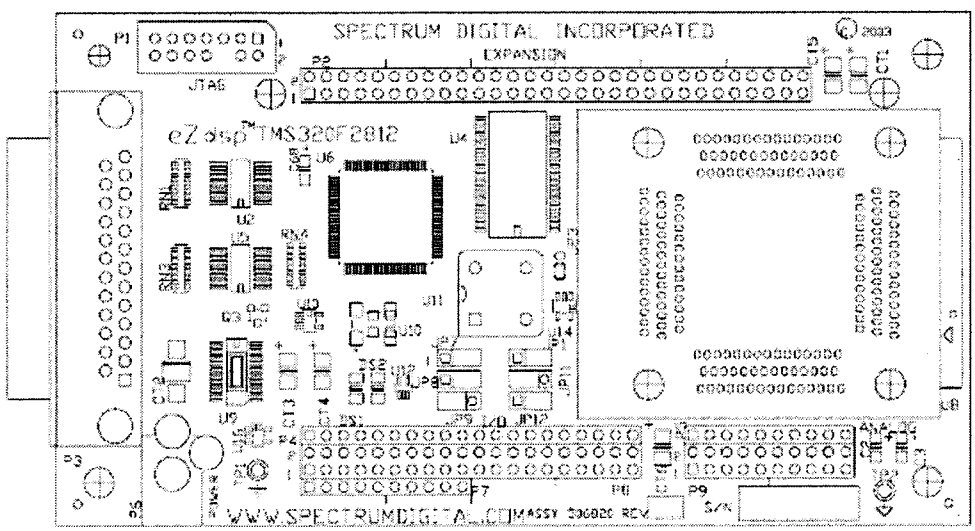

Fig. C-2 Layout of Socketed version of the eZdspTM F2812

Appendix D

Schematics of Electric Circuits

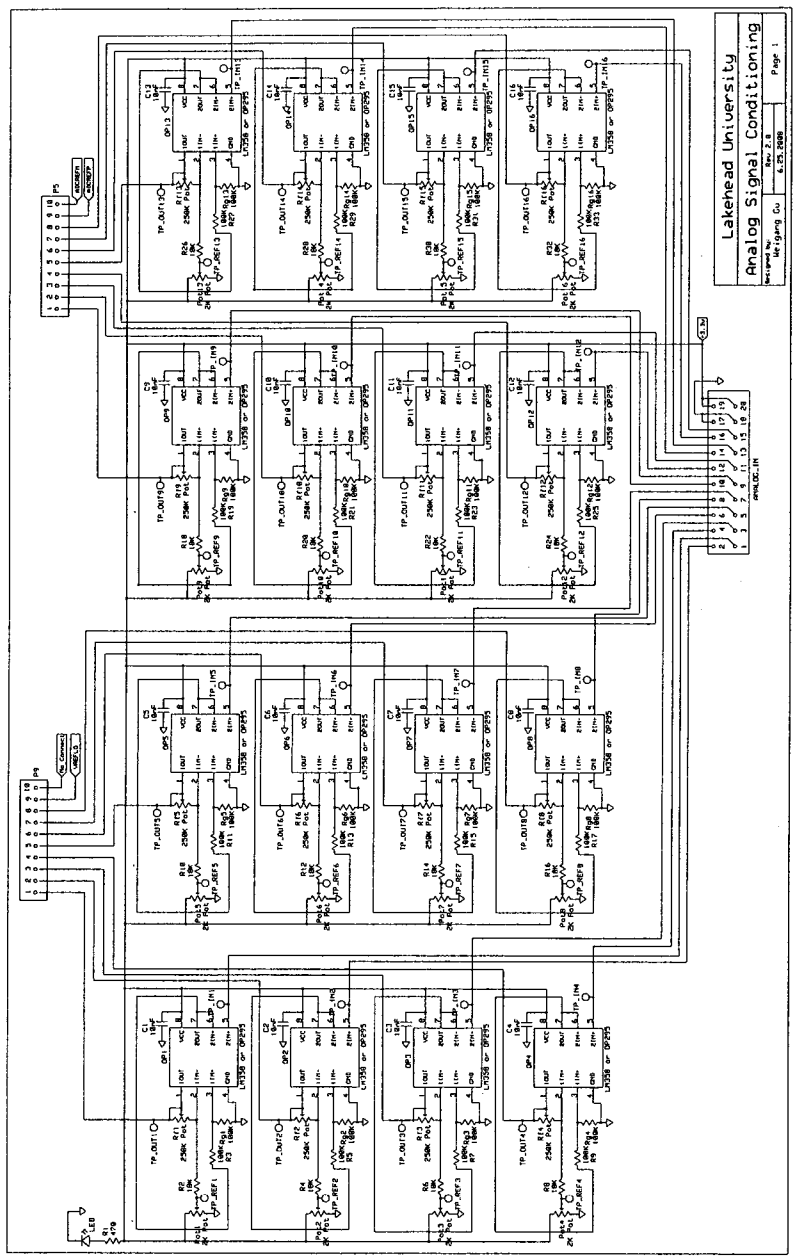

Fig. D-1 Schematics of analog signal conditioning circuit

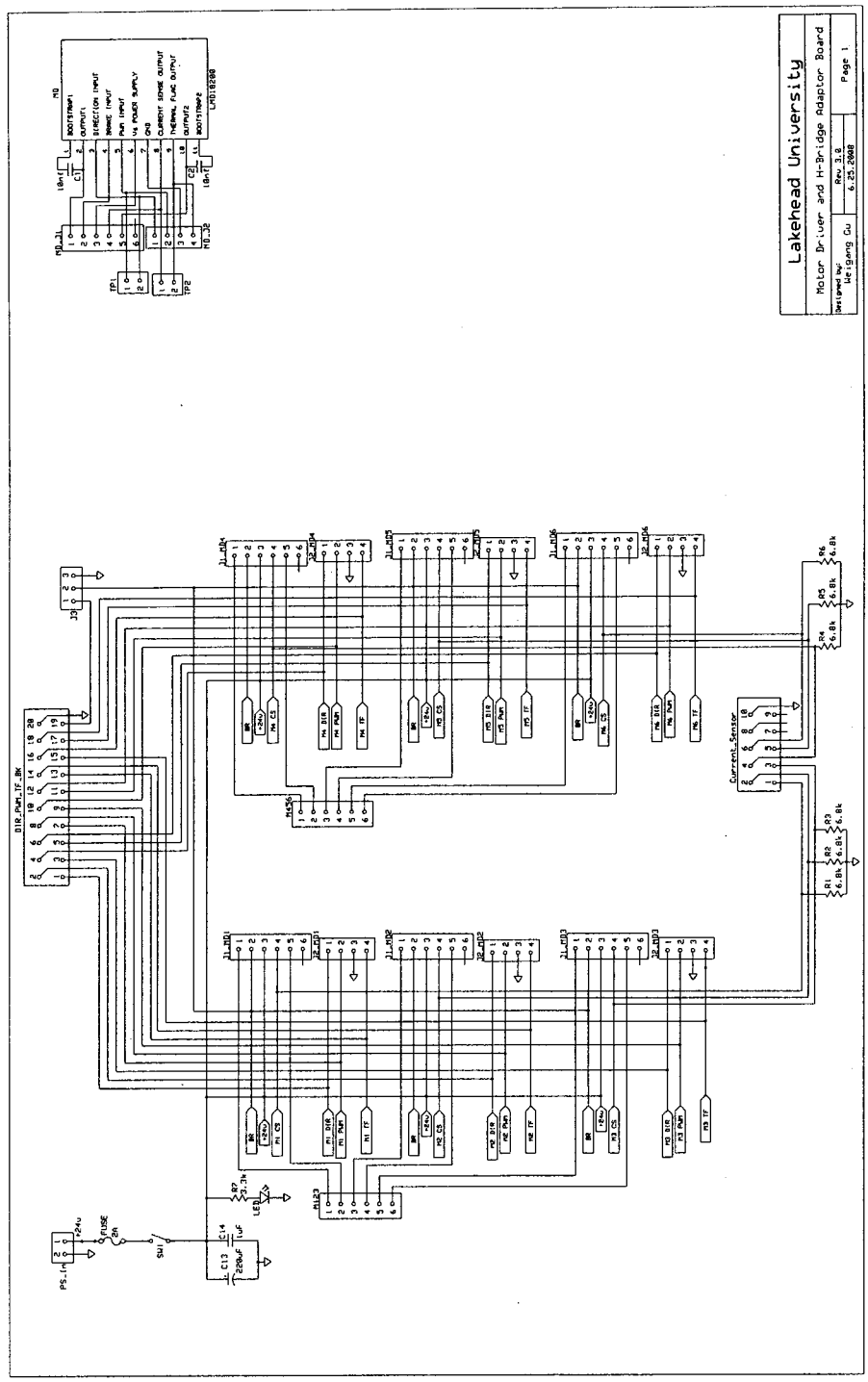

Fig. D-2 Schematics of motor driver circuit and H-bridge adaptor circuit

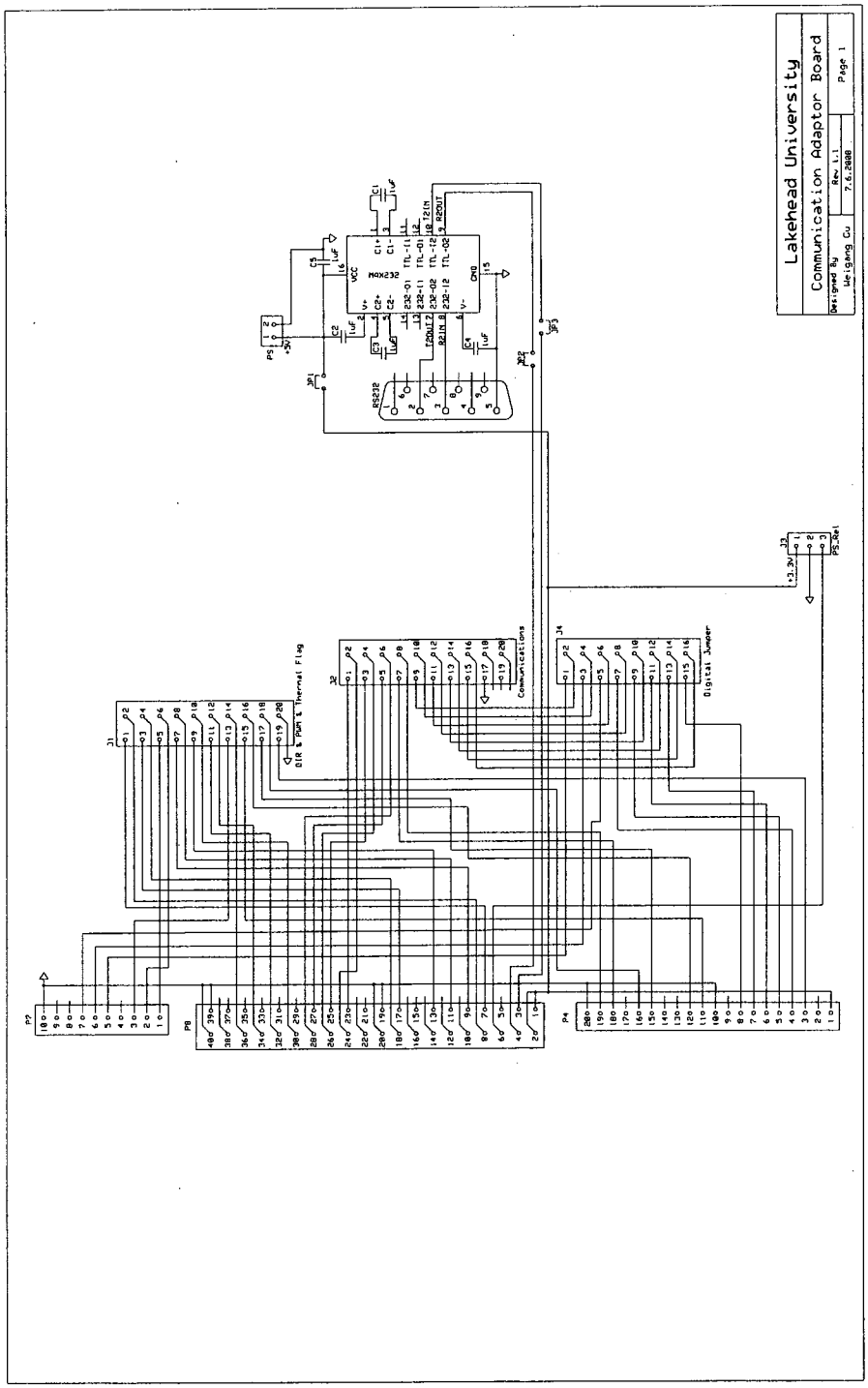

Fig. D-3 Schematics of communication circuit

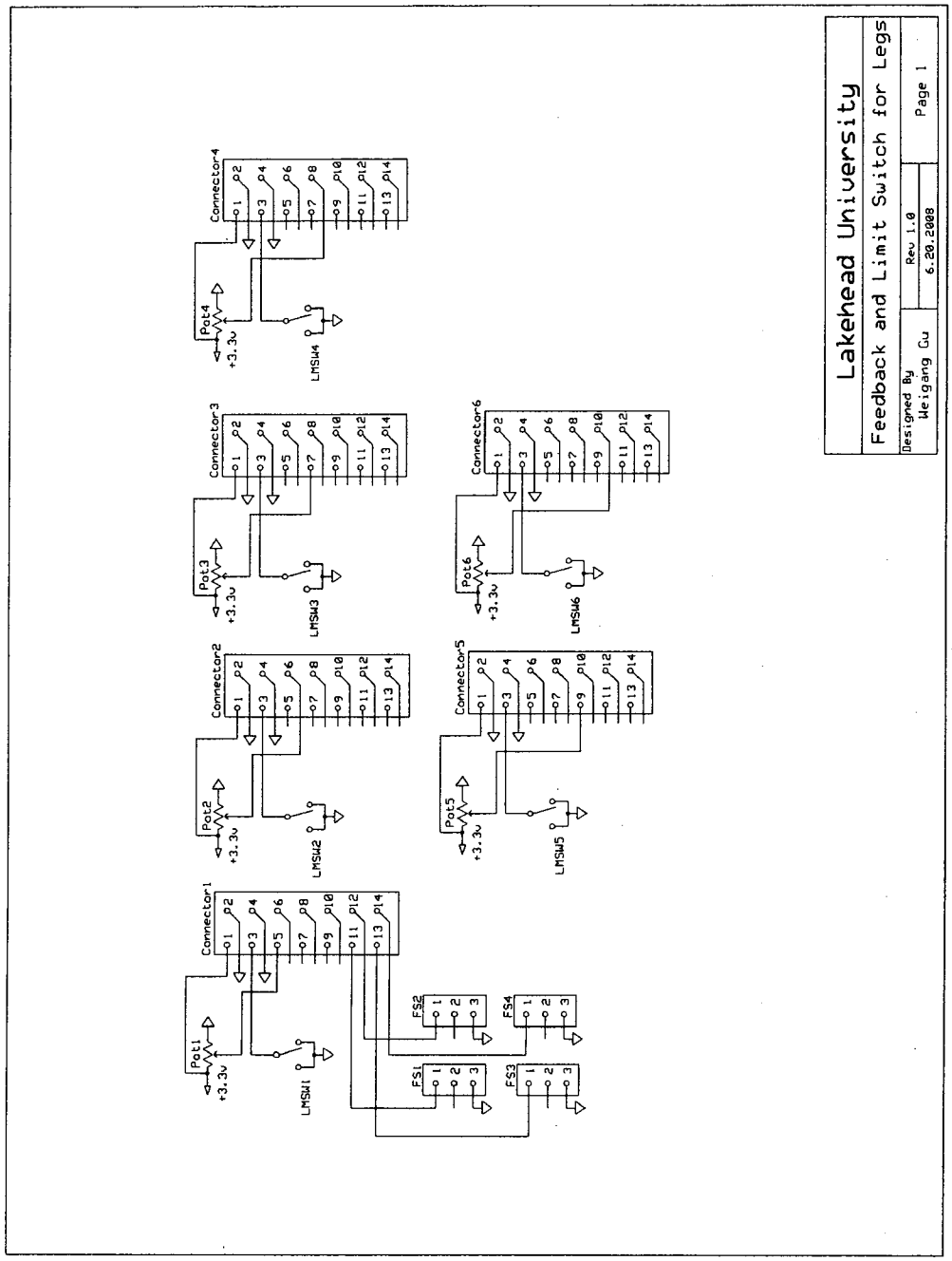

Fig. D-4 Schematics of potentiometer feedback and limit switch circuit

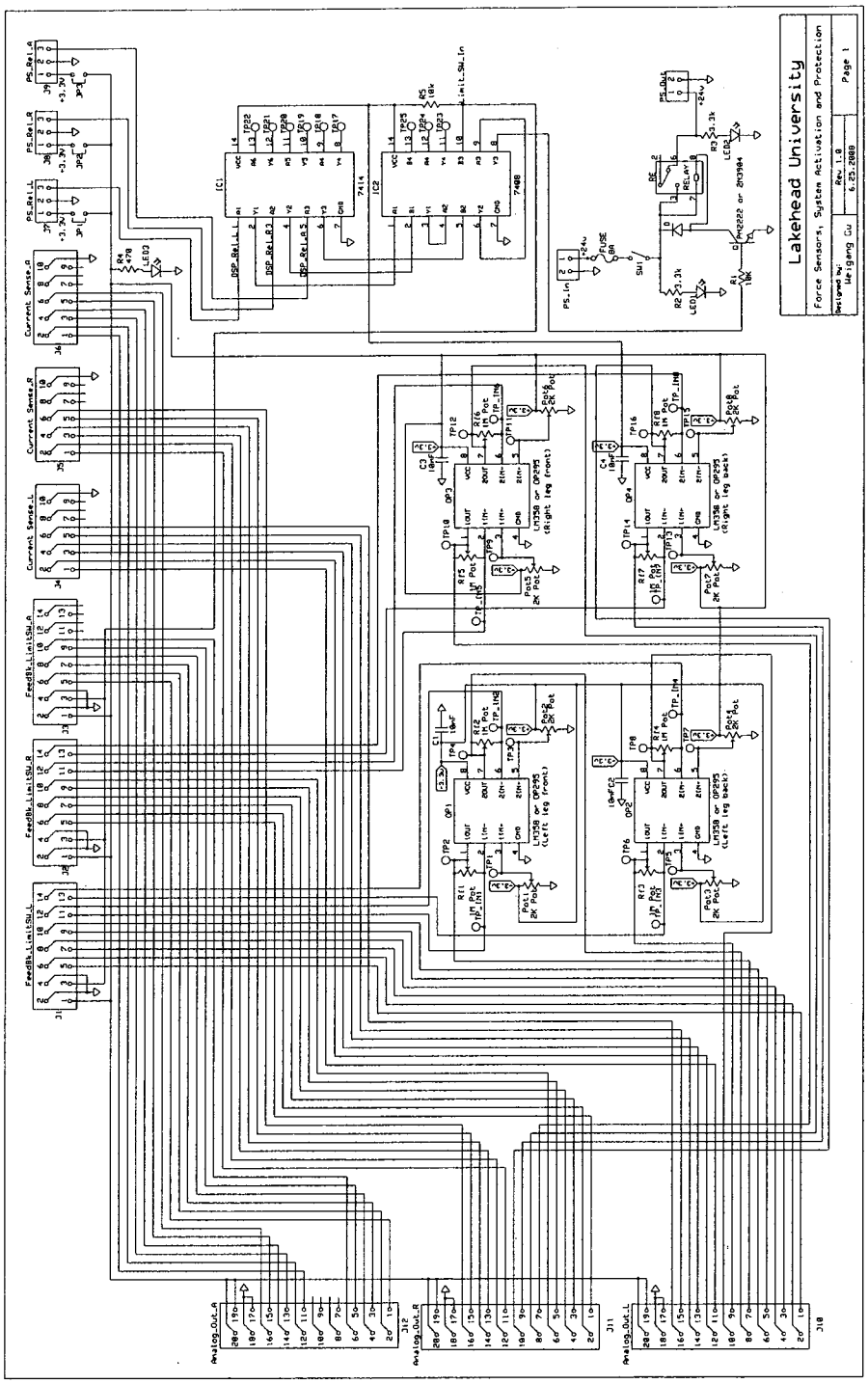

Fig. D-5 Schematics of force sensor, system activation and protection circuit

Appendix E

PCB Artwork and Components Layout Schematics

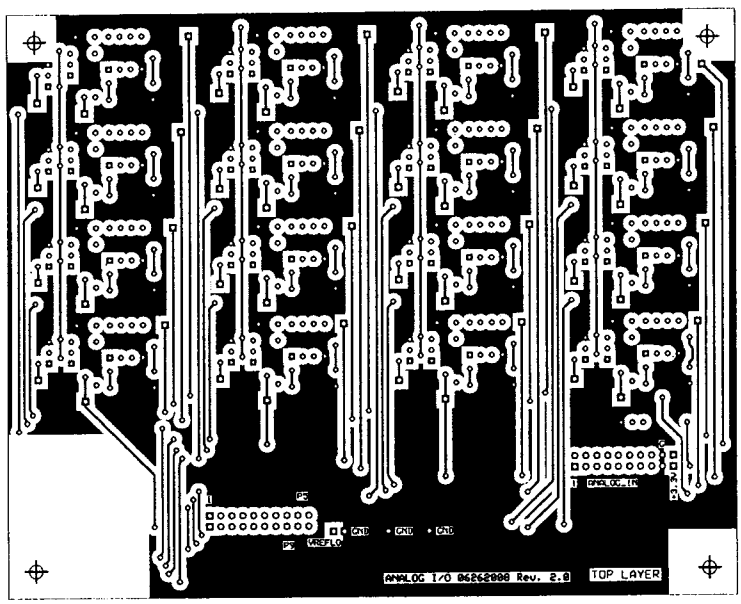

Fig. E-1 Analog signal conditioning board: top layer

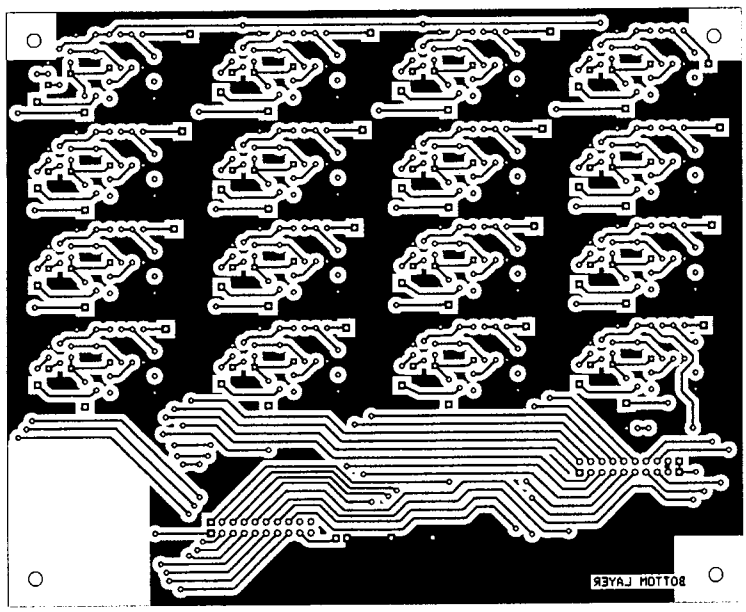

Fig. E-2 Analog signal conditioning board: bottom layer

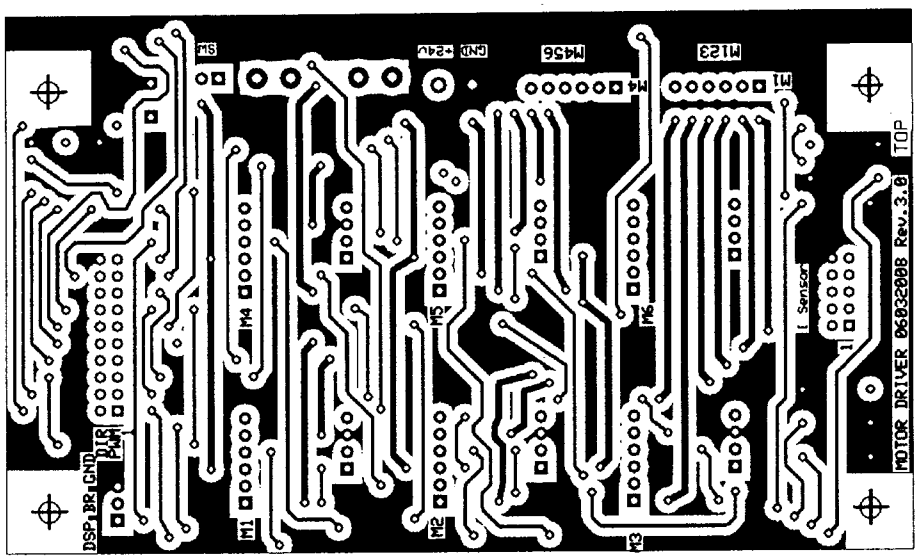

Fig. E-3 Motor driver board: top layer

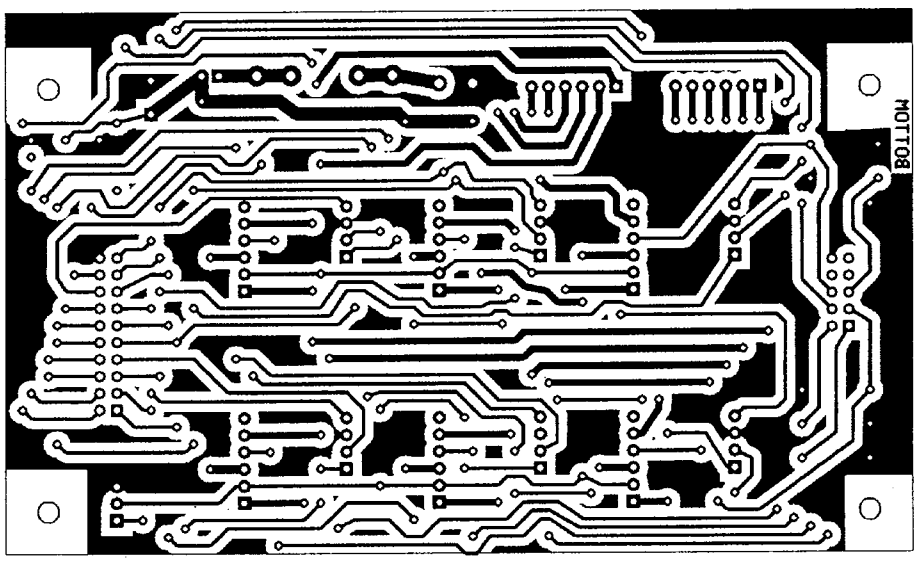

Fig. E-4 Motor driver board: bottom layer

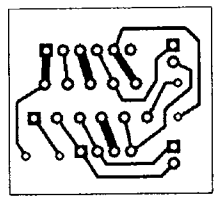

Fig. E-5 H-bridge adaptor board: top layer

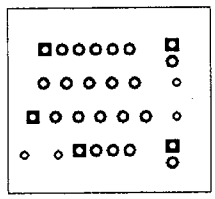

Fig. E-6 H-bridge adaptor board: bottom layer

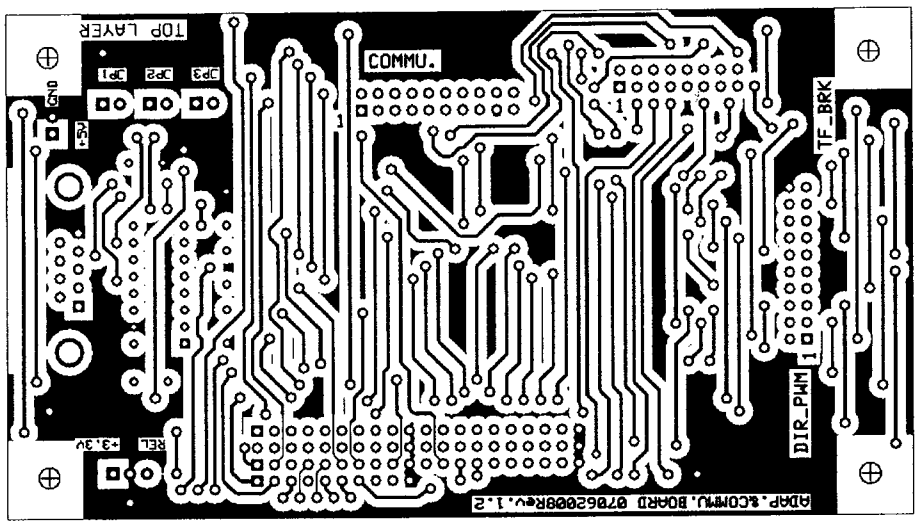

Fig. E-7 Communication adaptor board: top layer

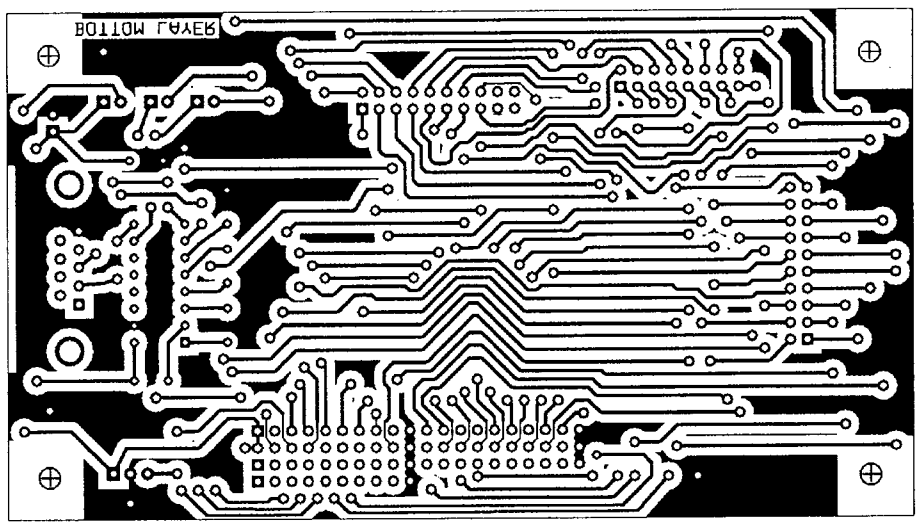

Fig. E-8 Communication adaptor board: bottom layer

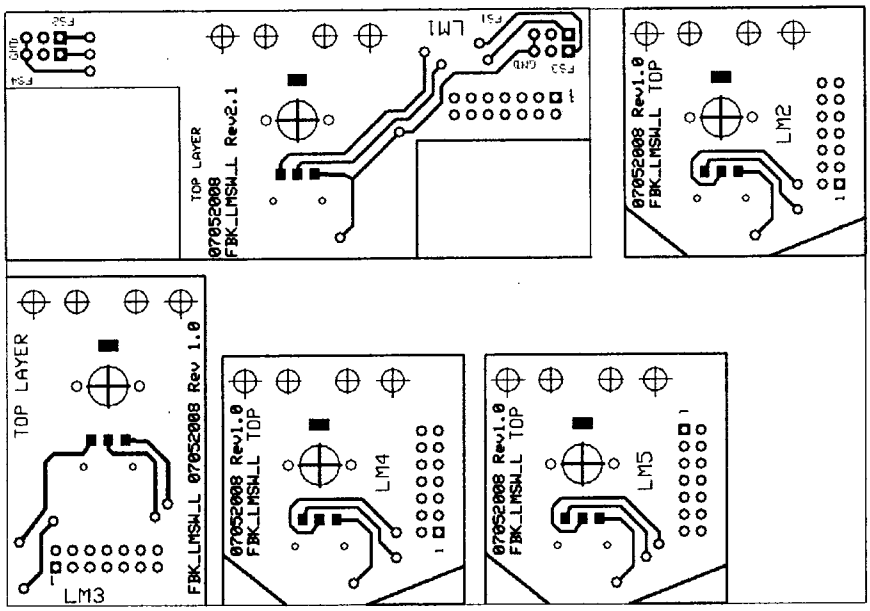

Fig. E-9 Feedback and limit switch board for left leg: top layer

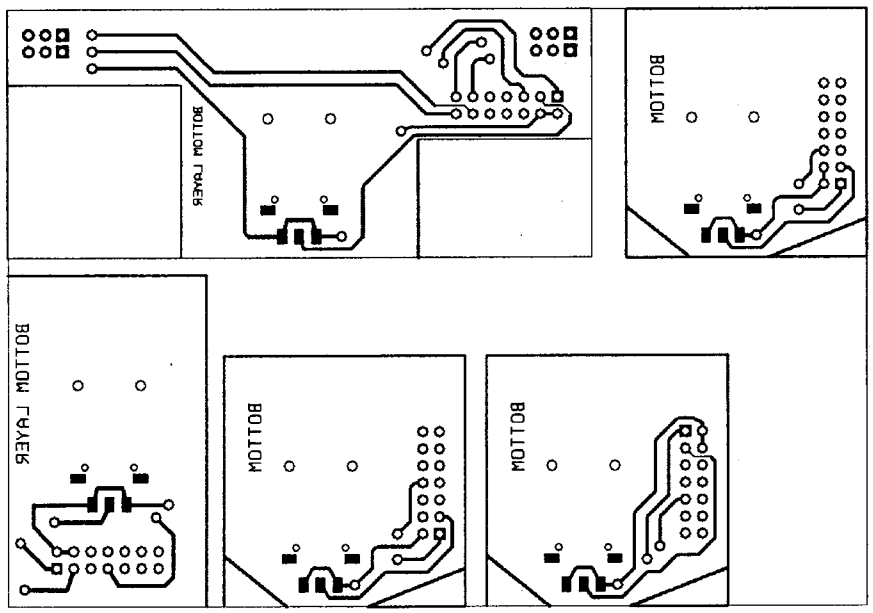

Fig. E-10 Feedback and limit switch board for left leg: bottom layer

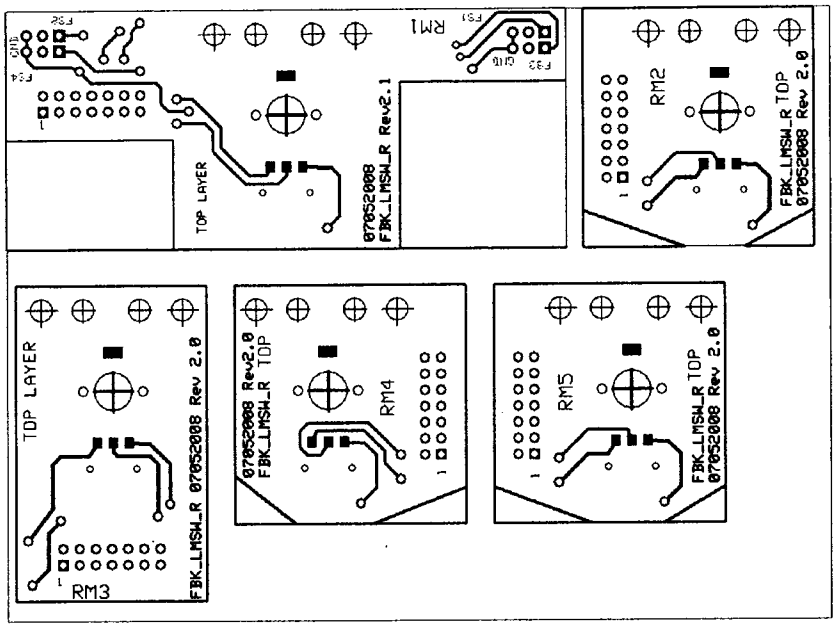

Fig. E-11 Feedback and limit switch board for right leg: top layer

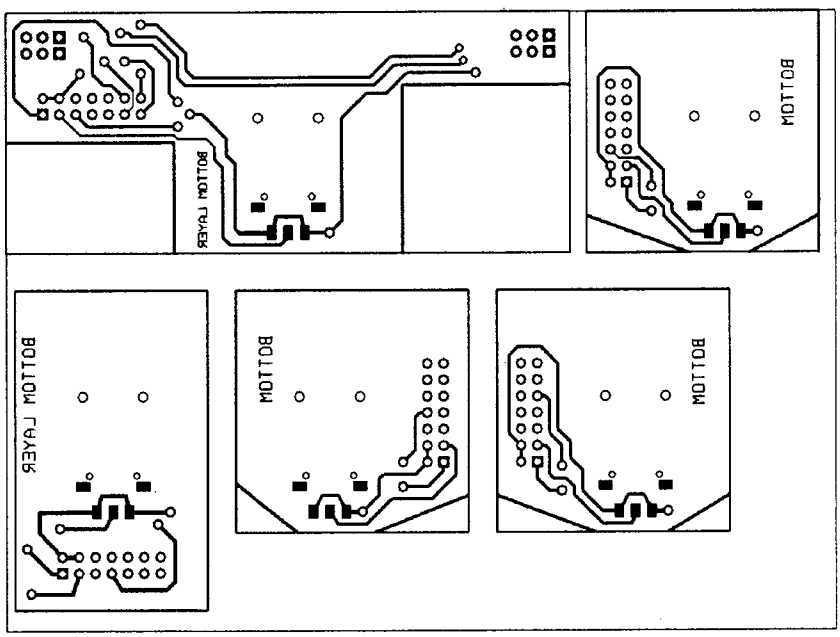

Fig. E-12 Feedback and limit switch board for right leg: bottom layer

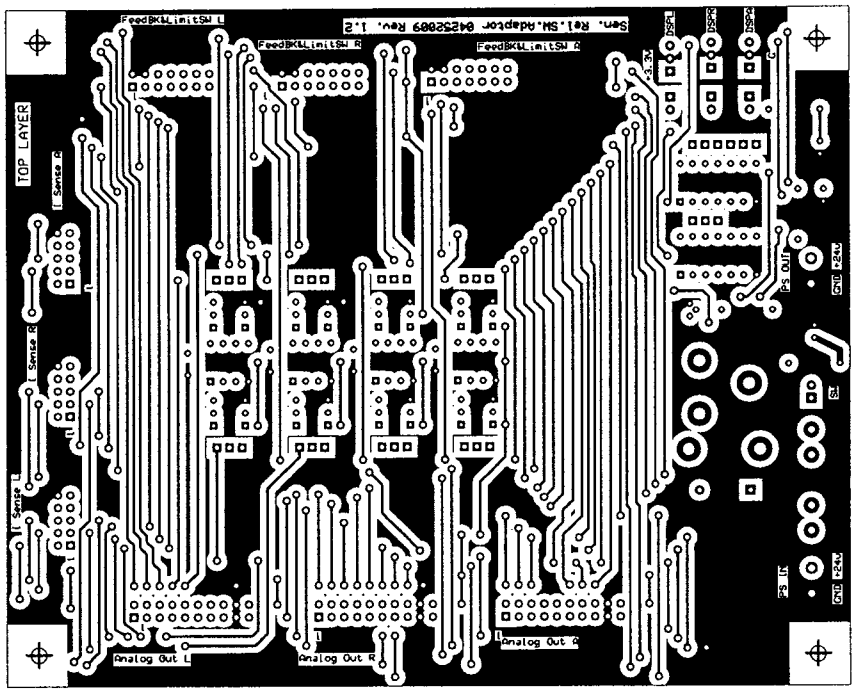

Fig. E-13 Force sensor, system activation and protection board: top layer

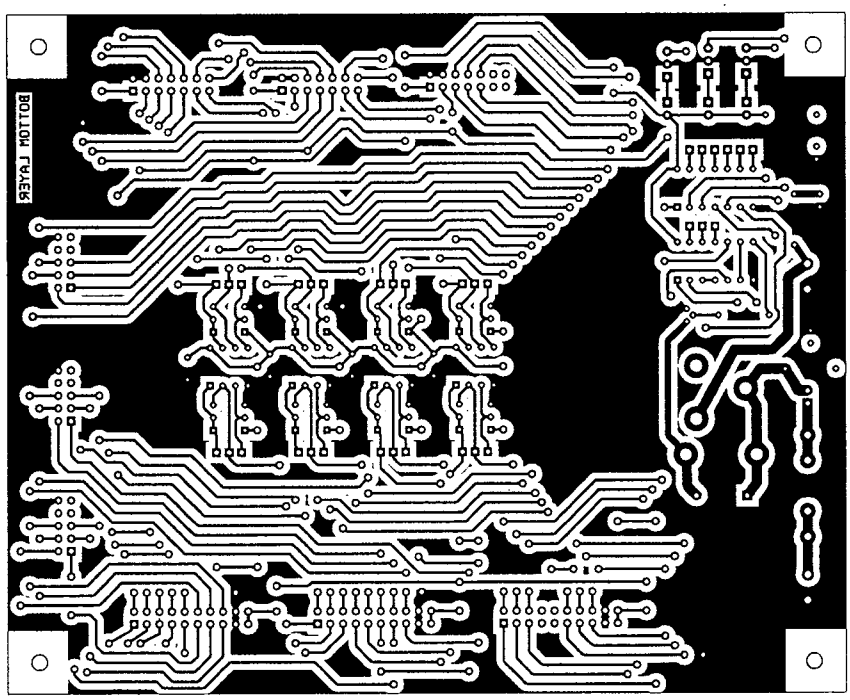

Fig. E-14 Force sensor, system activation and protection board: bottom layer

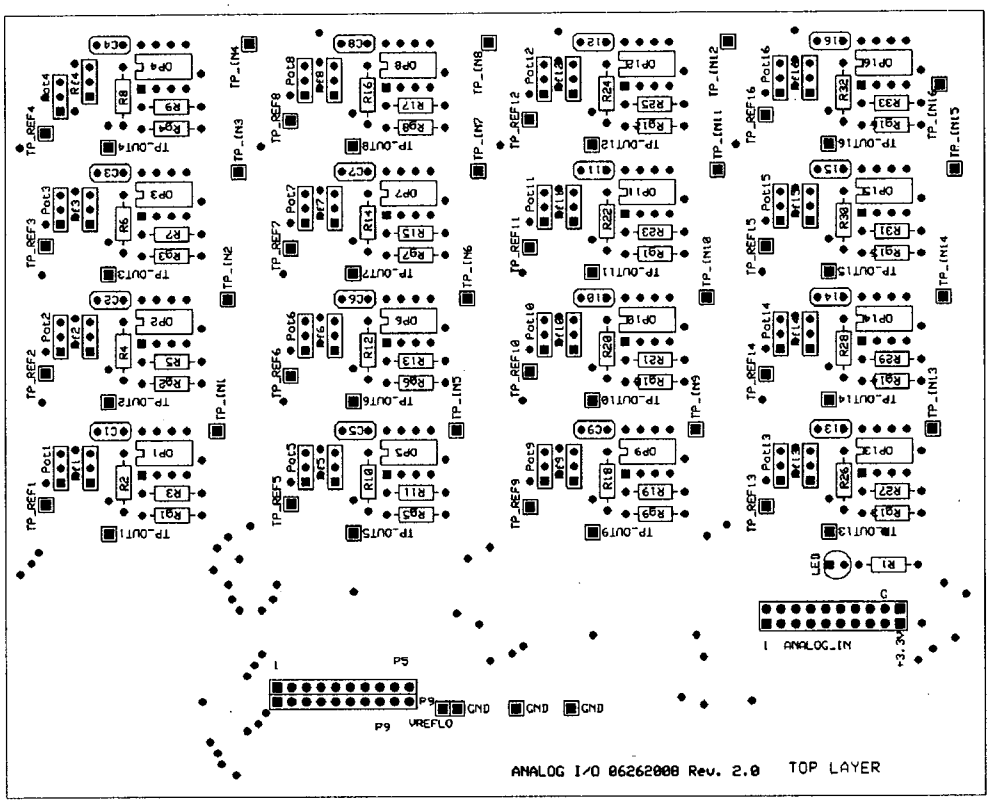

Fig. E-15 Analog signal conditioning board: components layout

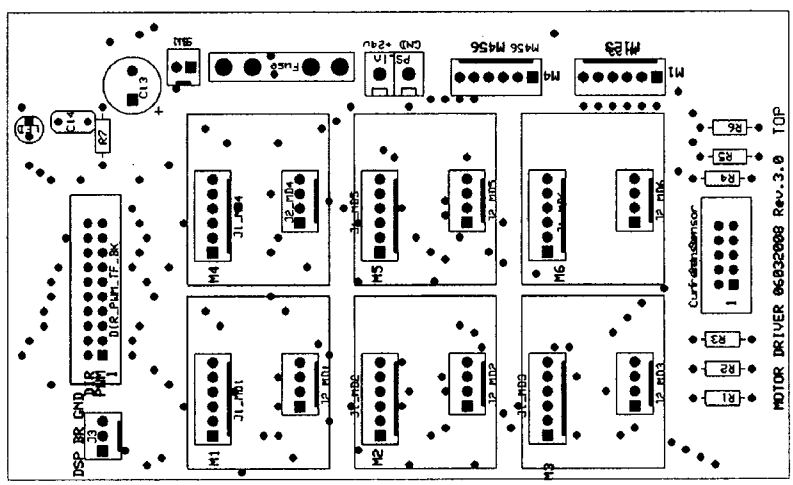

Fig. E-16 Motor driver board: components layout

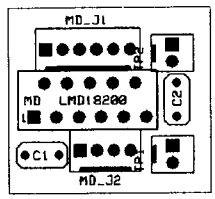

Fig. E-17 H-bridge adaptor board: components layout

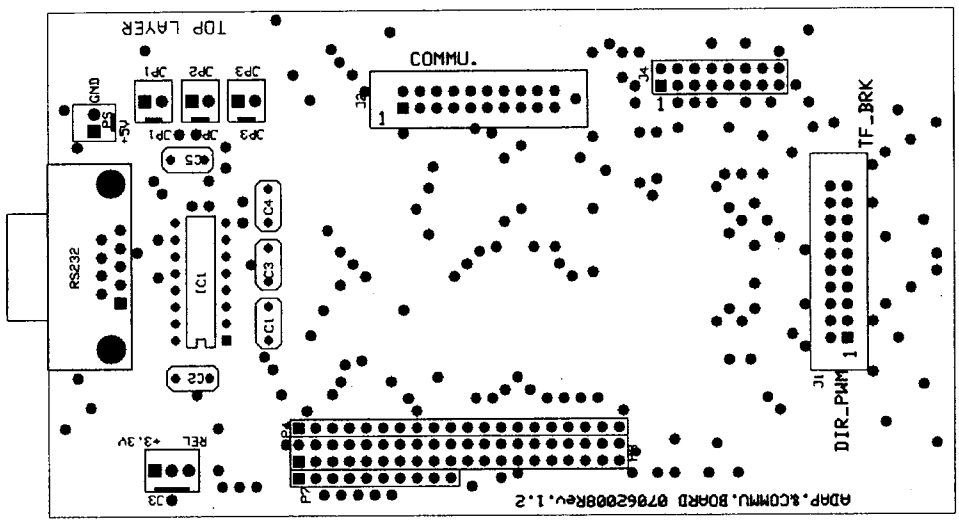

Fig. E-18 Communication Adaptor board: components layout

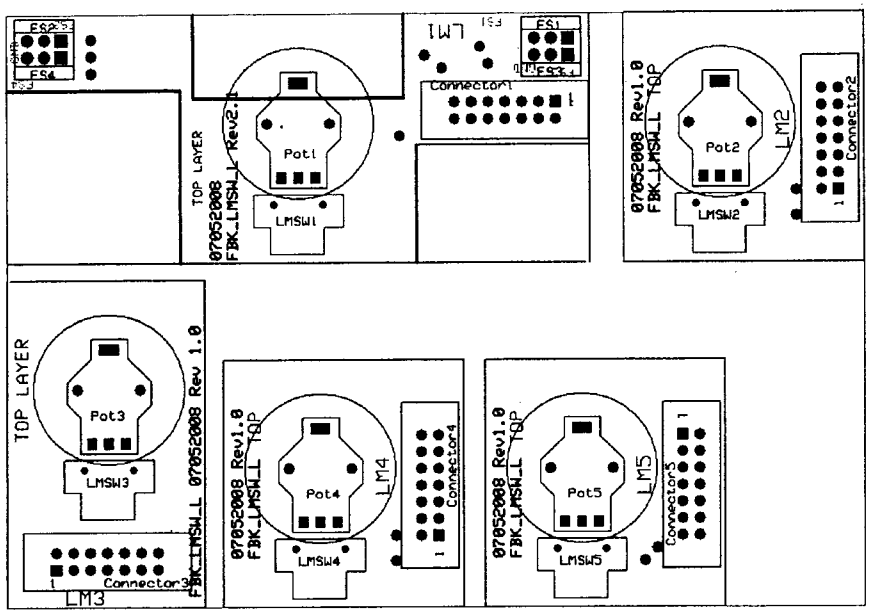

Fig. E-19 Feedback and limit switch board for left leg: components layout

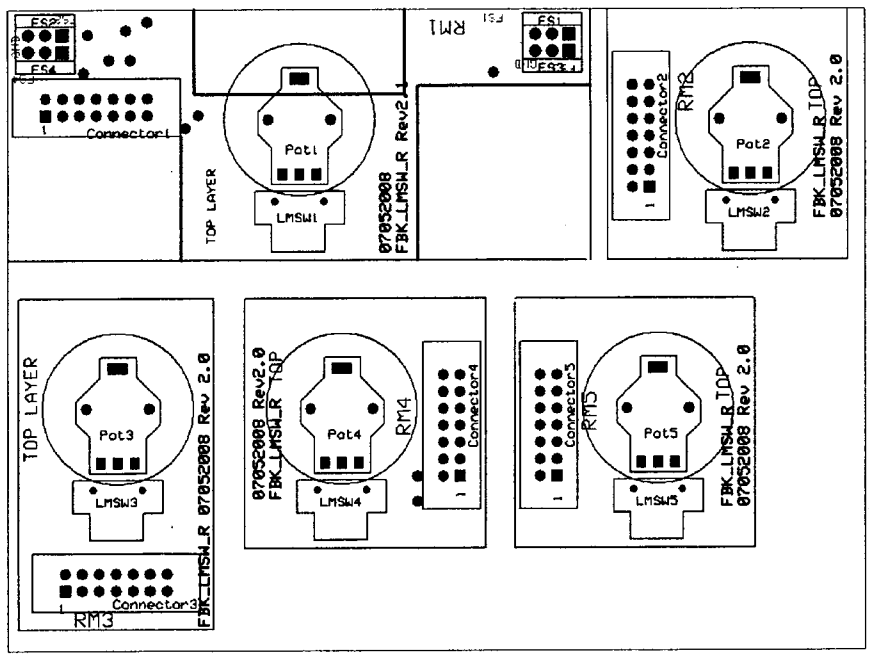

Fig. E-20 Feedback and limit switch board for right leg: components layout

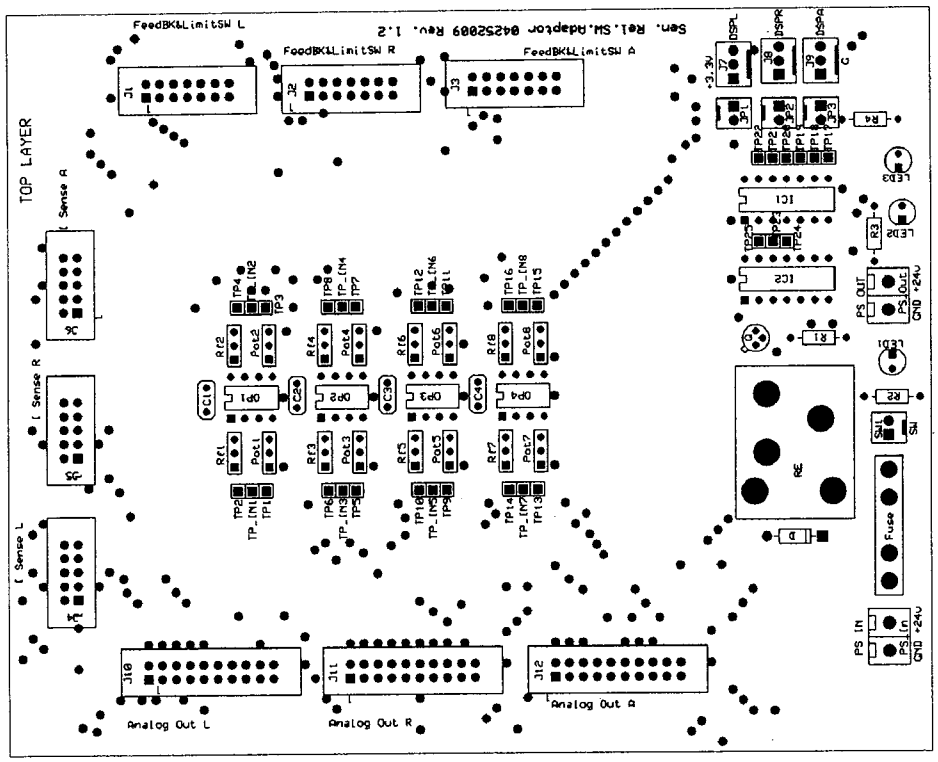

Fig. E-21 Force sensor, system activation and protection board: components layout

Appendix F

MATLAB Simulink Programs

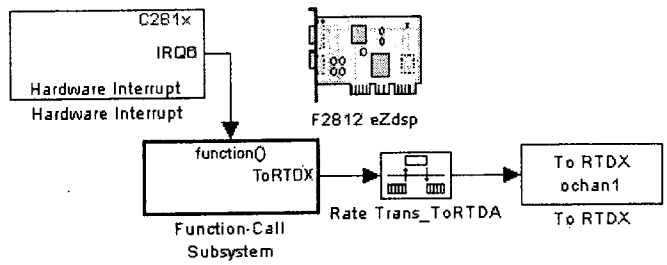

Fig. F-1 Main program for left leg

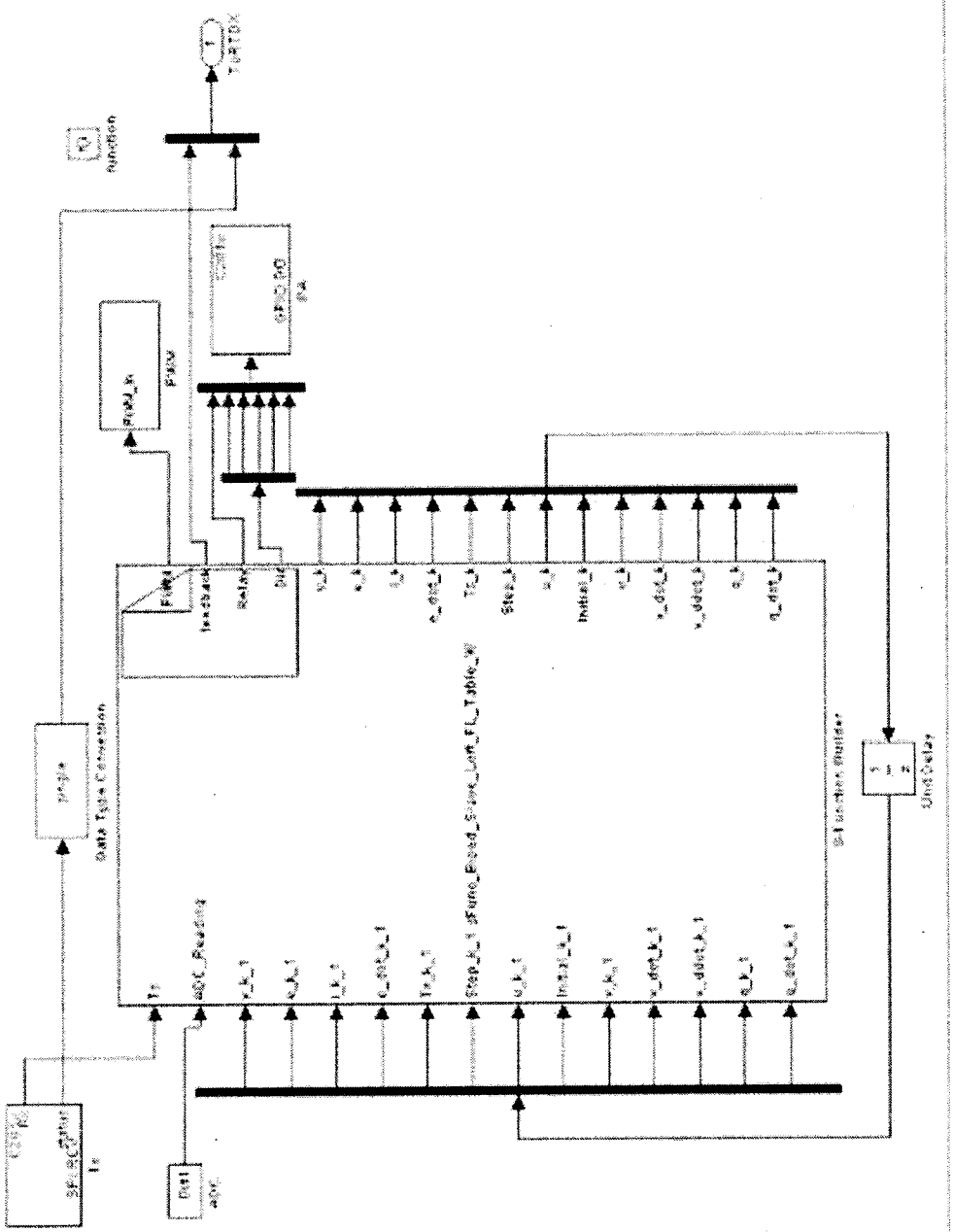

Fig. F-2 Function-call subsystem diagram for left leg

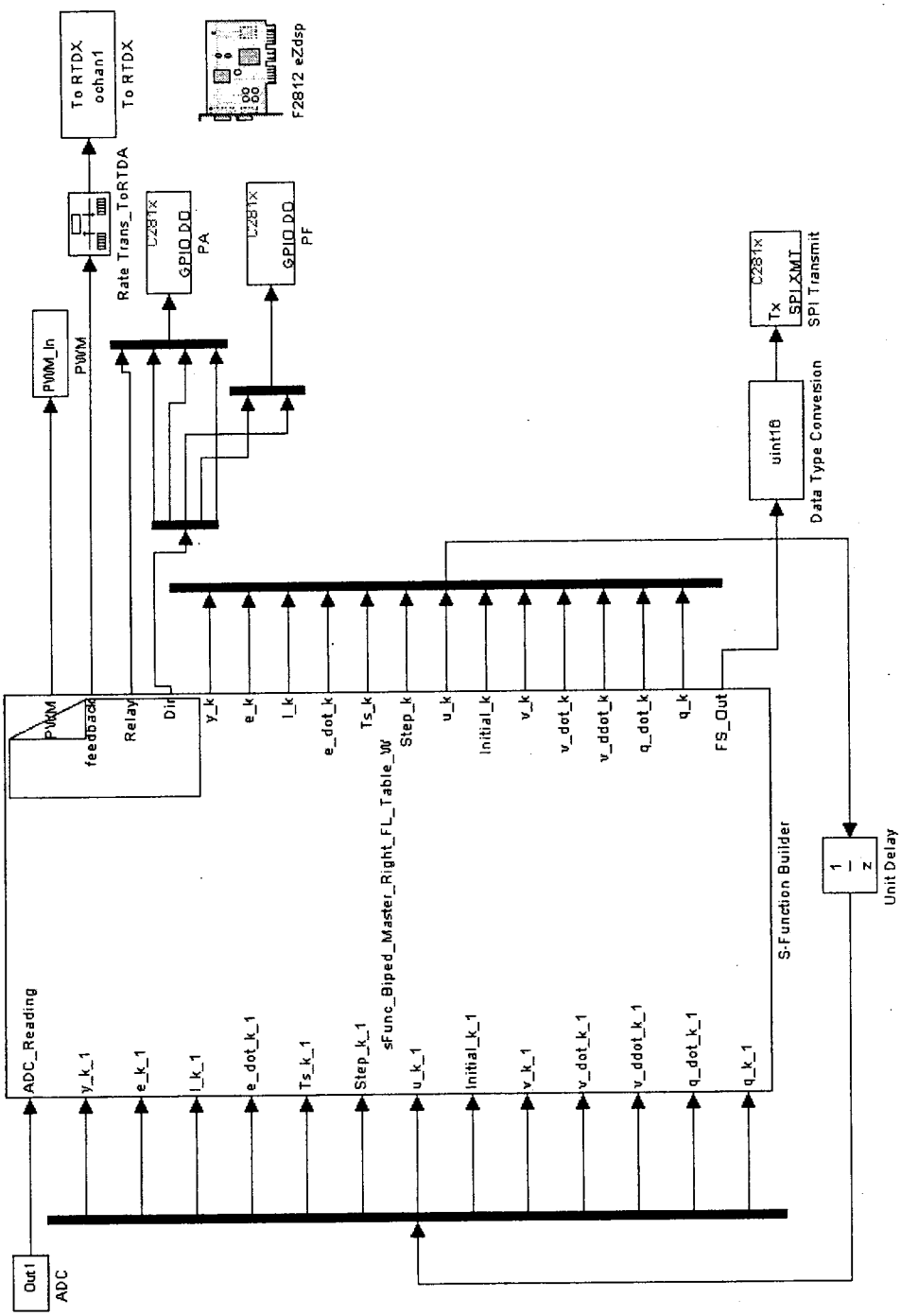

Fig. F-3 Main program for right leg

Appendix G

DC Motors and Gearheads Data Sheets

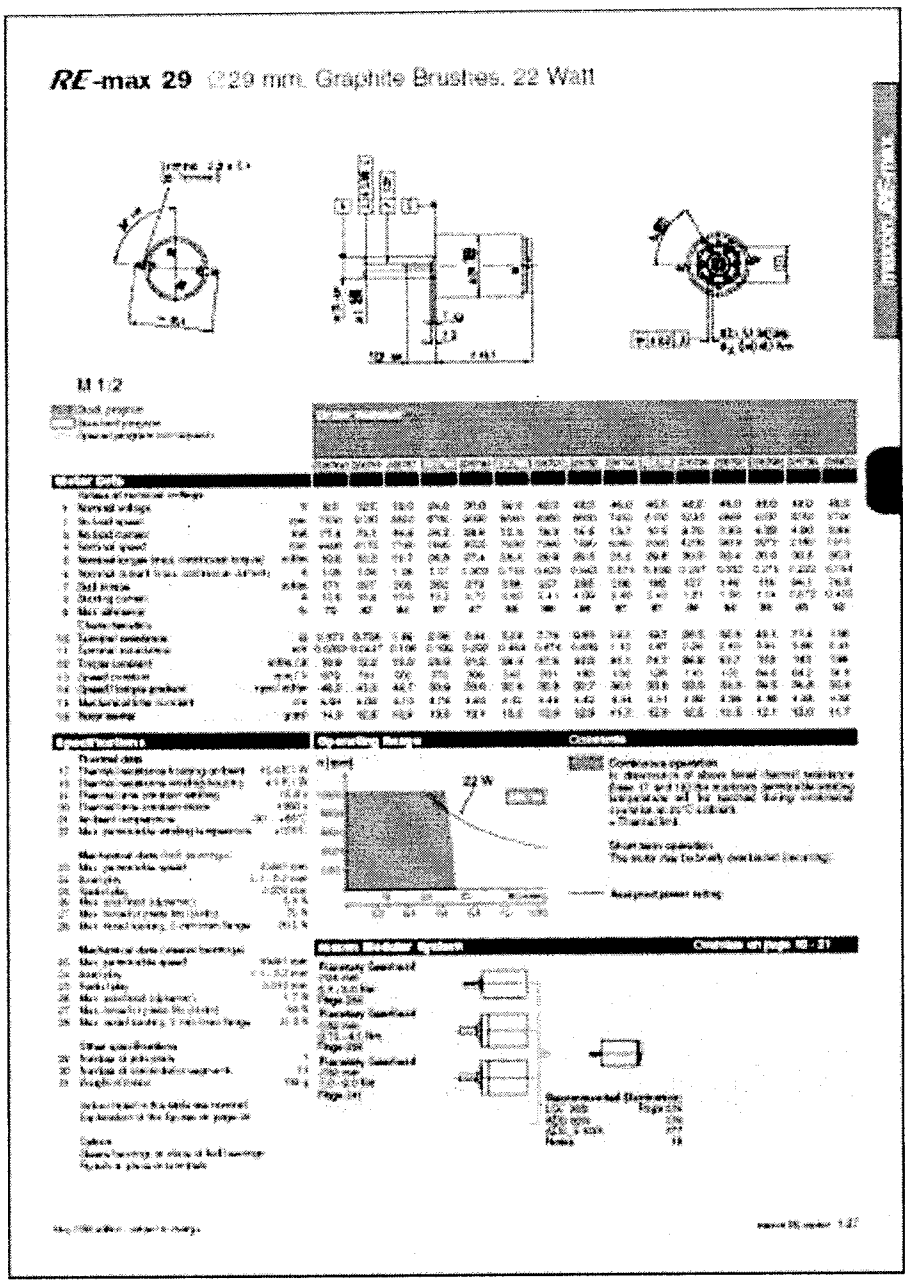

Fig. G-1 Maxon motor RE-max 29

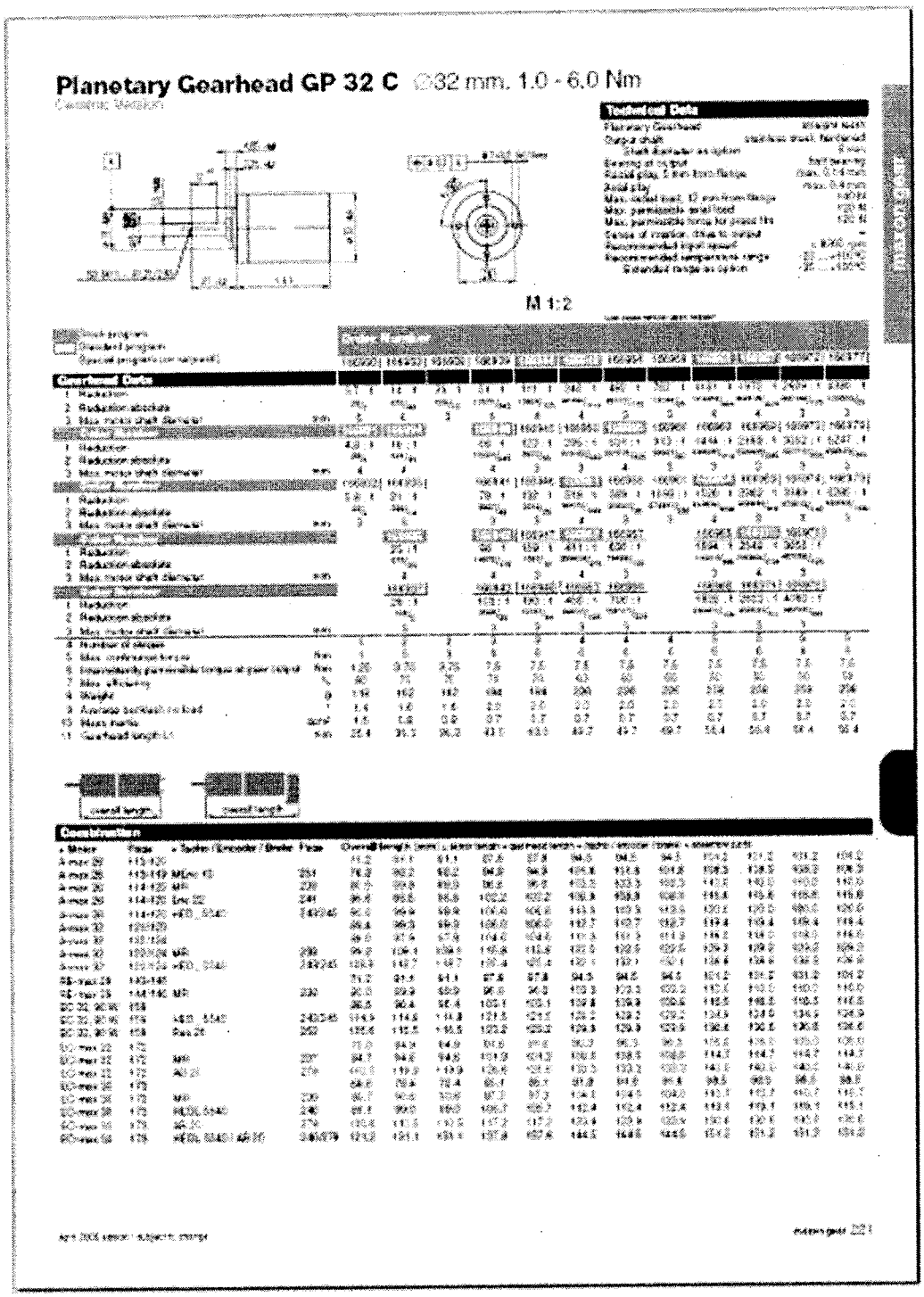

Fig. G-2 Maxon planetary gearhead GP32C

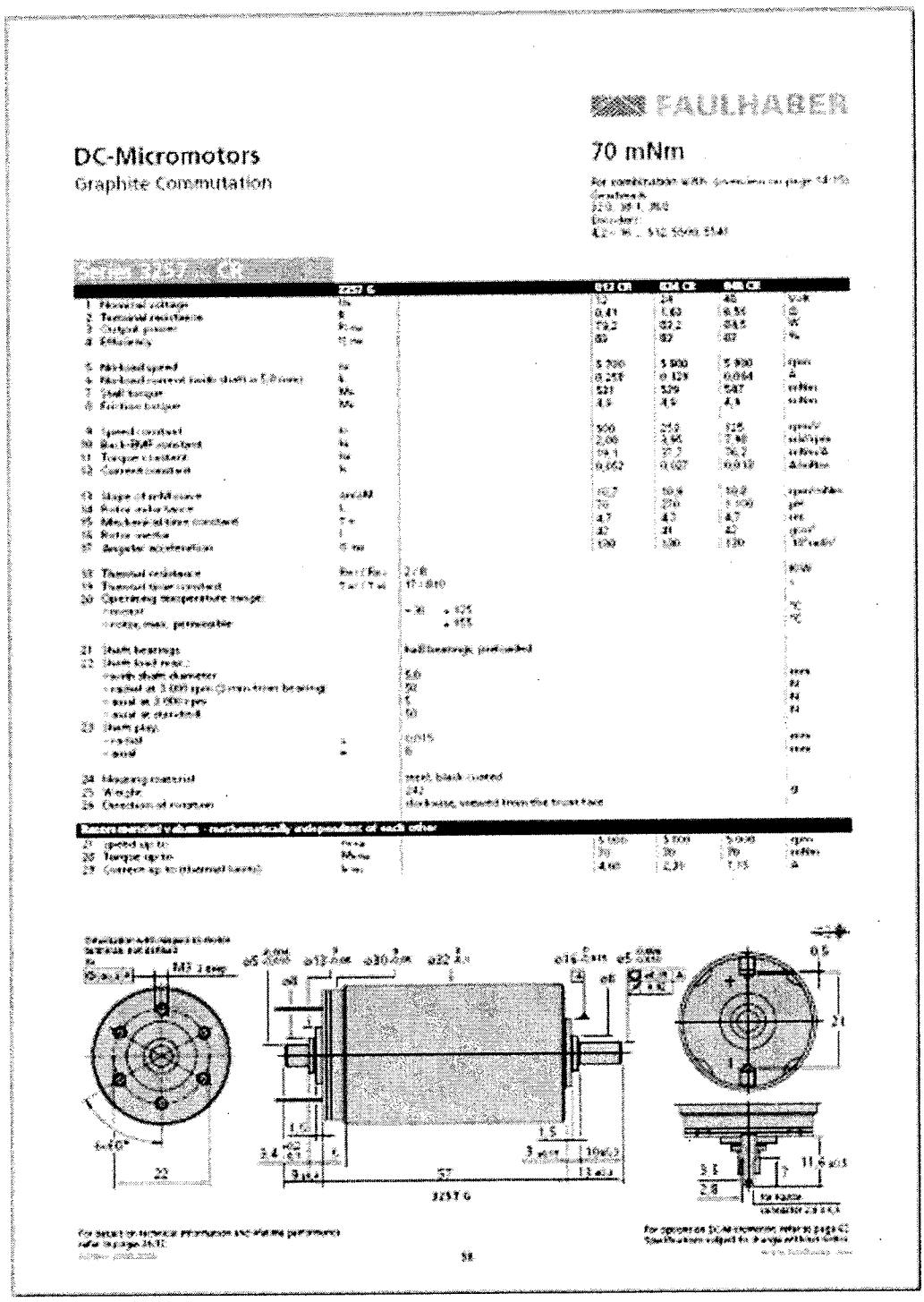

FAULHABER

DC-Micromotors

Graphite Commutation

70 mNm

Fig. G-3 Faulhaber motor 3257CR

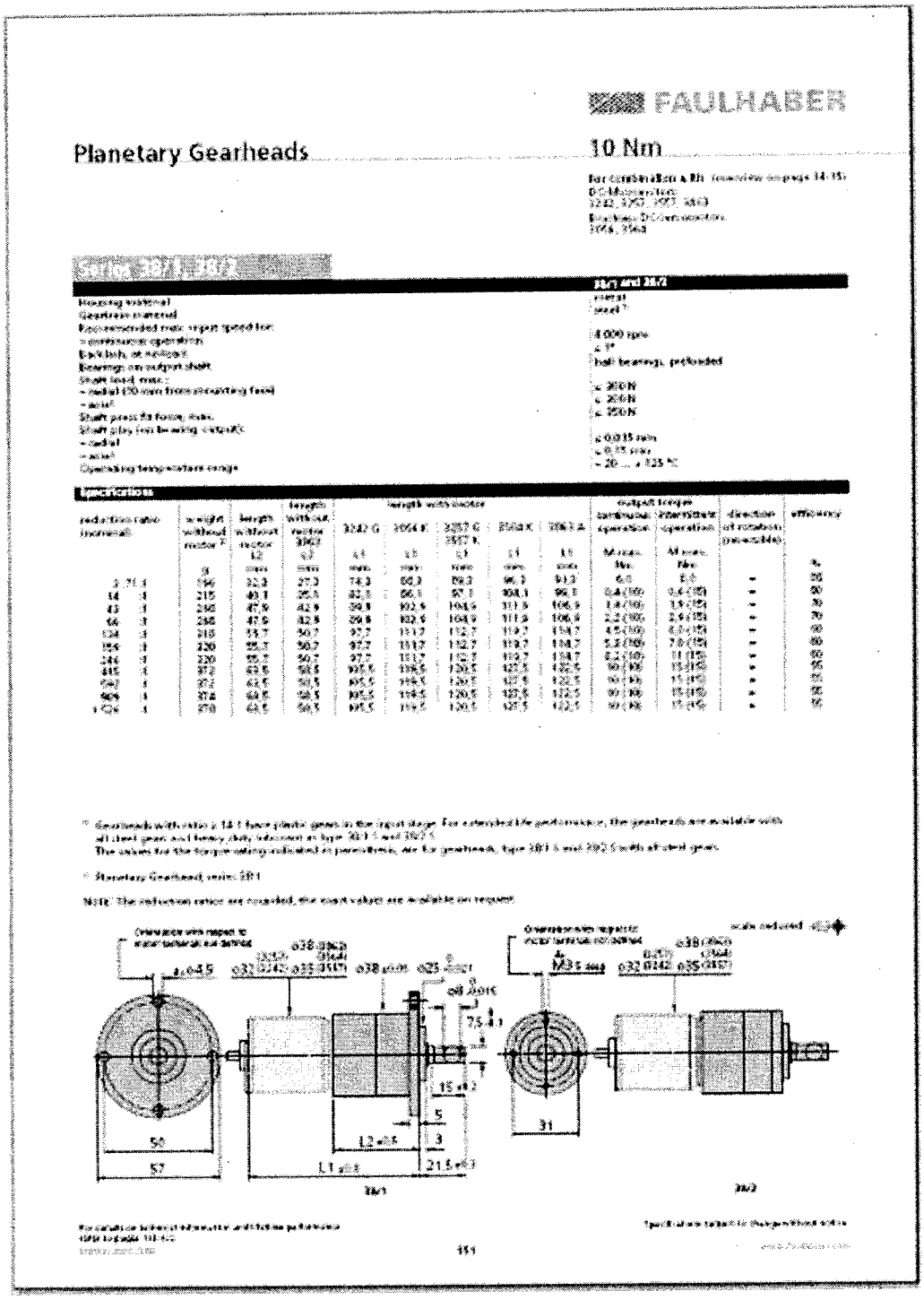

Fig. G-4 Faulhaber gearhead 38/2

Appendix H

I/O Ports Description for Electrical Circuit Boards

Table H-1 I/O Ports Description for the Analog Conditioning Board

I/O	Pin #	Description
ANALOG_IN (Analog signal inputs)	1	Voltage feedback 1 from joint 1
	2	Voltage feedback 2 from joint 2
	3	Voltage feedback 3 from joint 3
	4	Voltage feedback 4 from joint 4
	5	Voltage feedback 5 from joint 5
	6	Voltage feedback 6 from joint 6
	7	Voltage measurement 1 for force sensor 1
	8	Voltage measurement 2 for force sensor 2
	9	Voltage measurement 3 for force sensor 3
	10	Voltage measurement 4 for force sensor 4
	11	Current sense signal 1 from H-bridge 1
	12	Current sense signal 2 from H-bridge 2
	13	Current sense signal 3 from H-bridge 3
	14	Current sense signal 4 from H-bridge 4
	15	Current sense signal 5 from H-bridge 5
	16	Current sense signal 6 from H-bridge 6
	17	GND
	18	GND
	19	+3.3 v
	20	+3.3 v
P9 (To connector P9 on DSP board)	1	Analog output 1 for DSP ADCINA0 (P9 Pin1)
	2	Analog output 2 for DSP ADCINA1 (P9 Pin2)
	3	Analog output 3 for DSP ADCINA2 (P9 Pin3)
	4	Analog output 4 for DSP ADCINA3 (P9 Pin4)
	5	Analog output 5 for DSP ADCINA4 (P9 Pin5)
	6	Analog output 6 for DSP ADCINA5 (P9 Pin6)
	7	Analog output 7 for DSP ADCINA6 (P9 Pin7)
	8	Analog output 8 for DSP ADCINA7 (P9 Pin8)
	9	For DSP VREFLO (P9 Pin9) Short to GND
	10	No connect
P5 (To connector P5 on DSP board)	1	Analog output 9 for DSP ADCINB0 (P5 Pin1)
	2	Analog output 10 for DSP ADCINB1 (P5 Pin2)
	3	Analog output 11 for DSP ADCINB2 (P5 Pin3)
	4	Analog output 12 for DSP ADCINB3 (P5 Pin4)
	5	Analog output 13 for DSP ADCINB4 (P5 Pin5)

Table H-1 I/O Ports Description for the Analog Conditioning Board (Contd.)

I/O	Pin #	Description
P5 (To connector P5 on DSP board) (Contd.)	6	Analog output 14 for DSP ADCINB5 (P5 Pin6)
	7	Analog output 15 for DSP ADCINB6 (P5 Pin7)
	8	Analog output 16 for DSP ADCINB7 (P5 Pin8)
	9	For DSP ADCREFP (P5 Pin9) Not use.
	10	For DSP ADCREFP (P5 Pin10) Not use.

Table H-2 I/O Ports Description for the Motor Driver Board

I/O	Pin #	Description
PS_In (Power from activation board)	1	+24 v
	2	GND
M123 (Motor 1, 2 and 3 power supply)	1	Voltage supply 1 for the motor 1
	2	
	3	Voltage supply 2 for the motor 2
	4	
	5	Voltage supply 3 for the motor 3
	6	
M456 (Motor 4, 5 and 6 power supply)	1	Voltage supply 4 for the motor 4
	2	
	3	Voltage supply 5 for the motor 5
	4	
	5	Voltage supply 6 for the motor 6
	6	
DIR_PWM_TF_BK (Direction, PWM, thermal flag and brake signals)	1	Direction signal 1 from DSP for H-bridge 1
	2	Direction signal 2 from DSP for H-bridge 2
	3	Direction signal 3 from DSP for H-bridge 3
	4	Direction signal 4 from DSP for H-bridge 4
	5	Direction signal 5 from DSP for H-bridge 5
	6	Direction signal 6 from DSP for H-bridge 6
	7	PWM signal 1 from DSP for H-bridge 1
	8	PWM signal 2 from DSP for H-bridge 2
	9	PWM signal 3 from DSP for H-bridge 3
	10	PWM signal 4from DSP for H-bridge 4
	11	PWM signal 5 from DSP for H-bridge 5
	12	PWM signal 6 from DSP for H-bridge 6
	13	H-bridge 1 Thermal flag signal 1 to DSP
	14	H-bridge 2 Thermal flag signal 2 to DSP
	15	H-bridge 3 Thermal flag signal 3 to DSP
	16	H-bridge 4 Thermal flag signal 4 to DSP
	17	H-bridge 5 Thermal flag signal 5 to DSP
	18	H-bridge 6 Thermal flag signal 6 to DSP
	19	Brake signal from DSP (short pin1 and pin2 of J3 to enable)
	20	GND
Current_Sense (Current sensing outputs)	1	Current sensing output signal 1 from H-bridge 1
	2	Current sensing output signal 2 from H-bridge 2
	3	Current sensing output signal 3 from H-bridge 3
	4	Current sensing output signal 4 from H-bridge 4
	5	Current sensing output signal 5 from H-bridge 5
	6	Current sensing output signal 6 from H-bridge 6

Table H-2 I/O Ports Description for the Motor Driver Board (Contd.)

I/O	Pin #	Description
Current_Sense (Current sensing outputs) (Contd.)	7	No connect
	8	No connect
	9	No connect
	10	GND
J3 (Jumpers)	1	Brake signal from DIR_PWM_TF_BK pin19
	2	To BRAKE INPUT of all H-bridges
	3	GND
J1_MD1 J2_MD1 (Connectors for H-bridge adaptor)		H-bridge 1 Adaptor
J1_MD2 J2_MD2 (Connectors for H-bridge adaptor)		H-bridge 2 Adaptor
J1_MD3 J2_MD3 (Connectors for H-bridge adaptor)		H-bridge 3 Adaptor
J1_MD4 J2_MD4 (Connectors for H-bridge adaptor)		H-bridge 4 Adaptor
J1_MD5 J2_MD5 (Connectors for H-bridge adaptor)		H-bridge 5 Adaptor
J1_MD6 J2_MD6 (Connectors for H-bridge adaptor)		H-bridge 6 Adaptor

Table H-3 I/O Ports Description for the Communication Adaptor Board

I/O	Pin #	Description
P8 (From connector P8 on DSP board)	1	+3.3 v to P4 pin1, J3 pin1 and JP1
	2	
	3	SCITXDA to JP3
	4	SCIRXDA to JP2
	5	No connect
	6	GPIO A8 to J3 pin3
	7	GPIO A9 to J1 pin1
	8	GPIO A10 to J1 pin2
	9	PWM1 to J1 pin7
	10	No connect
	11	PWM3 to J1 pin8
	12	No connect
	13	PWM5 to J1 pin9
	14	No connect
	15	
	16	
	17	GPIO A11 to J1 pin3
	18	GPIO A12 to J1 pin4
	19	GND
	20	
	21	No connect
	22	
	23	SPISIMOA to J2 pin1
	24	SPISOMIA to J2 pin2
	25	SPICLKA to J2 pin3
	26	SPISTEA to J2 pin4
	27	CANTXA to J2 pin5
	28	CANRXA to J2 pin6
	29	No connect
	30	PWM7 to J1 pin10
	31	No connect
	32	PWM9 to J1 pin11
	33	No connect
	34	PWM11 to J1 pin12
	35	No connect
	36	GPIO B8 to J1 pin14
	37	No connect
	38	
	39	GND
	40	

Table H-3 I/O Ports Description for the Communication Adaptor Board (Contd. 1)

I/O	Pin #	Description
P4 (From connector P4 on DSP board)	1	+3.3 v to P8 pin1, P8 pin2, J3 pin1 and JP1
	2	No connect
	3	GPIO F8 to J1 pin19
	4	GPIO F9 to J4 pin7
	5	GPIO F10 to J4 pin9
	6	GPIO F11 to J4 pin11
	7	GPIO F12 to J4 pin13
	8	GPIO F13 to J4 pin15
	9	No connect
	10	GND
	11	GPIO B9 to J1 pin15
	12	GPIO B10 to J1 pin16
	13	No connect
	14	
	15	GPIO B11 to J1 pin17
	16	GPIO B12 to J1 pin18
	17	No connect
	18	SCITXDB (P4 pin18)
	19	SCIRXDB (P4 pin19)
	20	GND
P7 (From connector P7 on DSP board)	1	GPIO A13 to J1 pin5
	2	GPIO A14 to J1 pin6
	3	GPIO A15 to J1 pin13
	4	No connect
	5	GPIO B13 to J4 pin1
	6	GPIO B14 to J4 pin3
	7	GPIO B15 to J4 pin5
	8	No connect
	9	
	10	GND
PS (Optional external +5 v)	1	Optional external +5 v (JP1 must open)
	2	GND
JP1		Jumper always open
JP2		Jumper to connect DSP SCIRXDA (P8 pin4) to MAX232 pin 9
JP3		Jumper to connect DSP SCITXDA (P8 pin3) to MAX232 pin10

Table H-3 I/O Ports Description for the Communication Adaptor Board (Contd. 2)

I/O	Pin #	Description
J1 DIR & PWM & Thermal Flag (Direction, PWM, thermal flag and brake signals)	1	Direction signal 1 from DSP GPIO A9 (P8 pin7)
	2	Direction signal 2 from DSP GPIO A10 (P8 pin8)
	3	Direction signal 3 from DSP GPIO A11 (P8 pin17)
	4	Direction signal 4 from DSP GPIO A12 (P8 pin18)
	5	Direction signal 5 from DSP GPIO A13 (P7 pin1)
	6	Direction signal 6 from DSP GPIO A14 (P7 pin2)
	7	PWM signal 1 from DSP PWM1 (P8 pin9)
	8	PWM signal 2 from DSP PWM3 (P8 pin11)
	9	PWM signal 3 from DSP PWM5 (P8 pin13)
	10	PWM signal 4 from DSP PWM7 (P8 pin30)
	11	PWM signal 5 from DSP PWM9 (P8 pin32)
	12	PWM signal 6 from DSP PWM11 (P8 pin34)
	13	Thermal flag signal 1 to DSP GPIO A15 (P7 pin3)
	14	Thermal flag signal 2 to DSP GPIO B8 (P8 pin36)
	15	Thermal flag signal 3 to DSP GPIO B9 (P4 pin11)
	16	Thermal flag signal 4 to DSP GPIO B10 (P4 pin12)
	17	Thermal flag signal 5 to DSP GPIO B11 (P4 pin15)
	18	Thermal flag signal 6 to DSP GPIO B12 (P4 pin16)
	19	Break signal from DSP GPIO F8 (P4 pin3)
	20	GND
J2 Communication (SPI, SCI_B and 8 digital I/Os)	1	DSP SPISIMOA (P8 pin23)
	2	DSP SPISOMIA (P8 pin24)
	3	DSP SPICLKA (P8 pin25)
	4	DSP SPISTEA (P8 pin26)
	5	DSP CANTXA (P8 pin27)
	6	DSP CANRXA (P8 pin28)
	7	DSP SCITXDB (P4 pin18)
	8	DSP SCIRXDB (P4 pin19)
	9	J4 pin2
	10	J4 pin4
	11	J4 pin6
	12	J4 pin8
	13	J4 pin10
	14	J4 pin12
	15	J4 pin14
	16	J4 pin16
	17	GND
	18	No connect
	19	No connect
	20	No connect

Table H-3 I/O Ports Description for the Communication Adaptor Board (Contd. 3)

I/O	Pin #	Description
J3 PS_Rel (+3.3 v and relay signal from DSP)	1	+3.3 v from DSP (P8 pin1, pin 2 and P4 pin1)
	2	GND
	3	Relay activation signal from DSP GPIO A8 (P8 pin6)
J4 Digital Jumper (Jumpers to enable J2 pin9 to J2 pin16)	1	DSP GPIO B13 (P7 pin5)
	2	J2 pin9
	3	DSP GPIO B14 (P7 pin6)
	4	J2 pin10
	5	DSP GPIO B15 (P7 pin7)
	6	J2 pin11
	7	DSP GPIO F9 (P4 pin4)
	8	J2 pin12
	9	DSP GPIO F10 (P4 pin5)
	10	J2 pin13
	11	DSP GPIO F11 (P4 pin6)
	12	J2 pin14
	13	DSP GPIO F12 (P4 pin7)
	14	J2 pin15
	15	DSP GPIO F13 (P4 pin8)
	16	J2 pin16

Table H-4 I/O Ports Description for the Feedback and Limit Switch Boards (Leg)

Joint 1

I/O	Pin #	Description
Connector 1	1	+3.3 v
	2	GND
	3	Middle lead of the limit switch
	4	GND
	5	Middle lead of feedback potentiometer
	6	No connect
	7	
	8	
	9	
	10	
	11	FS1 pin1
	12	FS2 pin1
	13	FS3 pin1
	14	FS4 pin1
FS1 (Force sensor 1)	1	Force sensor 1 pin1
	2	Force sensor 1 pin2
	3	Force sensor 1 pin3, GND
FS2 (Force sensor 2)	1	Force sensor 2 pin1
	2	Force sensor 2 pin2
	3	Force sensor 2 pin3, GND
FS3 (Force sensor 3)	1	Force sensor 3 pin1
	2	Force sensor 3 pin2
	3	Force sensor 3 pin3, GND
FS4 (Force sensor 4)	1	Force sensor 4 pin1
	2	Force sensor 4 pin2
	3	Force sensor 4 pin3, GND

Joint 2

I/O	Pin #	Description
Connector 2	1	+3.3 v
	2	GND
	3	Middle lead of the limit switch
	4	GND
	5	No connect
	6	Middle lead of feedback potentiometer
	7	No connect
	8	
	9	
	10	
	11	
	12	
	13	
	14	

Joint 3

I/O	Pin #	Description
Connector 3	1	+3.3 v
	2	GND
	3	Middle lead of the limit switch
	4	GND
	5	No connect
	6	
	7	Middle lead of feedback potentiometer
	8	No connect
	9	
	10	
	11	
	12	
	13	
	14	

Joint 4

I/O	Pin #	Description
Connector 4	1	+3.3 v
	2	GND
	3	Middle lead of the limit switch
	4	GND
	5	No connect
	6	
	7	
	8	Middle lead of feedback potentiometer
	9	No connect
	10	
	11	
	12	
	13	
	14	

Joint 5

I/O	Pin #	Description
Connector 5	1	+3.3 v
	2	GND
	3	Middle lead of the limit switch
	4	GND
	5	No connect
	6	
	7	
	8	
	9	Middle lead of feedback potentiometer
	10	No connect
	11	
	12	
	13	
	14	

Joint 6

I/O	Pin #	Description
Connector 6	1	+3.3 v
	2	GND
	3	Middle lead of the limit switch
	4	GND
	5	No connect
	6	
	7	
	8	
	9	
	10	Middle lead of feedback potentiometer
	11	No connect
	12	
	13	
	14	

Table H-5 I/O Ports Description for the Feedback and Limit Switch Boards (Arms)

Left Arm Joint 1

I/O	Pin #	Description
J_L1	1	+3.3 v
	2	GND
	3	Middle lead of the limit switch
	4	GND
	5	Middle lead of feedback potentiometer
	6	No connect
	7	
	8	
	9	
	10	

Left Arm Joint 2

I/O	Pin #	Description
J_L2	1	+3.3 v
	2	GND
	3	Middle lead of the limit switch
	4	GND
	5	No connect
	6	Middle lead of feedback potentiometer
	7	No connect
	8	
	9	
	10	

Left Arm Joint 3

I/O	Pin #	Description
J_L3	1	+3.3 v
	2	GND
	3	Middle lead of the limit switch
	4	GND
	5	No connect
	6	
	7	Middle lead of feedback potentiometer
	8	No connect
	9	
	10	

Table H-5 I/O Ports Description for the Feedback and Limit Switch Boards (Arms) (Contd.)

Right Arm Joint 1

I/O	Pin #	Description
J_R1	1	+3.3 v
	2	GND
	3	Middle lead of the limit switch
	4	GND
	5	No connect
	6	
	7	
	8	Middle lead of feedback potentiometer
	9	No connect
	10	

Right Arm Joint 2

I/O	Pin #	Description
J_R2	1	+3.3 v
	2	GND
	3	Middle lead of the limit switch
	4	GND
	5	No connect
	6	
	7	
	8	
	9	Middle lead of feedback potentiometer
	10	No connect

Right Arm Joint 3

I/O	Pin #	Description
J_R3	1	+3.3 v
	2	GND
	3	Middle lead of the limit switch
	4	GND
	5	No connect
	6	
	7	
	8	
	9	
	10	Middle lead of feedback potentiometer

Table H-6 I/O Ports Description for the Force Sensor, System Activation and Protection Board

I/O	Pin #	Description
Analog_Out_L (Analog signals and +3.3 v supply for analog conditioning board for left leg)	1	Voltage feedback 1 for left leg (FeedBK_LimitSW_L pin 5)
	2	Voltage feedback 2 for left leg (FeedBK_LimitSW_L pin 6)
	3	Voltage feedback 3 for left leg (FeedBK_LimitSW_L pin 7)
	4	Voltage feedback 4 for left leg (FeedBK_LimitSW_L pin 8)
	5	Voltage feedback 5 for left leg (FeedBK_LimitSW_L pin 9)
	6	Voltage feedback 6 for left leg (FeedBK_LimitSW_L pin 10)
	7	Voltage measurement 1 for left foot force sensor 1 (OP1 pin 1)
	8	Voltage measurement 2 for left foot force sensor 2 (OP1 pin 7)
	9	Voltage measurement 3 for left foot force sensor 3 (OP2 pin 1)
	10	Voltage measurement 4 for left foot force sensor 4 (OP2 pin 7)
	11	Left leg current sensing output signal 1 (Current Sense_L pin1)
	12	Left leg current sensing output signal 2 (Current Sense_L pin2)
	13	Left leg current sensing output signal 3 (Current Sense_L pin3)
	14	Left leg current sensing output signal 4 (Current Sense_L pin4)
	15	Left leg current sensing output signal 5 (Current Sense_L pin5)
	16	Left leg current sensing output signal 6 (Current Sense_L pin6)
	17	GND
	18	
	19	+3.3 v (Pin1 of PS_Rel_L or PS_Rel_R or PS_Rel_A)
	20	+3.3 v (Pin1 of PS_Rel_L or PS_Rel_R or PS_Rel_A)
Analog_Out_R (Analog signals and +3.3 v supply for analog conditioning board for right leg)	1	Voltage feedback 1 for right leg (FeedBK_LimitSW_R pin 5)
	2	Voltage feedback 2 for right leg (FeedBK_LimitSW_R pin 6)
	3	Voltage feedback 3 for right leg (FeedBK_LimitSW_R pin 7)
	4	Voltage feedback 4 for right leg (FeedBK_LimitSW_R pin 8)
	5	Voltage feedback 5 for right leg (FeedBK_LimitSW_R pin 9)
	6	Voltage feedback 6 for right leg (FeedBK_LimitSW_R pin 10)
	7	Voltage measurement 1 for right foot force sensor 1 (OP3 pin 1)
	8	Voltage measurement 2 for right foot force sensor 2 (OP3 pin 7)
	9	Voltage measurement 3 for right foot force sensor 3 (OP4 pin 1)
	10	Voltage measurement 4 for right foot force sensor 4 (OP4 pin 7)
	11	Right leg current sensing output signal 1 (Current Sense_R pin1)
	12	Right leg current sensing output signal 2 (Current Sense_R pin2)
	13	Right leg current sensing output signal 3 (Current Sense_R pin3)
	14	Right leg current sensing output signal 4 (Current Sense_R pin4)
	15	Right leg current sensing output signal 5 (Current Sense_R pin5)
	16	Right leg current sensing output signal 6 (Current Sense_R pin6)
	17	GND
	18	

Table H-6 I/O Ports Description for the Force Sensor, System Activation and Protection Board (Contd. 1)

I/O	Pin #	Description
Analog_Out_R (Analog signals and +3.3 v supply for analog conditioning board for right leg) (Contd.)	19	+3.3 v (Pin1 of PS_Rel_L or PS_Rel_R or PS_Rel_A)
	20	+3.3 v (Pin1 of PS_Rel_L or PS_Rel_R or PS_Rel_A)
Analog_Out_A (Analog signals and +3.3 v supply for analog conditioning board for arm)	1	Voltage feedback 1 for left arm (FeedBK_LimitSW_A pin 5)
	2	Voltage feedback 2 for left arm (FeedBK_LimitSW_A pin 6)
	3	Voltage feedback 3 for left arm (FeedBK_LimitSW_A pin 7)
	4	Voltage feedback 1 for right arm (FeedBK_LimitSW_A pin 8)
	5	Voltage feedback 2 for right arm (FeedBK_LimitSW_A pin 9)
	6	Voltage feedback 3 for right arm (FeedBK_LimitSW_A pin 10)
	7	No connect
	8	
	9	
	10	
	11	Left arm current sensing output signal 1 (Current Sense_L pin1)
	12	Left arm current sensing output signal 2 (Current Sense_L pin2)
	13	Left arm current sensing output signal 3 (Current Sense_L pin3)
	14	Right arm current sensing output signal 1 (Current Sense_L pin4)
	15	Right arm current sensing output signal 2 (Current Sense_L pin5)
	16	Right arm current sensing output signal 3 (Current Sense_L pin6)
	17	GND
	18	GND
	19	+3.3 v (Pin1 of PS_Rel_L or PS_Rel_R or PS_Rel_A)
	20	+3.3 v (Pin1 of PS_Rel_L or PS_Rel_R or PS_Rel_A)
J1 FeedBK_LimitSW_L (feedback, limit switch and force sensor feedbacks from left leg)	1	+3.3 v (Pin1 of PS_Rel_L or PS_Rel_R or PS_Rel_A)
	2	GND
	3	Limit switch signal (Pin3 of PS_Rel_L, PS_Rel_R and PS_Rel_A)
	4	GND
	5	Voltage feedback 1 for left leg
	6	Voltage feedback 2 for left leg
	7	Voltage feedback 3 for left leg
	8	Voltage feedback 4 for left leg
	9	Voltage feedback 5 for left leg
	10	Voltage feedback 6 for left leg
	11	Resistance measurement 1 for left foot force sensor 1
	12	Resistance measurement 2 for left foot force sensor 2
	13	Resistance measurement 3 for left foot force sensor 3
	14	Resistance measurement 4 for left foot force sensor 4

Table H-6 I/O Ports Description for the Force Sensor, System Activation and Protection Board (Contd. 2)

I/O	Pin #	Description
J2 FeedBK_LimitSW_R (feedback, limit switch and force sensor feedbacks from right leg)	1	+3.3 v (Pin1 of PS_Rel_L or PS_Rel_R or PS_Rel_A)
	2	GND
	3	Limit switch signal (Pin3 of PS_Rel_L, PS_Rel_R and PS_Rel_A)
	4	GND
	5	Voltage feedback 1 for right leg
	6	Voltage feedback 2 for right leg
	7	Voltage feedback 3 for right leg
	8	Voltage feedback 4 for right leg
	9	Voltage feedback 5 for right leg
	10	Voltage feedback 6 for right leg
	11	Resistance measurement 4 for right foot force sensor 4
	12	Resistance measurement 1 for right foot force sensor 1
	13	Resistance measurement 2 for right foot force sensor 2
	14	Resistance measurement 3 for right foot force sensor 3
J3 FeedBK_LimitSW_A (feedback and limit switch feedbacks from arm)	1	+3.3 v (Pin1 of PS_Rel_L or PS_Rel_R or PS_Rel_A)
	2	GND
	3	Limit switch signal (Pin3 of PS_Rel_L, PS_Rel_R and PS_Rel_A)
	4	GND
	5	Voltage feedback 1 for left arm
	6	Voltage feedback 2 for left arm
	7	Voltage feedback 3 for left arm
	8	Voltage feedback 1 for right arm
	9	Voltage feedback 2 for right arm
	10	Voltage feedback 3 for right arm
	11	No connect
	12	
	13	
	14	
J4 Current Sense_L (Current sensing outputs from motor driver board for left leg)	1	Current sensing output signal 1 from left leg H-bridge 1
	2	Current sensing output signal 2 from left leg H-bridge 2
	3	Current sensing output signal 3 from left leg H-bridge 3
	4	Current sensing output signal 4 from left leg H-bridge 4
	5	Current sensing output signal 5 from left leg H-bridge 5
	6	Current sensing output signal 6 from left leg H-bridge 6
	7	No connect
	8	
	9	
	10	

Table H-6 I/O Ports Description for the Force Sensor, System Activation and Protection Board (Contd. 3)

I/O	Pin #	Description
J5 Current Sense_R (Current sensing outputs from motor driver board for right leg)	1	Current sensing output signal 1 from right leg H-bridge 1
	2	Current sensing output signal 2 from right leg H-bridge 2
	3	Current sensing output signal 3 from right leg H-bridge 3
	4	Current sensing output signal 4 from right leg H-bridge 4
	5	Current sensing output signal 5 from right leg H-bridge 5
	6	Current sensing output signal 6 from right leg H-bridge 6
	7	No connect
	8	
	9	
	10	
J6 Current Sense_A (Current sensing outputs from motor driver board forarm)	1	Current sensing output signal 1 from left arm H-bridge 1
	2	Current sensing output signal 2 from left arm H-bridge 2
	3	Current sensing output signal 3 from left arm H-bridge 3
	4	Current sensing output signal 4 from right arm H-bridge 4
	5	Current sensing output signal 5 from right arm H-bridge 5
	6	Current sensing output signal 6 from right arm H-bridge 6
	7	No connect
	8	
	9	
	10	
J7 PS_Rel_L (+3.3 v and relay signal from DSP for left leg)	1	+3.3 v from DSP for left leg (P8 pin1, pin 2 and P4 pin1)
	2	GND
	3	Relay activation signal from DSP for left leg GPIO A8 (P8 pin6)
J8 PS_Rel_R (+3.3 v and relay signal from DSP for right leg)	1	+3.3 v from DSP for right leg (P8 pin1, pin 2 and P4 pin1)
	2	GND
	3	Relay activation signal from DSP for right leg GPIO A8 (P8 pin6)
J9 PS_Rel_A (+3.3 v and relay signal from DSP for arm)	1	+3.3 v from DSP for arm (P8 pin1, pin 2 and P4 pin1)
	2	GND
	3	Relay activation signal from DSP for arm GPIO A8 (P8 pin6)
PS_In (+24 v power input)	1	+24 v from power supply
	2	GND
PS_Out (+24 v power output)	1	+24 v to motor driver boards
	2	GND
JP1		Jumper to enable +3.3 v from DSP for left leg
JP2		Jumper to enable +3.3 v from DSP for right leg
JP3		Jumper to enable +3.3 v from DSP for arm

Appendix I

Electrical Circuit Boards Inter-wiring Schematics

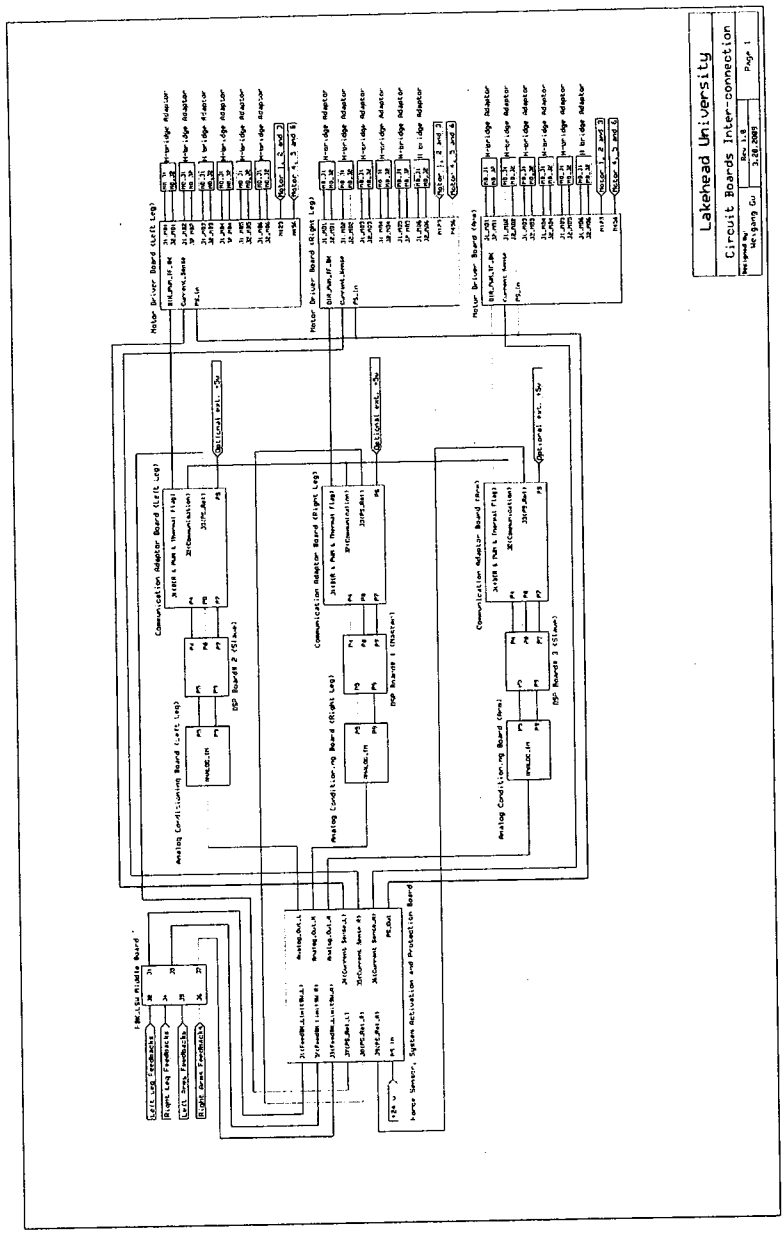

Fig. I-1 Circuit boards inter-wiring